Development of quorum-sensing circuits for metabolic flux control in *Escherichia coli*

by

Christina V. Dinh

M.S. Chemical Engineering Practice
Massachusetts Institute of Technology, 2016

B.S. Chemical Engineering
University of Minnesota – Minneapolis, 2015

Submitted to the Department of Chemical Engineering
in partial fulfillment of the requirements for the degree of

Doctor of Philosophy in Chemical Engineering
at the
MASSACHUSETTS INSTITUTE OF TECHNOLOGY

February 2020

Signature of Author .....
Christina V. Dinh
Department of Chemical Engineering
December 17, 2019

Certified by .....
Kristala L. Jones Prather
Arthur D. Little Professor of Chemical Engineering
Thesis Supervisor

Accepted by .....
Patrick S. Doyle
Robert T. Haslam Professor of Chemical Engineering
Chairman, Committee for Graduate Students

Development of quorum sensing circuits for metabolic flux control in *Escherichia coli*

Christina V. Dinh

Submitted to the Department of Chemical Engineering on December 17, 2019 in Partial Fulfillment of the Requirements for the Degree of Doctor of Philosophy in Chemical Engineering

Abstract

Metabolic engineering seeks to reprogram microbial cells to efficiently produce value-added chemicals. Traditionally, this is achieved by overexpressing the production pathway and/or knocking out competing endogenous pathways. However, limitations in some pathways are more effectively addressed through dynamic metabolic flux control to favor different objectives over the course of the fermentation. This thesis aims to develop autonomous and pathway-independent regulation tools that can be applied to controlling metabolic fluxes in these contexts to improve production. To this end, quorum-sensing (QS)-based circuits were constructed, characterized, and applied to regulating metabolic fluxes in a cell-density-dependent manner.

The first tool is a bifunctional QS circuit in which each control module regulates transcription under circuits derived from different QS systems. Characterization showed that the switching dynamics of both circuits can be tuned by varying the expression level of circuit components. To address major limitations in the naringenin and salicylic acid pathways, one module was used to delay transcription of key heterologous genes to overcome enzyme inhibition and growth burden while the second module controlled expression of CRISPRi components to silence competing endogenous pathways. Application of these regulation schemes resulted in significant production improvements in both pathways.

Especially when aiming to dynamically down-regulate enzyme activity, post-translational control can offer faster response dynamics. To develop a post-translational control tool, expression of a protease linker was regulated under a QS circuit, resulting in selective degradation of tagged enzymes. This circuit was applied to regulating phosphofructokinase (Pfk) levels with the ultimate goal of dynamic composition control in co-culture fermentations. Application of this control circuit in a naringenin-producing co-culture system resulted in improved composition profiles, which benefited production. Finally, a second post-translational control system that co-localizes proteins in response to cell-density changes was constructed and characterized. Such a system can be applied to actuate changes in reaction rates with minimal dependence on host cell machinery.

Overall, this work developed QS-based circuits and showed they can be powerful tools for addressing key limitations in microbial syntheses.

Thesis supervisor: Kristala L. J. Prather
Title: Arthur D. Little Professor of Chemical Engineering

Acknowledgments

There are many people who have shaped my path to get me to this point. I would first like to thank my thesis advisor, Kris Prather, for being an amazing mentor and role model. Your optimism and encouragement made the obstacles in the lab seem surmountable and your willingness to give me the freedom to make mistakes and pursue questionable ideas has allowed me to hone my problem-solving skills. I would also like to thank my thesis committee, Professors Gregory Stephanopoulos and Kevin Esvelt for their input and scientific guidance during the project.

I would like to acknowledge the other academic mentors who have contributed to my development as a scientist. First among those is my undergrad research mentor, Rachel, for being the first to show me what hard work and good science looks like. Your mentorship was influential in my decision to pursue a research career and the skills I gained under your guidance certainly eased my transition to graduate school. I would also like to thank the many other outstanding teachers and professors who have instilled in me curiosity and a love of learning.

I would like to thank my friends and colleges in the Prather lab for their steady willingness to lend advice, support, and precious lab materials. This list is far from complete, but I'd like to thank a few. To Apoorv, thank you for guiding me through my first few semesters in the lab. To Stephanie, thank you for listening to and talking through all my questions about research and life. To Cynthia, thanks for being a thoughtful friend and for reminding me to laugh at myself. To Jennifer, thanks for your positive energy and willingness to step up for the lab. To Kevin, thanks for all the chats about the undergrad days and all other Minnesota-related things. To Jason, Kristina, and Wesley, thanks for your valuable technical advice, insightful questions, and willingness to help us grad students. To Crystal, thanks for all your help, hard work and positive attitude. I'm excited to hear about your future accomplishments. And of course, thanks Gwen for all that you do to make things run smoothly around here.

I am grateful to all the amazing people I've met at MIT, especially my classmates. Thank you for being there as we ventured through grad school together and thanks for making a new place feel like home.

Last but not least, I need to thank my family for their love and support. To my parents, I would not be here without your dedication to giving me everything I need to succeed. You inspire me to aim for my best every day. To my sister Tracy, I couldn't have asked for a better partner in crime.

Christina V. Dinh

Table of Contents

List of Figures

List of Tables

List of Abbreviations

Abbreviation	Complete name
AHL	N-acyl homoserine lactone
AI-2	Autoinducer-2
AIP	Auto-inducing peptide
aTc	Anhydrotetracycline
C12-AHL	*N*-(3-oxododecanoyl)-L-homoserine lactone
CA	*p*-coumaric acid
CHI	Chalcone isomerase
CHS	Chalcone synthase
CoA	Coenzyme-A
DAS+4	Protein degradation tag AADENYSENYADAS
DO	Dissolved oxygen
DPD	dihydroxypentanedione
E. coli	*Escherichia coli*
FPP	Farnesyl pyrophosphate
G6P	Glucose-6-phosphate
GFP	Green fluorescent protein
HPLC	High pressure liquid chromatography
IDR	Intrinsically disordered region
IPTG	β-D-1-thiogalactopyranoside
LB	Luria-Bertani medium
LVA	Protein degradation tag AANDENYALVA
MIOX	*Myo*-inositol oxygenase
MOPS	3-(N-morpholino) propansulfonic acid
OD_{600}	Optical density at 600 nm wavelength
PCR	Polymerase chain reaction
Pfk	phosphofructokinase

QS	Quorum sensing
RBS	Ribosome binding site
RFP	Red fluorescent protein
SD	Standard deviation
TAL	Tyrosine ammonia lyase
3OC6HSL	*N*-(3-oxohexanoyl)-L-homoserine lactone
3OC12HSL	*N*-(3-oxododecanoyl)-L-homoserine lactone
4CL	4-coumaryl-CoA ligase

1. Introduction

Abstract

Metabolic engineering strategies have led to an expansion in the set of molecules that can be efficiently produced through microbial synthesis. Traditionally, these gains are realized by up-regulating metabolic fluxes in the production pathway and down-regulating competing endogenous pathways. Inspired by the way that cells naturally regulate gene expression to adapt to changing environmental conditions, recent studies have focused on developing systems that similarly respond to stimuli to dynamically control metabolic fluxes to favor certain reactions during different phases in the fermentation. With the rapid development of synthetic biology tools, control circuits that respond to cell density, metabolite concentration, and fermentation conditions have now been developed and employed in microbial production systems to overcome production limitations and achieve significant improvements. In this dissertation, quorum-sensing (QS)-based tools were developed to offer generalizable control methods that may be used to overcome limitations in challenging production pathways.

This chapter contains material adapted from:

Dinh, C. V. & Prather, K. L. J. Layered and multi-input autonomous dynamic control strategies for metabolic engineering. In preparation.

1.1. Dynamic metabolic flux control

Metabolic engineering seeks to reprogram cells with the goal of producing value-added chemicals that are well suited to microbial synthesis. Such chemicals vary widely, including ones used in biofuels, plastics, and pharmaceuticals. Enzymes that produce stereochemically pure products simplify downstream separation requirements in fine chemical production. For commodity chemical production, microbial synthesis may allow for utilization of inexpensive or renewable feedstocks. Additionally, microbial synthesis typically occurs under mild conditions, offering safety, energy conservation, and environmental benefits.

Challenges that limit efficient production can arise when heterologous pathways are imported or when endogenous metabolic fluxes are manipulated. For example, flux through heterologous pathways may inhibit cell growth by generating toxic products or consuming essential endogenous metabolites. Strategies for overcoming these challenges focus on balancing growth and production through controlling reaction fluxes. The static balancing approach aims to maintain fixed reaction fluxes in an intermediate regime such that neither objective dominates whereas the dynamic approach generally regulates gene expression to favor accumulating biomass or key metabolites early, before diverting metabolic fluxes towards product formation. While more difficult to implement in practice, dynamic control is required for efficient production in some pathways. Key computational and experimental demonstrations of metabolic flux control are detailed in the following sections.

1.1.1. Dynamic control in computational models

Cells naturally dynamically regulate their metabolic fluxes to adapt and survive in changing environmental conditions. These native regulation systems allow for decreased protein demand while maintaining metabolic fluxes through key pathways, resulting in faster growth rates under a broad range of environmental conditions. For example, carbon catabolite repression ensures that *E. coli* cells prioritize the uptake of their preferred carbon source, glucose, by preventing uptake of other sugars in its presence. *E. coli* additionally minimizes the protein burden associated with

unnecessary catabolic pathways by repressing expression of these pathways in the presence of glucose (1). More recently, analysis of the amino acid pathways has shown that these pathways utilize a "just-in-time" pathway expression routine in which upstream pathway enzymes have faster activation response times and higher maximum expression levels. Such regulation schemes enable cells to rapidly achieve their production goal with a relatively low enzyme requirement (2). A more comprehensive analysis revealed that there is wide-spread transcriptional regulation of endogenous metabolic pathways in *E. coli.* Additionally, the study found that the likelihood of regulation at an individual pathway step depends on the cost (i.e. total mass) of the enzyme that catalyzes that reaction. These results suggest that cells naturally employ dynamic regulation to manage a trade-off between surviving in diverse environments and minimizing enzyme cost (3).

The concept of dynamic control to only produce enzymes when needed can also be applied to engineered microbial production systems. Gadkar et al. performed bilevel optimizations on computational models of glycerol and ethanol production. Their optimization algorithm allowed a key metabolic flux to switch from OFF to ON or ON to OFF during the course of the fermentation and predicted significant productivity improvements in both glycerol and ethanol production systems (4). Anesiadis et al. extended the ethanol production model to incorporate the kinetics of a toggle switch composed of the *lac* and *lux* regulation circuits to confirm that dynamic control still improves production under more gradual transition between states (5). This group additionally generalized their model to predict how dynamic regulation can similarly improve serine production (6). While the above models employ simple regulation schemes that control only one reaction step, Klipp et al. developed an optimization algorithm that allowed for control of each pathway enzyme. With these additional degrees of freedom, the optimal regulation scheme showed the same trends that occur in natural systems – sequential expression of production pathways results in high productivity for relatively low protein demand (7).

1.1.2. Pathway-dependent dynamic control strategies

Natural just-in-time transcription mechanisms rely on metabolite sensing circuitry to convey information about the concentration of pathway molecules. Build-up of an intermediate could

result in up-regulation of downstream pathways genes and/or down-regulation of upstream pathway genes. Engineered regulatory circuits have adapted machinery from the endogenous circuits that actuate these responses to dynamically control metabolic fluxes at key reaction steps in a metabolite-responsive manner.

Farmer and Liao adapted a native *E. coli* promoter that turns on transcription in response to acetyl phosphate accumulation to divert pyruvate utilization from glycolysis to the lycopene production pathway. Since acetyl phosphate is a downstream metabolite of pyruvate, its accumulation indicates excess flux that can be diverted to the lycopene pathway. To realize this metabolic shift, they placed the genes *idi* and *pps* under control of the acetyl phosphate-responsive promoter. *idi* encodes the enzyme that converts acetyl phosphate to the first intermediate in the lycopene pathway and *pps* encodes the enzyme that converts acetyl phosphate to the upstream glycolytic intermediate, PEP. Application of this regulation scheme resulted in a greater-than 50% improvement in lycopene production compared to a control that constitutively expresses *idi* and *pps* (8).

As synthetic biology tools have advanced, recent studies have modified components of native systems to obtain more favorable response profiles. For example, Zhang et al. improved fatty acid ethyl ester (FAEE) production using fatty acid biosensor variants that contain hybrid promoters with different dynamic ranges. The control circuit contains a transcription factor, FadR, that represses expression from the fatty acid-responsive promoter in its unbound state and releases from the promoter upon binding to fatty acid. Based on previous work, they aimed to improve a FAEE producer strain through two pathways that are each subject to a major limitation. The first pathway converts pyruvate to FAEE through three enzymatic steps, that involves ethanol as a toxic intermediate. The second pathway converts acetyl-CoA to FAEE by overexpressing *tesA* to convert fatty acyl-ACP to free fatty acid which is converted fatty acyl-CoA by *fadD*. Regulation in this second pathway is required to prevent to overconsumption of fatty acids by the FadD-catalyzed reaction, which sequesters fatty acids from the endogenous cell membrane biosynthesis pathways. These challenges were addressed by controlling the entire ethanol-generating pathway genes along with *fadD* under the fatty acid-responsive promoter variants and screening for the top

combinations. Implementation of the regulation scheme resulted in a 3-fold improvement in FAEE yield compared to the uncontrolled strain (9).

To more precisely control flux at a key metabolic node, Xu et al. developed a sensor pair that can be used to control both generation and consumption reactions for improving fatty acid production. Their regulation system employs two promoters that exhibit opposite responses to changing malonyl-CoA levels. The first promoter, a hybrid derived from the T7 promoter, is repressed by the regulator protein, FapR, in the absence of malonyl-CoA and is de-repressed in its absence. The second promoter, a hybrid of the GAP promoter, is activated by unbound FapR such that transcription turns from ON to OFF in the presence of malonyl-CoA. Since malonyl-CoA is both an essential metabolite required for cell membrane biosynthesis and a product precursor, it is important to balance metabolism between cell growth and product formation. To achieve this balance, they controlled malonyl-CoA-producing genes under the promoter that turns OFF in the presence of malonyl-CoA and the fatty acid synthesis pathway that consumes malonyl-CoA under the promoter that turns ON in the presence of malonyl-CoA. Characterization of the malonyl-CoA profile under this regulation strategy revealed an oscillating pattern, indicative of switching between malonyl-CoA generation and fatty acid synthesis modes. Implementation of this regulation system led to a 2.1-fold improvement in fatty acid titer compared to the strain carrying the uncontrolled metabolic pathway (10).

While the studies above clearly demonstrate the functionality of biosensor-based control for addressing some metabolic engineering challenges, this approach is limited to contexts in which there is a biosensor for the relevant molecule. However, Dahl et al. showed that in the absence of a previously characterized biosensor system, whole genome transcript analysis can be used to mine for metabolite-responsive promoters. This study was interested in identifying a metabolite-responsive promoter to mitigate the growth effects due to accumulation of the intermediate, farnesyl pyrophosphate (FPP). To this end, the authors performed whole genome transcript analysis on their unregulated strain that accumulates FPP and identified a panel of genes which exhibited varying transcript levels throughout exponential and stationary phase. The FPP-producing and FPP-consuming pathway genes were placed under control of promoters that turn OFF and ON transcription in the presence of FPP, respectively. Implementation of this control

strategy and screening through different promoters led to identification of a top producer that improved amorphadiene production two-fold over that which employed inducible or constitutive promoters (11).

Even when there is a native control system that can be coopted for engineered regulation, each new biosensor must be tuned and characterized before application in a metabolic flux regulation context. This limitation motivated focus on the class of pathway-independent control methods discussed in the following section.

1.1.3. Pathway-independent control methods

While pathway-dependent regulation circuits respond to a change in the concentration of a relevant metabolite, pathway-independent methods respond to exogenous stimuli or conditions, such as cell-density or pH, that change in most fermentations. Early demonstrations of pathway-independent control used the former strategy whereas more recent studies have focused on autonomous methods. The most common inducible circuit is the one based on the *lac* operon in which a regulator protein, LacI, represses expression from a family of promoters that contain the *lacO* binding sequence. The repression is relieved when a lactose analog, β-D-1-thiogalactopyranoside (IPTG), binds to LacI, causing it to unbind from the promoter. Today, many production systems place heterologous pathway genes under control of IPTG-inducible promoters to delay induction until mid-exponential phase to mitigate growth effect due to protein burden. Of course, IPTG-inducible systems can be used to address other challenges as well. For example, Santos et al. overcame enzyme inhibition by an intermediate through delaying production of the inhibiting molecule (12).

Although all applications previously mentioned involve OFF-to-ON control of gene expression, there are many scenarios in which ON-to-OFF dynamic control of endogenous genes would benefit production. For example, in the case of a heterologous pathway that uses an endogenous precursor that is also an essential metabolite, knockout of the genes encoding the enzyme(s) that consumes the precursor is not feasible. Therefore, to accumulate the precursor, it would be desirable to switch from a growth phase, characterized by precursor utilization in endogenous pathways, to a

production phase, characterized by precursor utilization in the production pathway. Brockman and Prather demonstrated a method by which a chemically-induced control circuit can achieve such a regulation scheme. Their system was developed with the goal of improving the production of *myo*-inositol, which is derived from glucose-6-phosphate (G6P). They envisioned a regulation system that would begin with a growth phase during which G6P is consumed in glycolysis and a production phase during with G6P is consumed by the heterologous enzyme. To realize this regulation scheme, they controlled phosphofructokinase (Pfk) activity at the post-translational level using an anhydrotetracycline (aTc)-inducible circuit to trigger Pfk degradation. Implementation of this regulation system and identification of the optimal switching time resulted in a 2-fold increase in the yield and titer of *myo*-inositol (13).

While effective at a lab scale, controls circuits that are triggered by chemical inducer addition are not practical at an industrial scale due to the high cost of these inducers and transport limitations. Additionally, the responses from these circuits are inherently irreversible as inducer molecules are not consumed by design. With the aim of overcoming these limitations, Zhao et al. developed a light-inducible and a dark-inducible regulation circuit. Light-based control is interesting because light is relatively low-cost, levels can be controlled very precisely, and reversibly. To construct a transcriptional regulation circuit, they coopted components from the EL222 transcription system that involves a light-responsive transcription factor that binds to the P_{C120} promoter. They ported this system to *Saccharomyces cerevisiae* by expressing a fusion protein containing a light-responsive transcription factor domain and a yeast transcriptional activator domain and controlling expression of their target gene under the P_{C120} promoter. They additionally constructed a light-repressible gene circuit by inverting the responsive from the prior light-inducible circuit. By applying both modalities for switching between growth and production phases, they were able to achieve up to 8.5 g/L of isobutanol and 2.4 g/L of 2-methyl-1-butanol from glucose (14).

Recently, studies on pathway-independent control have focused on the development of autonomous systems, which do that require external stimuli. Microbial cells autonomously regulate gene expression in response to changing cell density using quorum sensing (QS) mechanisms. While QS systems employ diverse circuit components and molecular interactions, they all involve the production of a signaling molecule that exits the cell to trigger changes in gene

expression at a threshold concentration. Components from these QS circuits have been assembled in host organisms to control expression of target genes. Application of QS circuits for dynamically controlling metabolic fluxes in production systems has resulted in significant improvements in glucaric acid, shikimate, bisabolene, and isobutanol production (15–17). In these early demonstrations, QS circuits were used to increase availability of a key precursor(15, 16) and to delay expression of a heterologous pathway (17).

1.2. New strategies in metabolic engineering

With the rapid development of synthetic biology tools, it is possible to design, construct, and tune more complicated control circuits. This has led to the recent focus on "layered" autonomous strategies that use one or more stimuli to influence multiple metabolic fluxes (18–20). Advances in metabolic engineering tools have also led to an expansion in the set of molecules that can be produced through microbial synthesis, although these pathways may be complex and more burdensome to the cell. These trends have motivated recent interest in co-culturing as a method of distributing metabolic burden or segregating conflicting objectives between two or more strains (21–23). Additionally, researchers have implemented regulatory circuits to dynamically coordinate population behavior (24–30). Finally, the discovery of membrane-less organelles, or biomolecular condensates, that dynamically facilitate rapid reaction rates by clustering certain proteins and nucleic acids has inspired research into synthetic co-localization systems. These synthetic systems can be applied to clustering pathway enzymes to dynamically switch between metabolic branches (31).

1.2.1. Layered control methods

To address challenging pathways that require flux balancing at multiple nodes, recent studies have developed layered control methods capable of actuating metabolic flux changes at two or more nodes. For example, one layer can divert flux from endogenous pathways to heterologous pathways while a second delays expression of heterologous pathway genes to overcome enzyme instability (19), product inhibition (20), or growth burden (18, 20) (Figure 1-1A). These layered

approaches combine modules of the single-input control circuits (Figure 1-1B) and the choice of modules dictates the level of independent control the user has over the dynamics of each circuit. In this section, two illustrative examples of recent work on layered dynamic control are presented, highlighting the differences in tunability that result from the module choices.

Yang et al. developed bifunctional control circuit in which up- and down-regulation modes are fully coupled to overcome challenges in muconic acid production (Figure 1-1C) (18). To develop a sensor for muconic acid, they coopted components from the natural muconic acid response machinery in *Pseudomonas putida*. This systems uses CatR, a regulatory protein that binds to the muconic acid-responsive promoter (P_{MA}) and undergoes a conformation change in the presence of muconic acid such that transcription occurs in the presence of muconic acid (32). They envisioned using this sensor to construct a regulation system that would allow the cells to adapt to the fermentation environment before gradually turning ON the first two steps of the heterologous pathway and turning OFF carbon flux towards the TCA cycle. This regulation scheme was achieved by controlling certain pathway genes and anti-sense RNA for *ppc* down-regulation under the P_{MA} promoter. Implementation of the system showed that bifunctional regulation improves production over either up- or down-regulation mode alone.

A study by Doong et al. used two completely orthogonal regulation circuits (Figure 1-1D) to overcome limitations in the glucaric acid pathway (19). The first layer of regulation employs the quorum sensing (QS) circuit developed by Gupta et al. that turns off glycolytic flux to increase G6P availability for the heterologous glucaric acid pathway (15). To dynamically down-regulate glycolytic flux, they placed expression of degradation-tagged *pfk* under the P_{esaS} promoter, which turns from ON to OFF with increasing cell-density. The dynamics of this control layer are dictated by the rate of AHL accumulation, which is controlled by varying the expression level of the AHL synthase. The second layer of regulation addressed the instability of the heterologous pathway enzyme, MIOX, by coupling its expression to the concentration of its substrate, *myo*-inositol. This layer of regulation was realized using a *myo*-inositol biosensor composed of an IpsA transcription factor that represses expression from a hybrid promoter only in the absence of *myo*-inositol. Characterization of the circuit showed that the promoter's response curve can be controlled by varying the *ipsA* expression level. A combinatorial screen of the resulting glucaric acid producers

which turn OFF glycolysis and ON MIOX expression at varying times showed that the switching dynamics of both circuits are key parameters that drastically influence glucaric acid titers. Implementation of the *pfk* control layer only results in a greater than 4-fold titer increase and addition of the MIOX control layer led to an additional 2-fold increase.

These early applications of layered dynamic regulation have shown that control of two or more metabolic fluxes can result in significant production improvements by addressing two pathway limitations. These studies show two approaches for bifunctional regulation which primarily differ in the extent to which the two regulation modes are coupled. The study that employed an orthogonal control scheme showed that production is highly dependent on switching dynamics, confirming the importance of independent tunability. However, since there is a trade-off between simplicity and tunability, the combination of modules should be chosen to suit the application. For example, if the impact of one control node is not highly dependent on switching time, the fully coupled regulation scheme would perhaps provide the simplest circuit without sacrificing production.

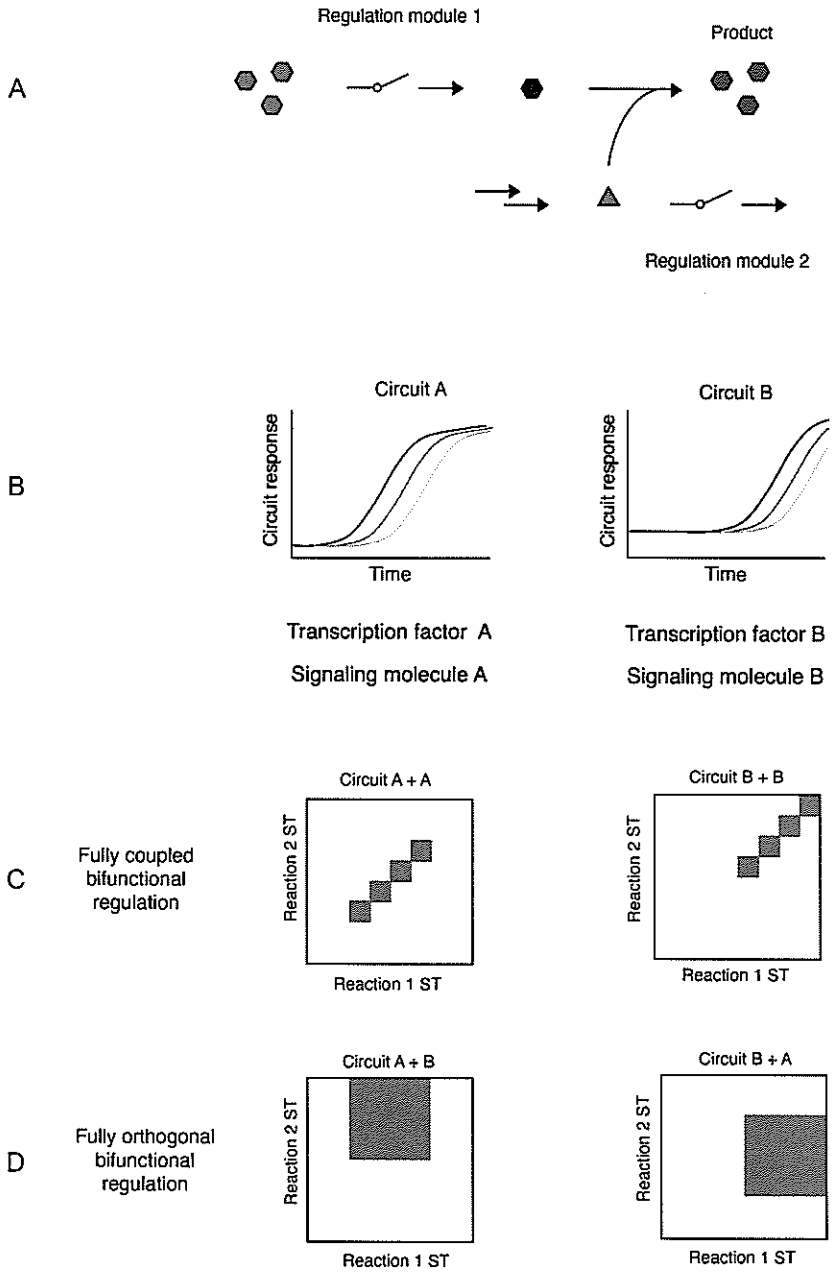

Figure 1-1. Illustration of layered control methods.
(**A**) Example of a regulation scheme that employs layered dynamic control. The first regulation module (green box) controls flux through the production pathway to delay intermediate and production formation. The second regulation module (red box) regulates consumption of a pathway precursor (triangle) by endogenous pathways. (**B**) Response curves for two different circuits – A and B. In each circuit the response curve shifts based on the expression level of the circuit components such as the transcription factor (or synthase for the signaling molecule in QS circuits). The two circuits respond to different transcription factors and signaling molecules. (**C**) Possible combinations of switching times (ST, shaded gray) with a fully coupled regulation system in which both modes are under control of the same circuit. (**D**) Possible combinations of switching times (ST) in a fully orthogonal bifunctional regulation system in which the two regulation modes are controlled under two different circuits.

1.2.2. Dynamic regulation in co-culture systems

The QS circuits discussed thus far have been contained within individual cells such that each cell both sends and receives signals to and from other population members. However, circuits can instead be designed to facilitate communication or behavior coordination between sub-populations of a co-culture. For example, one population could send signals (i.e. produce the signaling molecule) which would be received by the other population member that contains the rest of the QS circuit. This is the regulation scheme constructed in a study by Marchand and Collins in which they distributed components of the *agr* QS circuit between two strains of *Bacillus megaterium*. One strain was responsible for producing and processing the propeptide into a mature auto-inducing peptide (AIP), which was taken up by a second strain which contains the signal activator and response components. Characterization of the circuit showed that the AIP produced from one sub-population was able to induce GFP expression in a second sub-population (28).

While co-culturing is becoming an increasingly common production strategy for complex metabolic pathways, there have been few studies investigating methods for controlling the relative population sizes in a co-culture beyond the inoculum composition. Recently, two studies have applied QS and other circuits towards dynamically controlling the relative fitness of a co-culture sub-population. Kong et al. distributed different modules, or groups of genes, from the nisin and lactocaccin A biosynthesis pathways between two strains to engineer different interactions between the two strains. Nisin and lactocaccin A are both antimicrobials and the biosynthetic routes of both involve an antimicrobial production module, a translocation module, and an immunity module. Interactions between the two strains were then defined by the choice of modules present in each strain. For example, if one strain contains the entire nisin biosynthetic pathway, a second strain will survive only if it contains the nisin immunity module. By incorporating different circuit architectures, they were able to achieve interesting co-culture composition profiles in a qualitatively predictable manner (29). Rather than controlling microbial population dynamics through cell killing, Stephens et al. developed a composition control method based on a dynamic induction of a beneficial growth phenotype. Their system controls the growth rate of a receiver sub-population by controlling the expression of a gene that confers a growth benefit under a QS promoter. This strain could then be co-cultured with a sender strain which produces the signaling

molecule such that increasing the cell density of the sender strain leads to an increased growth rate of the receiver strain (30).

1.2.3. Enzyme clustering as a dynamic control method

The traditional metabolic engineering approach addresses bottlenecks in production pathways by increasing the expression level of the gene encoding the enzyme that catalyzes the limiting step (i.e. the target enzyme). However, this increase in expression level is dependent on sufficient cellular resources and may come at a cost to the growth rate. An alternative method for increasing the flux at this limiting node without increasing protein production cost, is co-localization of the target enzyme with the one immediately upstream. This strategy increases the local concentration of the substrate near the target enzyme to similarly accelerate the limiting reaction rate. Additionally, spatial control can be used to address other common metabolic engineering challenges such at toxic intermediates (33) or branched pathways (34–36). Previous strategies for co-localizing or compartmentalizing enzymes have employed synthetic scaffolds (37, 38), encapsulins (39), and localization to various membrane-bound organelles in eukaryotic hosts (40–42).

While studying the effect of enzyme clustering in a branched pathway, Castellana et al. observed that enzyme agglomeration to favor one branch can accelerate the consumption of certain intermediates such that cells can exhibit an auxotrophic phenotype for the down-stream metabolite of the excluded pathway. Their study sought to increase carbamoyl-phosphate utilization in the uracil pathway by clustering CarB, which is responsible for carbamoyl-phosphate production, with PyrB, which catalyzes the first step of the uracil-producing branch. This led to a lack of carbamoyl-phosphate availability for the arginine pathway, resulting in burdened growth in minimal medium, which could be restored by arginine supplementation (36). The findings from this study have motived the development of tools that enable dynamically controllable protein clustering to overcome growth limitation in the context of co-localization in branched pathways.

Phase transition has emerged as a wide-spread mechanism by which eukaryotic cells dynamically sequester biomolecules, facilitate certain reactions, and channel intracellular signaling. These clustering events are driven by intrinsically disordered regions (IDRs) in certain proteins which exhibit promiscuous interactions (i.e. electrostatic, dipole-dipole) between one another. IDRs are composed of sequences biased to R, G, S, and Y amino acids and these sequences alone are a sufficient driving force for condensation when present at a sufficient concentration (43–45). Previous studies have constructed synthetic systems that undergo clustering behavior by fusing an IDR domain to an oligomerizing protein. One such IDR domain that has been incorporated into synthetic clustering systems is the N-terminal of FUS, an RNA-binding protein involved in DNA repair, transcription, and pre-mRNA splicing. Shin et al. developed a light-induced clustering system by constructing a fusion protein that consists of a FUS domain and a Cry2 domain, where Cry2 is a light-sensitive protein that self-associates with light exposure (46).

Researchers have since applied this clustering mechanism to metabolic engineering applications. For example, Zhao et al. co-localized heterologous pathway enzymes to mitigate side-product formation in the deoxyviolacein pathway. The deoxyviolacein pathway contains a branchpoint at which the product of the VioE-catalyzed reaction can either be converted to deoxyviolacein by VioC or to prodeoxyviolacein non-enzymatically. With the goal of selectivity producing deoxyviolacein, they constructed two fusion proteins consisting of a light-sensitive oligomerizing domain, an N-terminal FUS domain, and an enzymatic domain, where the enzymatic domains in the two proteins are VioE and VioC. Induction of clustering in this system resulted in an 18.4-fold increase in ratio of the desired to undesired product, demonstrating that phase separation is a viable method of metabolic flux control (31).

1.3. Thesis objectives

As discussed in the previous section, a number of recent studies have developed and applied dynamic control circuits to manage conflicting cellular objectives such as growth and production. These studies have repeatedly confirmed the rationale for dynamic control by achieving significant production improvements. In the Prather lab, previous work has focused on pathway-independent

methods of metabolic flux control at the transcriptional and post-translational levels (13, 15, 19, 47), with the more recent studies focused on autonomous control strategies. Gupta et al. developed a QS circuit that was applied to dynamically down-regulating endogenous metabolic fluxes for precursor and product accumulation in the glucaric acid and shikimic acid pathways, respectively (15). Doong et al. developed a biosensor which responds to *myo*-inositol, a glucaric acid intermediate, with the aim of addressing another limiting step in the glucaric acid pathway (19). By layering the QS and myo-inositol-responsive biosensor to control metabolic fluxes at two nodes, they achieved significant improvements in glucaric acid titer over those from a single layer of control. Their study showed that the switching dynamics of both control layers were key parameters for obtaining efficient glucaric acid production. Motivated by these findings, the goal of this thesis was to develop a fully pathway-independent, tunable, and layered metabolic control circuit. QS circuits are attractive options for metabolic flux regulation due to the diversity in characterized QS circuits which may allow for orthogonal switching behavior of different nodes and the previous success in tuning the switching dynamics of these circuits. In addition to using QS promoters for direct transcriptional control, these circuits can drive expression of silencing systems such as CRISPRi components to expand their range of functions.

Beyond QS-based control at the transcriptional level, opportunities to apply QS circuits to regulating metabolic fluxes at the post-translational level were also explored. Protein degradation is an interesting option for controlling enzyme levels, allowing for a more rapid change in the target protein level. Brockman and Prather reported varying the degradation rates of target proteins by controlling the level of SspB, an adaptor protein that tethers target proteins to ClpXP (13, 48–50). Recently, protein clustering has emerged as an attractive method of regulating reaction rates and achieving very fast reaction kinetics (51–54). Natural and synthetic systems for clustering biomolecules employ proteins that contain an oligomerizing domain, which is responsible for co-localizing a disordered domain, which exhibit weak multivalent interactions with neighboring proteins (45, 55, 56). These systems facilitate the formation of biomolecular condensates upon oligomerization in response to the appropriate stimulus (31, 46).

In this context, the work presented in this dissertation aims to do the following:

1. Develop a bifunctional QS circuit by combining components for two different QS systems and characterize the impact of varying the expression level of circuit components on the switching dynamics of both regulation modes.

2. Apply the bifunctional QS circuit towards regulating metabolic fluxes in two different production pathways to overcome key production limitations.

3. Explore QS-based methods for metabolic flux control at the post-translational level and demonstrate how these tools can be promising alternative methods for improving microbial production.

1.4. Thesis organization

This thesis is organized into six chapters. Chapter 1 discusses the project motivation, provides background, and defines the scope of the project. Chapter 2 describes the construction and characterization of a bifunctional QS circuit that was used to overcome limitations in the naringenin and salicylic acid pathways. Chapter 3 discusses the development of a QS circuit that regulates at the post-translational level to control cellular growth rates. This circuit was applied towards regulating population dynamics in a co-culture to improve naringenin production. Chapter 4 describes the construction and initial characterization of a QS-based protein co-localization system. Chapter 5 discusses non-C6AHL QS circuits that were constructed and characterized and comments on the challenges of these circuits. Chapter 6 addresses the overall implications of the work and future directions for study.

2. Development of an autonomous and bifunctional quorum-sensing circuit for metabolic flux control

Abstract

Metabolic engineering seeks to reprogram microbial cells to efficiently and sustainably produce value-added compounds. Since chemical production can be at odds with the cell's natural objectives, strategies have been developed to balance conflicting goals. For example, dynamic regulation modulates gene expression to favor biomass and metabolite accumulation at low cell-densities before diverting key metabolic fluxes towards product formation. To trigger changes in gene expression in a pathway-independent manner without the need for exogenous inducers, researchers have coupled gene expression to quorum-sensing (QS) circuits, which regulate transcription based on cell-density. While effective, studies thus far have been limited to one control point. More challenging pathways may require layered dynamic regulation strategies, motivating the development of a generalizable tool for regulating multiple sets of genes. We have developed a QS-based regulation tool that combines components of the *lux* and *esa* QS systems to simultaneously and dynamically up- and down-regulate expression of two sets of genes. Characterization of the circuit revealed that varying the expression level of two QS components leads to predictable changes in switching dynamics and that using components from two QS systems allows for independent tuning capability. We applied the regulation tool to successfully address challenges in both the naringenin and salicylic acid synthesis pathways. Through these case studies, we confirmed the benefit of having multiple control points, predictable tuning capabilities, and independently tunable regulation modules.

This chapter contains material adapted from:

Dinh, C. V. & Prather, K. L. J. Development of an autonomous and bifunctional quorum-sensing circuit for metabolic flux control in engineered Escherichia coli. *Proc. Natl. Acad. Sci.* Accepted.

2.1. Introduction

Successful dynamic flux regulation strategies have been experimentally demonstrated in a number of production pathways by controlling activity of key pathway enzymes at the transcriptional or post-translational level. Many recent studies have focused on self-actuating dynamic control methods to minimize required human supervision and to avoid use of exogenous inducers, which can be costly. These control systems couple expression of pathway genes, anti-sense RNA, CRISPRi components, or proteases to relevant conditions such as external signals (57), internal cell state (metabolites, growth state, stress state) (8–11, 18, 19, 58–60), cell-density (15, 16, 61), glucose concentration (62, 63), or a combination of these (64–66). Control systems which respond to pathway-independent signals such as cell-density or O_2 level offer the additional advantage of applicability across different synthesis pathways without development of a new sensor for the relevant metabolite in each pathway. However, to our knowledge, there has not yet been a fully pathway-independent dynamic control system for independently regulating multiple metabolic fluxes, which may be required for efficient production of more challenging pathways.

With the goal of developing such a control system, we constructed a circuit containing genetic components from the *lux* and *esaR* QS systems. This system contains two constitutively expressed genes for the regulator proteins, LuxR and EsaR, which activate and repress the P_{lux} and P_{esaR} promoters, respectively, upon binding. The binding affinity between the regulators and their cognate promoters depends on the level of a common signaling molecule, 3-oxohexanoyl homoserine lactone (AHL) and thus, we can dynamically regulate the transcription level of the promoters in a cell-density dependent manner by constitutively expressing the gene encoding the AHL synthase, *esaI*. To ensure this system can be used to explore a broad metabolic control space, we varied the *luxR* and *esaI* expression levels to obtain a range of switching dynamics. The engineered regulatory circuits were applied towards controlling metabolic fluxes in two different synthesis pathways with unique trade-offs and metabolic control points. The significant improvement in product titers upon implementation of the control system in both case studies demonstrates the effectiveness of the control circuit for balancing multiple design objectives in synthesis pathways.

2.2. Materials and Methods

All strains and plasmids used in this study are summarized in Table 2-1 and Table 2-2, respectively. Promoter and RBS sequences are included in Appendix Table 1 and primer sequences are included in Appendix Table 2. For plasmid construction and gene/genome editing, cells were cultured in Luria-Bertani (LB) broth at either 30 °C or 37 °C. Temperature-sensitive plasmids were cured at 42 °C.

Table 2-1. All strains and corresponding genotypes relevant in Chapter 2.

The generalized denotation and genotype of strains used in fluorescence characterization, containing esaI and luxR expression cassettes with different promoter and or RBS sequences, is given as "LXX" for esaI.

Strain	Genotype	Description
BL21-LXX	BL21(DE3) *186(O)::apFABXX-apFABXX-esaI*	BL21(DE3) + *esaI* driven by a specific promoter and RBS, generalized as LXX here (Supplemental Table 3)
NST74	*aroH367, tyrR366, tna-2, lacY5, aroF394^{fbr}, -malT384, pheA101^{fbr}, pheO352, aroG397^{fbr}*	Tribe (1987)(67)
NST74-LXX	*aroH367, tyrR366, tna-2, lacY5, aroF394^{fbr}, -malT384, pheA101^{fbr}, pheO352, aroG397^{fbr} 186(O)::apFABXX-apFABXX-esaI*	NST74 + *esaI* driven by a specific promoter and RBS, generalized as LXX here (Supplemental Table 3)

Table 2-2. Summary of plasmids used in Chapter 2.

Plasmid	Functional Genotype	Source
pCOLA- P_{lux}-*mCherry*	mCherry under the P_{lux} promoter in the pCOLA DUET vector	This study
pCOLA-P_{esaR-H}-*mCherry*	mCherry under the Ptrc promoter with the *esaO* binding sequence in place of the *lacO* sequence and *esaR* under the apFAB104 promoter	This study
pCOLA-P_{esaR-H}-*TAL-4CL*	*TAL* (*Rhodotorula glutinis*) and *4CL* (*Petroselinum crispum*) under P_{esaR-H} promoters and *esaR* under the apFAB104 promoter	This study
pCOLA-P_{lux}-*TAL-4CL*	*TAL* (*Rhodotorula glutinis*) and *4CL* (*Petroselinum crispum*) under P_{lux} promoters	This study
pET-P_{T7}-*CHS-CHI*	*CHS* (*Petunia hybrida*) and *CHI* (*Medicago sativa*) under T7 promoters	This study
pACYC-P_{con10}-RBSX-luxR	*luxR* under control of a constitutive Anderson library promoter (Supplementary Table 3)	This study
pACYC-P_{lux}- *dCas9*-P_{con10} - RBSX-*luxR*	*dCas9* under the P_{lux} promoter and *luxR* under control of a constitutive Anderson library promoter (Supplementary Table 3)	This study
pCDF-P_{lux}-*sgRNA*	*sgRNA(s)* under the P_{lux} promoter	This study
pCOLA-*fapR*	*fapR* under the T7 promoter	Modified from Xu et al. (2014)(10)
pETM6-*fapO-eGFP*	eGFP expression controlled by bound state of the FapR binding sequence, *fapO*	Xu et al. (2014) (10)
pCOLA-P_{esaR}-*entC-pchB*	*entC* (*Escherichia coli*) and *pchB* (*Pseudomonas aeruginosa*) under P_{esaR-H} promoters and *esaR* under the apFAB104 promoter	This study
pOSIP-KO	Vector for integration into the 186 locus	St. Pierre (2013)(68)
pTet-FLP	*FLP* recombinase expression under the Tet promoter	Modified from St. Pierre (2013)(68)
pTrc-*GFP-LVA*	Degradation tagged GFP under the P_{trc} promoter	Brockman (2015)(69)

2.2.1. Strain construction

Synthase expression library integrations

The *esaI* expression cassette was integrated into the genome under the control of several different constitutive synthetic promoters (denoted BL2-LXX or NST74-LXX)(15). Integration was performed via "clonetegration" (68). The desired EsaI expression cassette was inserted into the pOSIP-KO backbone using restriction digestion and ligation. The ligation product was used to transform *E. coli* strain BL21(DE3) or NST74 for integration into the 186 locus. The phage integration genes and antibiotic resistance cassette were cured by transforming with a plasmid containing FLP under control of the P_{tet} promoter (pTet-FLP), yielding strains BL21-LXX or NST-LXX.

Fluorescence characterization of QS circuits

The P_{lux} promoter was amplified from pSB1A2-P_{lux}-*GFP*(70) using primers CD_211 and CD_212, *mCherry* was amplified from pFM301 (p15A ori, kanamycin resistance, mCherry-BBa_J06504 under constitutive promoter BBa_J23101) using primers CD_213 and CD_214, and the two products were joined using splicing by overlap extension PCR to yield P_{lux}-*mCherry*. This cassette was inserted into a modified pCOLA backbone without the T7 system components using restriction digestion and ligation to yield pCOLA-P_{lux}-*mCherry*. The P_{con10}-*luxR* cassette was amplified from pSB1A2-P_{lux}-*GFP*-P_{con10}-*luxR* (70) using primers CD_215 and CD_216 and inserted into the pACYC backbone using restriction digestion and ligation to yield pACYC-P_{con10}-*luxR*. The strength of the RBS driving *luxR* was decreased using primers lux_R1_a and luxR_R1_b and increased using primers luxR_R3_a, luxR_R3_b, luxR_R4_a, and luxR_R4_b, through Golden Gate cloning.

The P_{trc} promoter was amplified from the pTrc99A vector with the *esaO* operator sequence in place of the *lacO* sequence to yield the P_{trc}-*esaO* fragment ($P_{esaR\text{-}H}$) using primers esa_RFP_5 and esa_RFP_6. *mCherry* was amplified from pFM301 using esa_RFP_7 and esa_RFP8, *esaR* from a constitutive BIOFAB library promoter was amplified from pSB3K3-P_{esaR}-*GFP*-P_{con}-*esaR*(71) using esa_RFP_3 and esa_RFP_4, and the pCOLA backbone was amplified using esa_RFP_1 and

esa_RFP_2. These PCR products were assembled into the vector pCOLA-$P_{esaR\text{-}H}$-*mCherry* using Golden Gate cloning.

A custom synthesized gene fragment which contains BsaI restriction sites followed by the *sgRNA* scaffold sequence, flanked on both sides with bi-directional terminator B0015 (Genscript, New Jersey, USA), was amplified using primers sg_3 and sg_10. The pCDF backbone was amplified using primer sg_1 and sg_2. These two PCR products were combined to make pCDF-BsaI-BsaI-*sgRNA* using Golden Gate cloning. The 20-bp guide sequence targeting GFPmut3b was appended to P_{lux} using overhang PCR using the template pSB1A2-P_{lux}-*GFP* and primers A11 and A12 and inserted into pCDF-BsaI-BsaI-*sgRNA* using Golden Gate cloning to yield pCDF-P_{lux}-*sgGFP*.

dCas9 was amplified from pdCas9(72) with SapI sites preceding the gene using primers C9_1 and C9_2 and inserted into the pACYC backbone using restriction digestion and ligation to yield pACYC-SapI-SapI-*dCas9*. The P_{lux} promoter was PCR amplified from pSB1A2-P_{lux}-*GFP*(73) using primers A15 and A16, which add flanking SapI sites, and inserted into pACYC-SapI-SapI-dCas9 using Golden Gate cloning to yield pACYC-P_{lux}-*dCas9*. The RBS variants of the *luxR* cassette were amplified using C9_lux_3 and C9_lux_4 and the pACYC-P_{lux}-*dCas9* plasmid was amplified using C9_lux_1 and C9_lux_2. The resulting products were assembled using Golden Gate cloning to yield pACYC-P_{lux}-*dCas9*-P_{con}-RBSX-*luxR*.

Malonyl-CoA biosensor

The *lacI*-P_{T7}-*fapR* cassette was amplified from the pCDM4-*fapR* plasmid using primers fapR_3 and fapR_4 and the pCOLA backbone was amplified using fapR_1 and fapR_2 (74). The two products were assembled using Golden Gate cloning to yield pCOLA-*fapR*. This modification was to maintain origin of replication compatibility only.

Naringenin pathway

For QS-based transcriptional control of *TAL* and *4CL*, codon optimized sequences of each gene appended to P_{lux} were inserted into pCOLA using restriction digestion and ligation to yield pCOLA-P_{lux}-*TAL-4CL_v1* (Genscript, New Jersey, USA). The final pCOLA-P_{lux}-*TAL-4CL*

plasmid used in this study was obtained using primers T4_R20_(1-8) using Golden Gate cloning. This modification was carried out to take out the T7 system components from the backbone and to increase the strength of the RBS's driving *TAL* and *4CL* expression. Codon optimized sequences of *CHS* and *CHI* (Genscript, New Jersey, USA) were PCR amplified using primers CHS_T7F2 and CHS_T7R2 for *CHS* and CHI_T7F2 and CHI_T7R2 for *CHI*. Products were digested and ligated into MCS1 and MCS2 of the pET-duet vector to yield pET-*CHS-CHI*.

Dynamic control of ICS and IPL in the salicylic acid pathway

For QS-based transcriptional control of the genes encoding isochorismate synthase (Ics) and isochorismate pyruvate lyase (Ipl), the pCOLA backbone was amplified using EP_1 and EP_2, *esaR* was amplified from pSB3K3-P_{esaR}-GFP-p104-esaR using EP_3 and EP_4, $P_{esaR\text{-}H}$ was amplified from pCOLA-$P_{esaR\text{-}H}$-mCherry using EP_5 and EP_6 along with EP_9 and EP_10, *entC* (encoding Ics) was amplified from the *E. coli* genome using EP_7 and EP_8, and *pchB* (encoding Ipl) was amplified from the *Pseudomonas aeruginosa* genome using EP_11 and EP_12. The PCR products were assembled into the vector pCOLA-$P_{esaR\text{-}H}$-*entC-pchB* using Golden Gate cloning.

CRISPRi-mediated control of endogenous enzymes

For QS-based silencing of endogenous genes, the 20-bp guide sequence was changed from pCDF-P_{lux}-*sgGFP* by circular polymerase extension cloning using primers [gene name]_luxR_F, [gene name]_luxR_R, sg_CPEC_1 and sg_CPEC_2. The 20-bp guide sequences were obtained from either previous studies (75) or using predictions from ATUM's sgRNA design tool (www.atum.bio). To produce vectors which express multiple guides under the control of individual promoters, the pCDF-P_{lux}-*sgRNA* vectors which express a single guide RNA were used as templates in Golden Gate cloning using primer sg_(1-10).

2.2.2. Culturing and fermentations

Fluorescence characterization

Switching dynamics over varying expression levels of QS circuit components (*esaI* and *luxR*) were quantified using the BioLector microbioreactor system (m2p-labs, Baesweiler, Germany). Individual colonies were inoculated in LB medium and grown overnight at 30 °C. 1 mL cultures were inoculated from these seeds at OD_{600} 0.05 into BioLector 48-well flower plates and incubated at 30 °C, 1200 rpm (3 mm orbit), and 80% relative humidity. The plate was sealed with a gas-permeable sealing foil (m2p-labs). Cultures were monitored for OD (BioLector units), GFP, and RFP fluorescence over time.

Fermentations

Naringenin production trials were performed in glass vials with 5 mL working volume at 30 C and 80% humidity with 250 rpm shaking in modified MOPS minimal medium containing 5 g/L D-glucose, 500 mg/L tyrosine, 4 g/L NH_4Cl, 1 g/L K_2HPO_4, 2 mM $MgSO_4$, 0.1 mM $CaCl_2$, 40 mM MOPS, 4 mM Tricine, 50 mM NaCl, 100 mM Bis-Tris, 143 uM EDTA, 31 uM $FeCl_3$, 6.2 uM $ZnCl_3$, 0.76 uM $CuCl_2$. 0.42 uM $CoCl_2$, 1.62 uM H_3BO_3 and 0.081 uM $MnCl_2$. For strains containing plasmids with pET, pCOLA, pACYC, and pCDF vector backbones, the medium was also supplemented with 100 μg/mL carbenicillin, 50 μg/mL kanamycin, 34 μg/mL chloramphenicol, and 100 μg/mL spectinomycin, respectively, for plasmid maintenance. Strains were initially grown in 3 mL of LB medium at 30 °C overnight, then diluted 1:100 into 3-mL seed cultures of modified MOPS medium for ~24 h at 30 °C. These were used to inoculate working cultures at OD_{600} 0.05. Samples were taken periodically for quantification of cell density and extracellular metabolites. Fermentations were carried out for 48 hours.

For naringenin bioreactor production trials, colonies were inoculated into 50-mL seed cultures in 250-mL baffled shake flasks and incubated at 30 °C, 250 rpm, 8% humidity for ~16 h. Seed cultures were then sued to inoculate a 3-L Labfors bioreactor (Infors AG, Bottmingen, Switzerland; 1 L working volume) at OD_{600} 0.05. The pH was controlled at 7 using 4 M NaOH.

DO was controlled at 35% of maximum saturation by agitation rate (250-1000 rpm) and constant air sparging at 1 L per minute. Batch fermentation was carried out for 48 h, with 5-mL samples removed at 18, 24, and 48 h for optical density and titer measurements.

Salicylic acid production trials were performed in BioLector 48-well flower plates (m2p-labs, Baesweiler, Germany) with 1 mL working volume and 37 °C and 80% humidity with 900 rpm shaking in M9 minimal medium containing 10 g glycerol, 2.5 g glucose, 6g Na_2HPO_4, 0.5 g NaCl, 3 g KH_2PO_4, 1 g NH_4Cl, 245 mg $MgSO_4 \cdot 7H_2O$, 14.7 mg $CaCl_2 \cdot 2H_2O$, 2 g MOPS, and micronutrients including 2.0 mg vitamin B1, 1.25 mg H_3BO_3, 0.15 mg $NaMoO_4 \cdot 2H_2O$, 0.7 mg $CoCl_2 \cdot 2H_2O$, 0.25 mg $CuSO_4 \cdot 5H_2O$, 1.6 mg $MnCl_2 \cdot 4H_2O$, and 0.3 mg $ZnSO_4 \cdot 7H_2O$ per liter. For strains containing plasmids with pCOLA, pACYC, and pCDF vector backbones, the medium was supplemented with 50 μg/mL kanamycin, 34 μg/mL chloramphenicol, and 100 μg/mL spectinomycin, respectively, for plasmid maintenance. Strains were initially grown in 1 mL of M9 medium at 37 °C overnight and these cultures were used to inoculate working cultures at OD_{600} 0.05. Samples were taken periodically for quantification of cell density and extracellular metabolites. Fermentations were carried out for 24 hours.

2.2.3. Quantification of metabolites

Tyrosine, *p*-coumaric acid, naringenin, and salicylic acid were quantified by high performance liquid chromatography (HPLC) on an Agilent 1100 series instrument (Santa Clara, CA) with a ZORBAX Eclipse column (4.6 mm x 150 m x 3.5 um). The HPLC was run with a mixture of solution A (water + 0.1% TFA) and solution B (acetonitrile + 0.1% TFA) as the eluent at a flow rate of 1 mL/min. The following gradient was used: at 0 min, 90% solution A and 10% solution B, by 10 mins, 60% solution A and 40% solution B, by 15 mins, 40% solution A and 60% solution B, by 15.5 mins, 0 % solution A and 100% solution B, 15.5 – 21 min, 0 % solution A and 100 % solution B, by 21.5 min, 90% solution A and 10% solution B, 21.5 – 28 min, 90% solution A and 10% solution B. Compounds were quantified with 10 μL injections using diode-array detection at 270 nm (tyrosine) or 290 nm (*p*-coumaric acid, naringenin, and salicylic acid).

2.3. Results

2.3.1. Characterization of QS-based autonomous induction

We characterized two QS circuits for autonomous and dynamic gene expression control. The first QS circuit uses the transcriptional regulator LuxR, which forms a complex with AHL to activate transcription from the P_{lux} promoter (Figure 2-1A). For the second QS circuit, we constructed a hybrid promoter ($P_{esaR\text{-}H}$) that contains an EsaR binding site (*esaO*) downstream of the transcription start site of the P_{trc} promoter. In the absence of AHL, EsaR binds to the *esaO* sequence, repressing transcription from $P_{esaR\text{-}H}$. Upon binding to AHL, EsaR can no longer bind to the operator sequence, leading to de-repression (Figure 2-1B). Each circuit can be used to dynamically upregulate the expression of any gene of interest by placing the gene downstream of the P_{lux} or $P_{esaR\text{-}H}$ promoters.

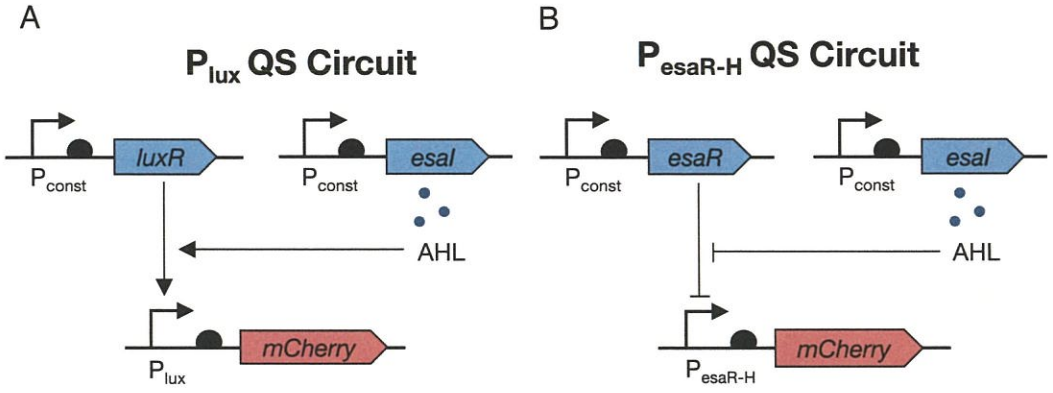

Figure 2-1. Architecture of the P_{lux} (**A**) and $P_{esaR\text{-}H}$ (**B**) QS circuits.

Transcription is activated from the P_{lux} promoter when AHL-bound LuxR binds to the promoter. EsaR binds to the $P_{esaR\text{-}H}$ promoter to block transcription, and this repression is relieved in the presence of AHL. Here, the arrow and ball represent the promoter and RBS, respectively.

Gupta et al. showed that the rate of AHL accumulation can be controlled by varying the constitutive expression level of the gene for the AHL synthase, *esaI* (15). By changing the AHL accumulation rate, we can tune the switching dynamics of these circuits. When applied to regulating enzyme expression, this tunability corresponds with the ability to vary the schedule of metabolic flux regulation in search of one that suits the desired application. To characterize relative switching dynamics from the P_{lux} and $P_{esaR\text{-}H}$ promoters, *esaI* was integrated into BL21(DE3) under

a library of promoter and RBS variants to make the BL21-LXX strain series. A P_{lux} or P_{esaR-H} promoter driving *mCherry* expression on a medium-copy plasmid (pCOLA-P_{lux}-*mCherry* or pCOLA-P_{esaR-H}-*mCherry*) was introduced into the BL21-LXX strain series. Strains testing the P_{lux} promoter required an additional plasmid with the *luxR* gene constitutively expressed from an Anderson library promoter (BBa_J23114) and varying RBS's on a low-copy plasmid (pACYC-P_{con}-RBSX-*luxR*). The pCOLA-P_{esaR-H}-*mCherry* vector contains *esaR* constitutively expressed from a BIOFAB library promoter (apFAB104).

Continuous fluorescence measurements of these strains produced a range of switching times in the up-regulation mode. In general, increasing the *esaI* expression level leads to earlier switching with both promoters (Figure 2-2A) and increasing the *luxR* expression level results in earlier switching from the P_{lux} promoter only (Figure 2-2B). These trends are consistent with expectations based on our understanding of the interactions in the QS circuits Figure 2-2C).

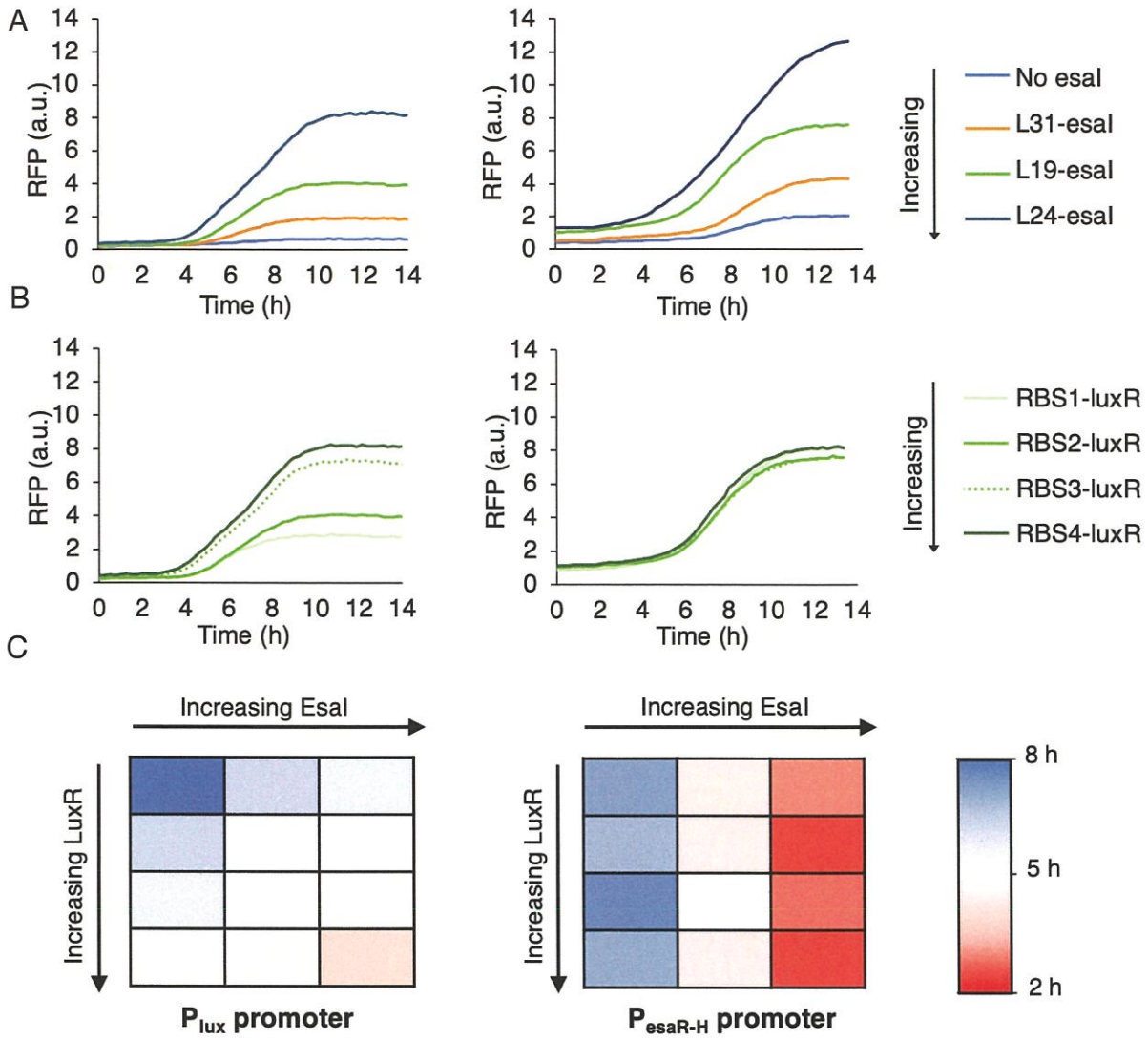

Figure 2-2. Characterization of *lux* and *esaR* quorum-sensing (QS) circuits.
(**A**) Representative fluorescence curves showing the response of P_{lux} (left) and $P_{esaR\text{-}H}$ (right) to varying esaI expression levels. Increasing esaI expression levels results in earlier switching from both promoters. (**B**) Representative fluorescence curves showing the response of P_{lux} (left) and $P_{esaR\text{-}H}$ (right) to varying luxR expression level. Increasing luxR expression results in earlier switching from the P_{lux} promoter only. (**C**) Summary of the trends in switching time from the P_{lux} and $P_{esaR\text{-}H}$ promoters varying luxR and esaI expression. Switching time was defined as the time at which fluorescence signal first surpasses a value equal to 90% of the maximum signal from the latest switcher (i.e. the lowest signal).

2.3.2. Dynamic gene regulation to control flux through the naringenin pathway

Naringenin is a natural plant-produced compound that is a common precursor of most flavonoids, natural plant products with a number of desirable therapeutic characteristics including anti-cancer and antiviral activity (76–78). One naringenin production pathway uses four enzymatic reactions to convert L-tyrosine and malonyl-CoA to (2S)-naringenin (Figure 2-3). This pathway has been widely studied in *E. coli* as a model system with relatively well-characterized challenges that may be addressed through dynamic control (12, 75, 79–81). For this reason, we applied our regulation system towards alleviating the limitations of the naringenin pathway.

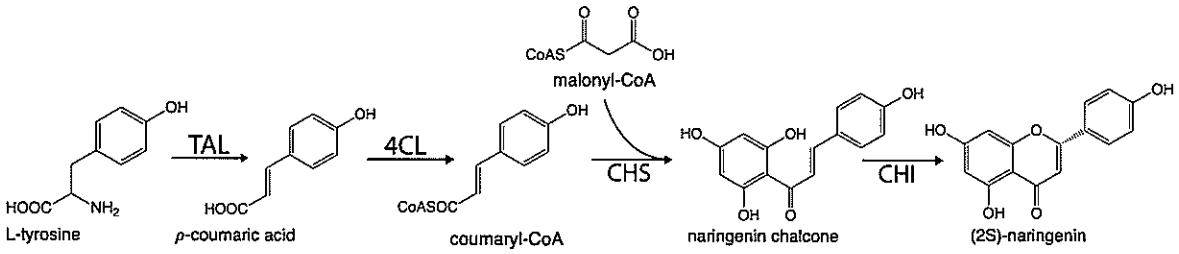

Figure 2-3. The naringenin pathway.

The naringenin pathway uses four heterologous enzymes - tyrosine ammonia lyase (TAL), 4-coumaryl-CoA ligase (4CL), chalcone synthase (CHS), and chalcone isomerase (CHI) - to convert L-tyrosine and malonyl-CoA to (2S)-naringenin. Each mole of naringenin requires one mole of L-tyrosine and three moles of malonyl-CoA.

Results from previous studies suggest that efficient naringenin production relies on maintaining high levels of chalcone synthase (CHS) and chalcone isomerase (CHI) relative to tyrosine ammonia lyase (TAL) and 4-coumaryl-CoA ligase (4CL), possibly due to an inhibitory interaction of coumaryl-CoA against TAL(12). This balance can be reached by delaying expression of *TAL* and *4CL*, while constitutively expressing *CHS* and *CHI*(12). To confirm that QS-based regulation can achieve this balancing effect, *TAL* and *4CL* were expressed from P_{lux} or $P_{esaR\text{-}H}$ promoters (pCOLA-P_{lux}-*TAL- 4CL* or pCOLA-$P_{esaR\text{-}H}$-*TAL- 4CL*) while *CHI* and *CHS* were each expressed from T7 promoters (pET-*CHI-CHS*), with IPTG added at inoculation. These plasmids, along with one that constitutively expresses *luxR* (pACYC-P_{con}-RBSX-*luxR*), were transformed into the BL21-LXX strain series to produce a set of strains that dynamically up-regulate *TAL* and *4CL* expression at varying cell densities.

Comparison of naringenin titers from dynamically and statically controlled strains confirmed that the naringenin pathway benefits from dynamic regulation of *TAL* and *4CL* expression under both the P_{lux} and $P_{esaR\text{-}H}$ promoters (Figure 2-4). With *TAL* and *4CL* expression under the P_{lux} promoter, static expression strains (i.e., with exogenous AHL added at inoculation) produced less than 10 μM naringenin, significantly less than the 204 ± 5 μM naringenin produced from the top strain with autonomous dynamic *TAL* and *4CL* regulation. Similarly, static *TAL* and *4CL* expression controlled from $P_{esaR\text{-}H}$ promoters produced less than 30 μM naringenin, also significantly less than the 196 ± 2 μM produced from the top autonomous dynamic strain. In both the P_{lux}- and $P_{esaR\text{-}H}$-controlled systems, an intermediate *esaI* expression level resulted in the maximum naringenin titer. This trend agrees with our current understanding of the pathway as early-switching strains might be subject to TAL inhibition and late-switching strains might be limited by low pathway fluxes. At the intermediate *esaI* level, naringenin titers from both QS circuits matched or exceeded those obtained with exogenous AHL addition, suggesting that the autonomous switching strategy can successfully replace exogenous inducer addition in this context.

Previous studies have suggested that naringenin production in *E. coli* is additionally limited by low endogenous malonyl-CoA levels (12, 75, 81). To confirm that this limitation exists in our system, all strains were cultured with and without cerulenin, an inhibitor of fatty acid synthesis that is known to elevate malonyl-CoA levels (82). Naringenin titers improved in all strains when cultured with cerulenin as expected, confirming that malonyl-CoA pools are limiting (Figure 2-4). In an effort to improve the naringenin titers using the P_{lux}-control system to match the top titer using the P_{esaR}-control system, we explored additional P_{lux} switching dynamics by testing additional *esaI* and *luxR* expression levels. However, none resulted in improved naringenin titers (Figure 2-5) and therefore, we decided to further build upon the regulation scheme with the $P_{esaR\text{-}H}$ promoter controlling *TAL* and *4CL* expression.

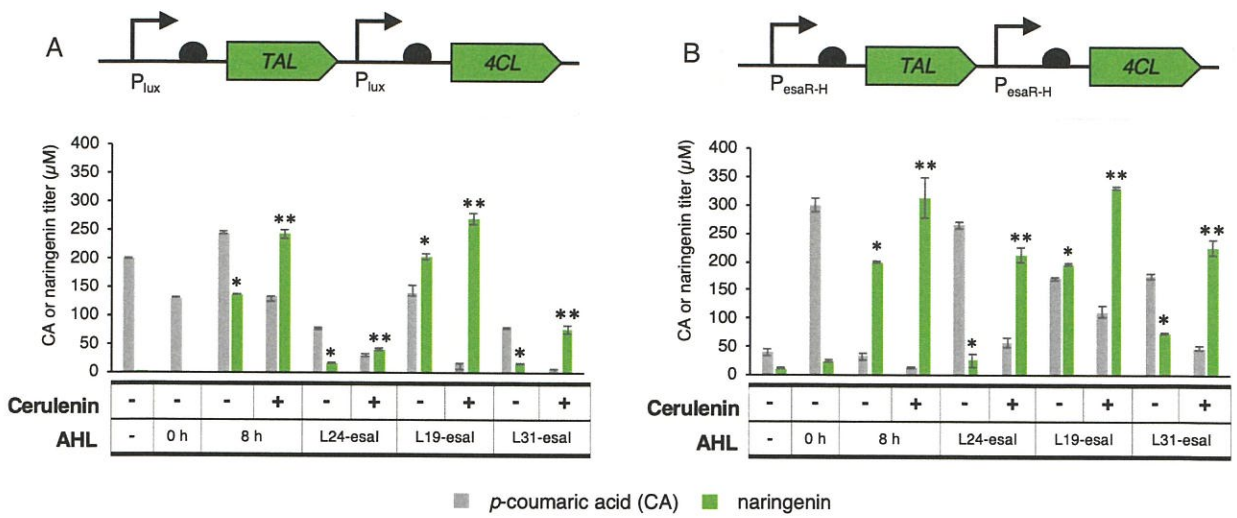

Figure 2-4. Preliminary characterization of the naringenin pathway

(**A**) *p*-Coumaric acid and naringenin titers with TAL and 4CL expression controlled under the P_{lux} promoter. Static expression of TAL and 4CL at the leaky expression level (AHL (-)) or at the fully induced expression level (AHL-0 h) results in low naringenin titers. Exogenous induction of TAL and 4CL expression during mid-exponential phase (AHL 8 h) improves naringenin titers more than 6-fold; EsaI-mediated induction is able to match that improvement. Addition of cerulenin to increase malonyl-CoA pools results in increased naringenin titers and a decrease in p-coumaric acid titers in all dynamic strains. (**B**) *p*-Coumaric acid and naringenin titers with TAL and 4CL expression controlled under the $P_{esaR\text{-}H}$ promoter. In general, all major trends follow those observed with TAL and 4CL under P_{lux} control. Error bars represent s.d. of triplicate trials. *P < 0.01 compared to static controls by two-tailed t test. **P < 0.01 compared to no cerulenin sample at same EsaI level by two-tailed t test.

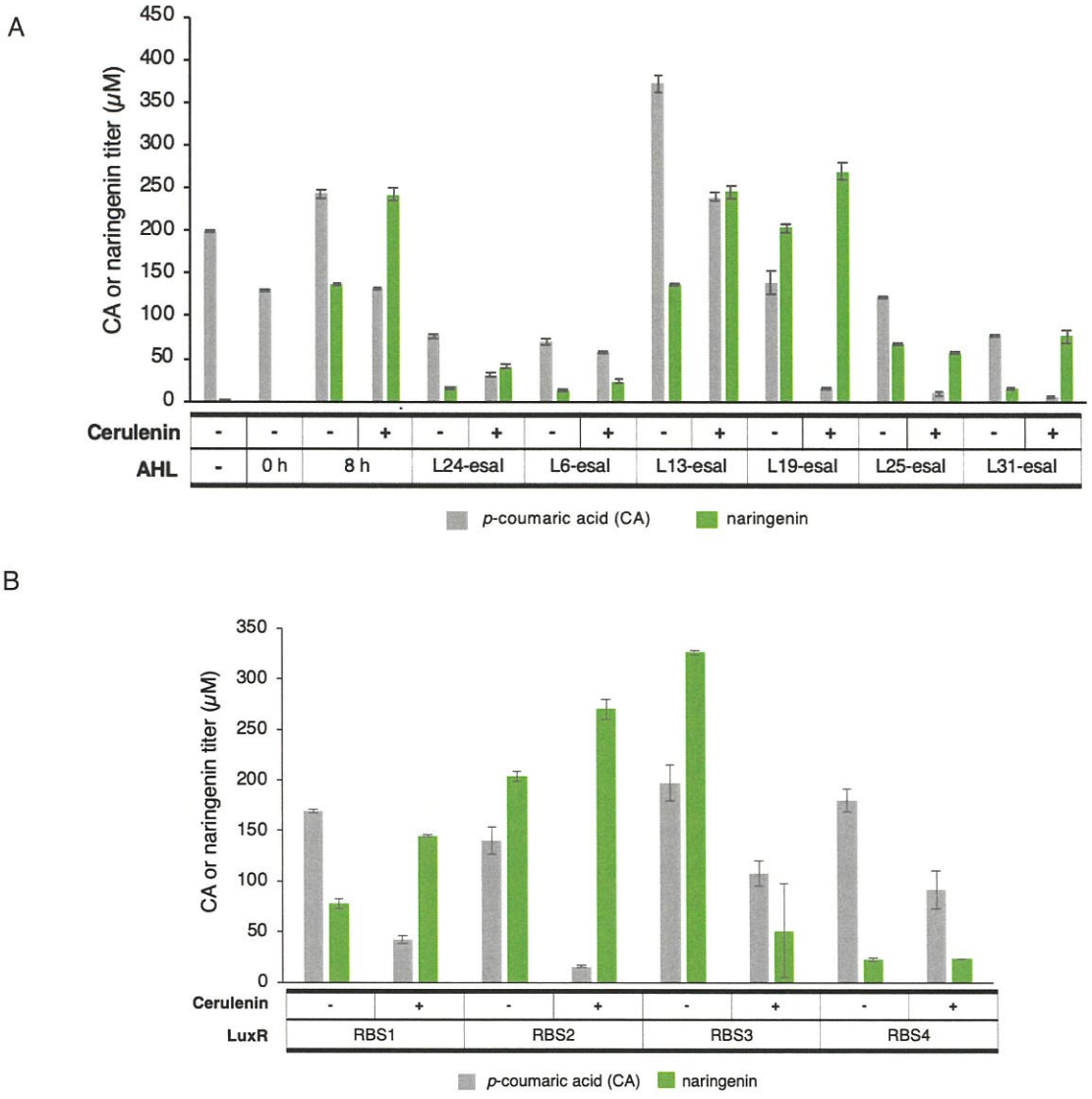

Figure 2-5. Additional screening of the P_{lux}-controlled naringenin pathway

(**A**) *p*-Coumaric acid and naringenin titers with varying EsaI levels with and without added cerulenin. Three additional esaI expression levels were tested (L6, L13, and L25) and the predicted expression levels are arranged in decreasing order from left to right. All three resulted in lower naringenin titers compared to the L19-esaI level. Error bars represent s. d. from triplicate trials. (**B**) *p*-Coumaric acid and naringenin titers at a constant EsaI and varying LuxR expression levels. The RBS number on the x-axis refers to the strength of the RBS driving luxR expression, increasing from 1 to 4. RBS2 was the one previously used when varying esaI expression. RBS3 results in the highest naringenin titers without cerulenin addition, but growth is severely burdened when grown with cerulenin. RBS1 and RBS4 result in relatively low naringenin titers. Error bars represent s. d. from triplicate trials.

2.3.3. Dynamic down-regulation of endogenous genes

While effective, cerulenin is not a cost-efficient solution for increasing malonyl-CoA pools and thus, we aimed to dynamically silence gene expression by using the P_{lux} promoter to drive expression of *dCas9* and guide RNA(s) (*sgRNA*) targeted towards dynamically down-regulating the gene(s) of interest. To characterize the down-regulation behavior, two P_{lux} promoters driving *dCas9* and *sgGFP* expression on low- and medium-copy plasmids, respectively (pACYC-P_{lux}-*dCas9*-P_{con10}-*luxR* and pCDF-P_{lux}-*sgGFP*), were introduced into the BL21-LXX strain series along with a plasmid that expresses degradation-tagged GFP (pTrc-*GFP-LVA*) (Figure 2-6A). In general, silencing dynamics from the P_{lux} promoter follow the expected trends based on the previous characterization of the *lux* circuit. That is, increasing *esaI* or *luxR* expression level leads to earlier *dCas9* and *sgRNA* expression and earlier down-regulation of the GFP signal (Figure 2-6B-C).

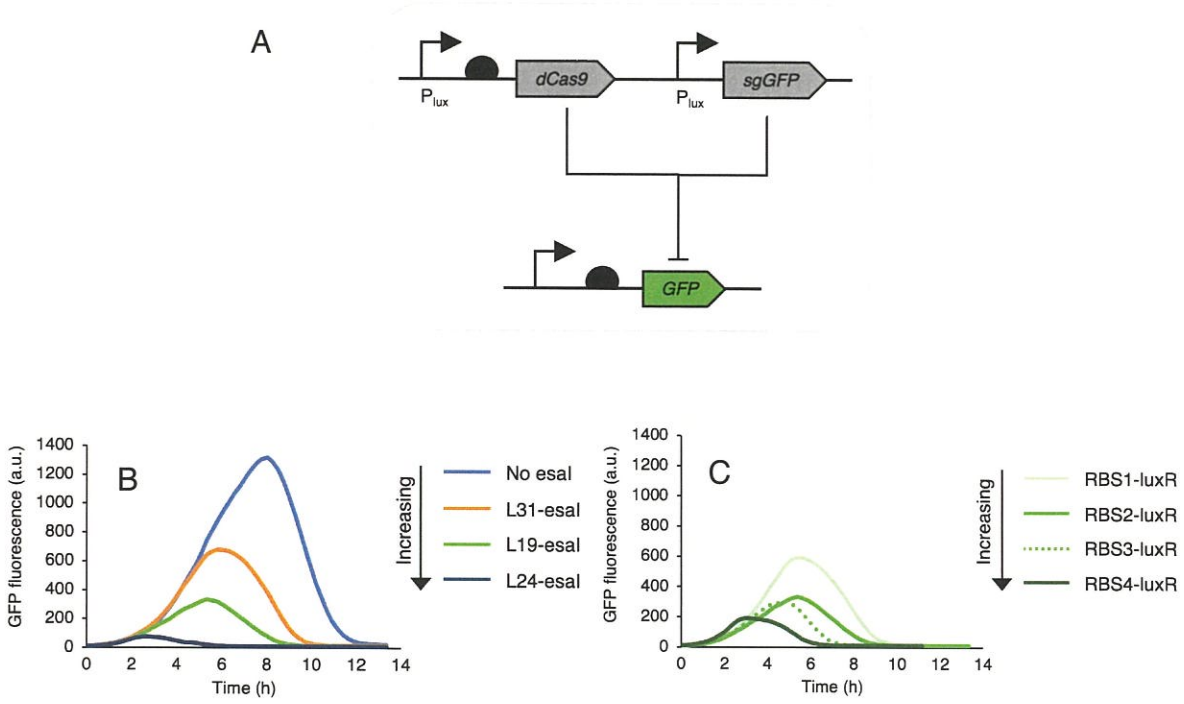

Figure 2-6. Characterization of the down-regulation dynamics from *lux*-controlled expression of CRISPRi components.

(**A**) Schematic of the regulation scheme. (**B**) Representative GFP fluorescence curves at varying EsaI levels and a fixed LuxR level (RBS2). ON-to-OFF switching occurs earlier with increasing EsaI levels. (**C**) Representative GFP fluorescence curves at varying LuxR levels and a fixed EsaI level. (L19).

dCas9 and *sgRNAs* targeted towards endogenous genes were expressed from the P_{lux} promoter (Figure 2-10C), with combinations of target genes chosen based on results from a previous study that used CRISPRi to elevate malonyl-CoA pools by down-regulating competing acetyl-CoA-consuming reactions and fatty acid synthesis cycle reactions (
Figure *2-7*) (75). The P_{lux}-sgRNA expression cassettes were expressed from the pCDF vector backbone and the P_{lux}-dCas9 cassette and P_{con}-luxR variants were expressed from pACYC. To ensure that the down-regulation module was having the desired effects, we first confirmed that transcript levels of the target gene are down-regulated in an EsaI level-dependent manner (Figure 2-8). We additionally confirmed that the decreased transcript levels resulted in elevated malonyl-CoA levels by utilizing a previously developed fluorescence-based sensor (10) (
Figure *2-9*).

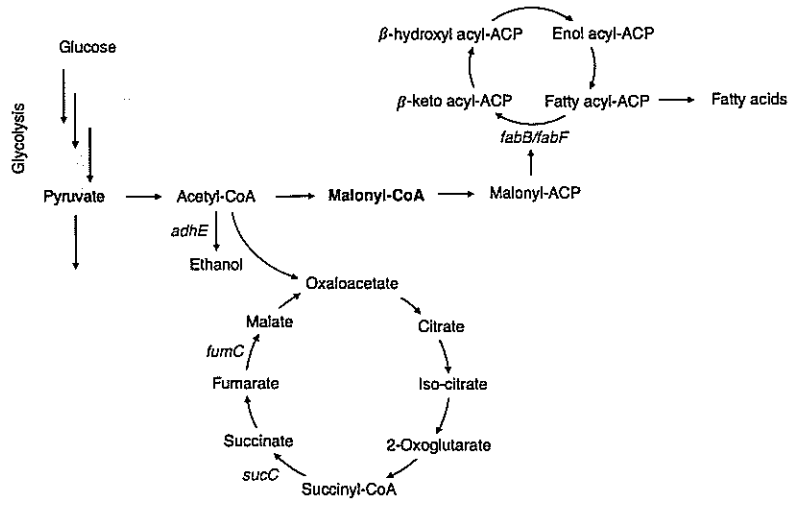

Figure 2-7. Map of down-regulation target genes in the context of *E. coli* metabolism.
The down-regulation target genes tested are labeled in red.

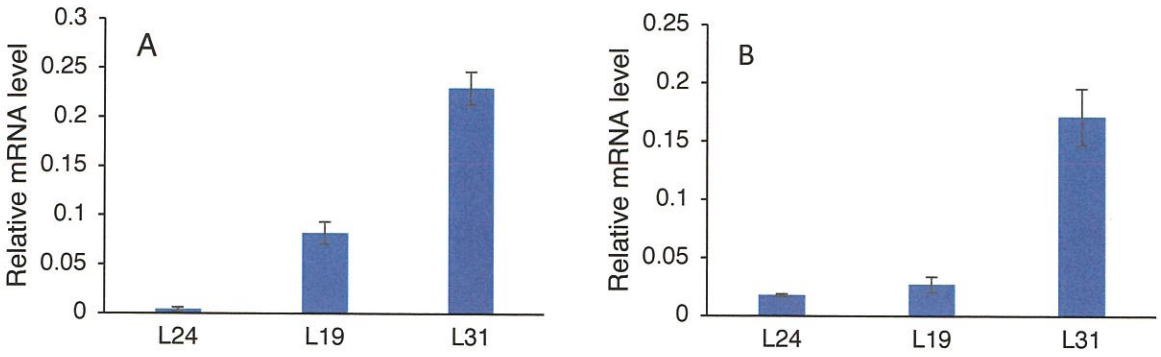

Figure 2-8. Relative transcript levels of target genes with CRISPRi expression under control of the *lux* QS system. All strains contain *dCas9* and *sgRNA* under control of P_{lux} promoters. The axis labels indicate the *esaI* expression level where LXX refers to a promoter-RBS combination (predicted strength L24 > L19 > L31). The *luxR* expression level (RBS2) is constant across all samples. (**A**) Relative transcript levels from *fabF* in a *sgRNA(fabF)*-expressing strain. (**B**) Relative transcript level of *sucC* in a *sgRNA(sucC)*-expressing strain. Levels are fold change compared to a control which expresses a non-specific guide RNA. Error bars indicate s.d. from triplicate trials.

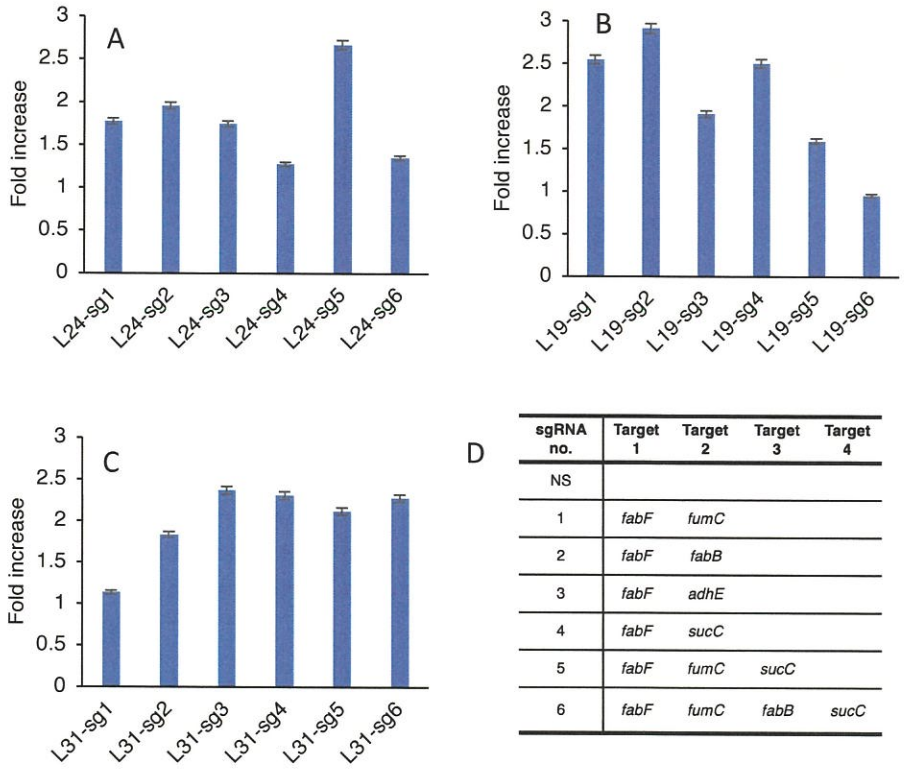

D

sgRNA no.	Target 1	Target 2	Target 3	Target 4
NS				
1	*fabF*	*fumC*		
2	*fabF*	*fabB*		
3	*fabF*	*adhE*		
4	*fabF*	*sucC*		
5	*fabF*	*fumC*	*sucC*	
6	*fabF*	*fumC*	*fabB*	*sucC*

Figure 2-9. Malonyl-CoA sensor output with varying down-regulation target genes and esaI expression levels. Fold increase values are reported with respect to a negative control strain which contains the sensor and down-regulation module expressing a non-specific guide. (**A**) Fold-increase in GFP fluorescence in a L24-esaI strain background with different down-regulation gene targets. (**B**) Fold-increase in GFP fluorescence in a L19-esaI strain background with different down-regulation gene targets. (**C**) Fold-increase in GFP fluorescence in a L31-esaI strain background with different down-regulation gene targets. (**D**) sgRNA gene targets. Error bars indicate s.d. from triplicate trials.

The plasmids harboring the P_{lux} down-regulation module (Figure 2-10C) were then imported into the naringenin producing strains which control TAL and 4CL expression under the P_{esaR-H} promoter (Figure 2-10B). Based on the previous observation that the L19-esaI expression level resulted in the highest naringenin titers under all conditions, we combinatorically tested LuxR levels and sgRNA target genes in the BL21-L19 strain background. Under this dual-regulation scheme (Figure 2-10A-C), increasing cell density leads to dynamic down-regulation of the sgRNA target genes and dynamic up-regulation of coumaryl-CoA-producing reactions.

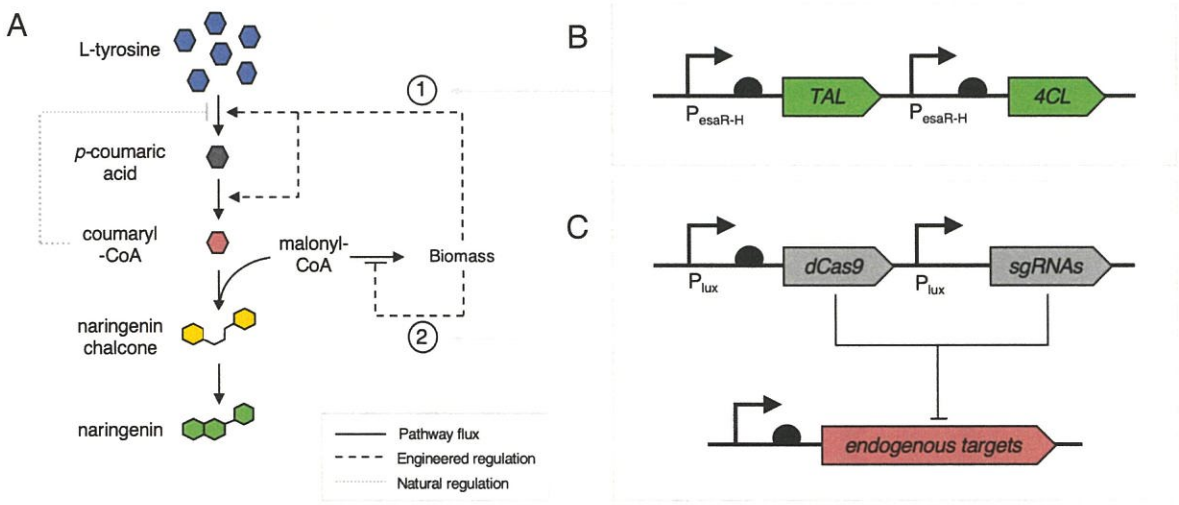

Figure 2-10. Dual regulation in the naringenin pathway
(**A**) Schematic of the regulatory strategy. Increasing cell density triggers two dynamic gene expression switches, one that up-regulates *TAL* and *4CL* expression and a second that down-regulates expression of endogenous genes that are associated with malonyl-CoA accumulation. Dotted lines represent QS circuit responses and solid lines represent metabolic reaction fluxes. (**B**) Diagram of the *TAL* and *4CL* upregulation module responsible for actuating the engineered response labeled (1). *TAL* and *4CL* are each under their own P_{esaR-H} promoters. In the presence of constitutive EsaR and EsaI, expression from the P_{esaR-H} promoter turns ON with increasing cell-density. (**C**) Diagram of downregulation module responsive for actuating the engineered response labeled (2). *dCas9* and each *sgRNA* are expressed from their own P_{lux} promoters. In the presence of constitutive LuxR and EsaI, expression of the target genes turns OFF with increasing cell density.

The library of LuxR levels and sgRNA targets resulted in a set of strains that produced varying naringenin titers (Figure 2-11B). Every strain with dual-regulation resulted in higher naringenin titers compared to the non-specific sgRNA control and half of the library resulted in higher naringenin titers compared to the cerulenin-treated non-specific sgRNA control, suggesting that the down-regulation module can effectively replace cerulenin addition in this context (Figure 2-11A). The top producer identified through this screen yields 463 ± 1 μM naringenin, 140%

higher than the strain with only the up-regulation module and 40% higher than the cerulenin-treated strain. Fermentation of the top producer on a bench-top bioreactor scale confirms that the improvement achieved through dual-regulation holds across fermentation scales (Figure 2-12).

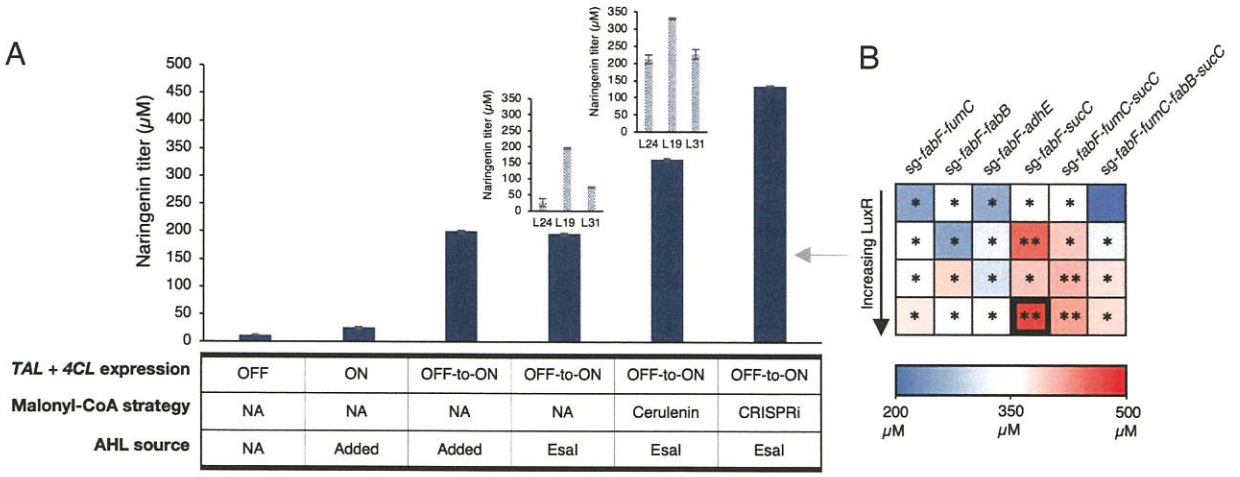

Figure 2-11. Naringenin titers with dual regulation.
(**A**) Naringenin titers with different regulatory schemes. Naringenin titers increase 6-fold over static strategies when TAL and 4CL expression are induced autonomously or with the addition of exogenous AHL. Cerulenin treatment improves naringenin titers in all esaI backgrounds and addition of the CRISPRi-mediated down-regulation module results in naringenin titers that are 40% higher than the top cerulenin-treated strain. (**B**) Heat map indicating naringenin titers with varying LuxR levels and down-regulation target genes. The square corresponding to the top producer is bolded. *P < 0.01 compared to TAL and 4CL controlled strain in L19 background. **P < 0.05 compared to TAL and 4CL controlled strain in L19 background with cerulenin. Error bars indicate s. d. of triplicate trials.

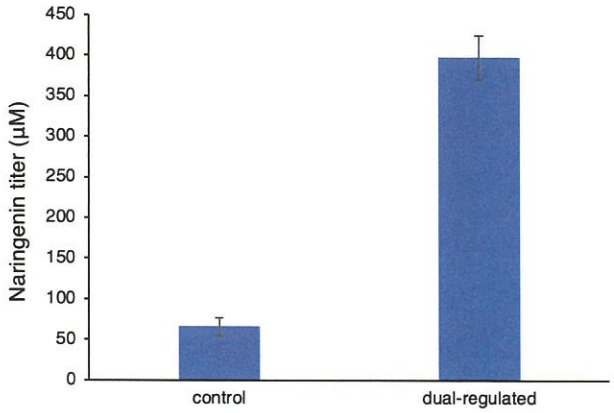

Figure 2-12. Naringenin titers from bioreactor fermentations.
The dual-switching strain is the top naringenin producer identified through screening at the 3-mL scale and the control strain constitutively expresses all naringenin pathway genes. Error bars represent s. d. of duplicate trials.

2.3.4. Dual regulation in the salicylic acid pathway

To test the generalizability of the regulatory circuits, we sought to apply the regulation strategy to a different production pathway that might also benefit from two points of dynamic control. One such pathway is the salicylic acid production pathway, which converts endogenous chorismate to salicylic acid using the enzymes, isochorismate synthase (Ics) and isochorismate pyruvate lyase (Ipl), produced from the genes *entC* and *pchB*, respectively (Figure 2-13A). Since salicylic acid can burden growth of *E. coli*, we hypothesized that production could be improved by delaying expression of pathway genes to manage the trade-off between growth and production. Additionally, chorismate is naturally consumed by the cell to produce the aromatic amino acids such that knocking out the consumption reactions to divert chorismate towards salicylic acid production results in an auxotrophic strain that requires aromatic amino acid supplementation. To create a salicylic acid producer that does not rely on amino acid supplementation, we used the dual-regulation system to (1) dynamically up-regulate *entC* and *pchB* expression to alleviate the growth burden and (2) dynamically down-regulate *pheA* and *tyrA* expression to divert chorismate pools towards the salicylic acid production pathway without introducing auxotrophies.

To implement the proposed control strategy, *entC* and *pchB* were expressed under the $P_{esaR\text{-}H}$ promoter and *dCas9* and *sgRNAs* targeted towards *pheA* and *tyrA* were expressed from the P_{lux} promoter. The $P_{esaR\text{-}H}$-*entC*, $P_{esaR\text{-}H}$-*pchB*, and P_{con}-*esaR* cassettes were expressed from the pCOLA-duet backbone (pCOLA-$P_{esaR\text{-}H}$-*entC-pchB*, Figure 2-13B). *dCas9* was expressed from the same plasmids as in the naringenin experiments (pACYC-P_{lux}-*dCas9*-P_{con}-RBSX-*luxR*) and the P_{lux}- *sgRNA* cassette was expressed from the pCDF backbone (pCDF-P_{lux}-*sg-pheA-tyrA*, Figure 2-13C). We tested this set of plasmids in a phenylalanine producer strain background that is commonly used for salicylic acid production (NST74) (83), with genomically integrated *esaI* (NST74-LXX). Under the proposed regulatory scheme, we can tune the up- and down-regulation modules by varying EsaI level and can tune the down-regulation module only by varying the LuxR level. Rather than holding expression of one of the QS components (EsaI or LuxR) constant in the optimization, we decided to combinatorically vary both since we were only interested in one combination of down-regulation targets in this context.

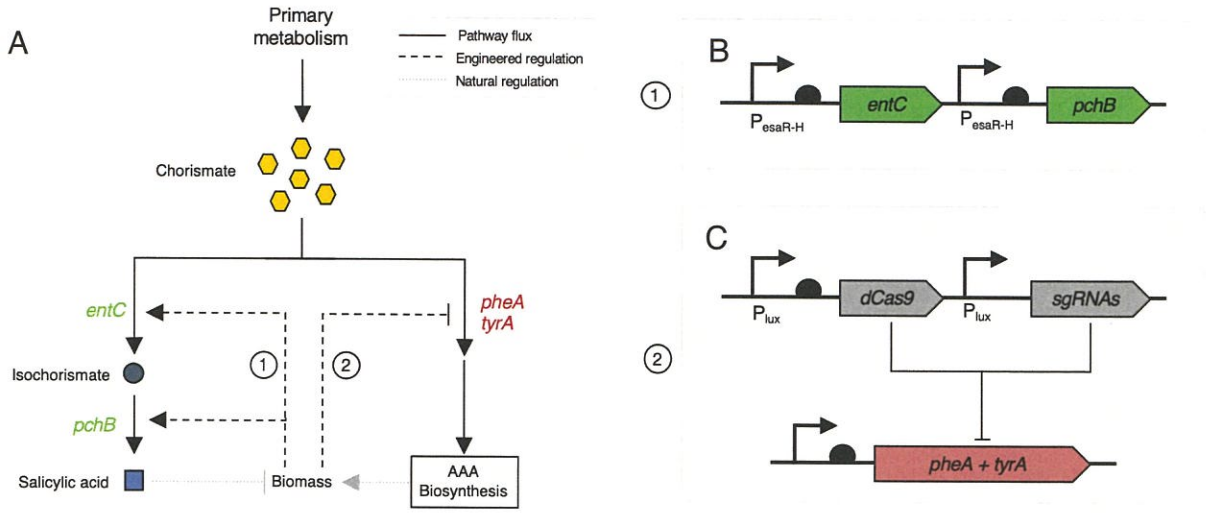

Figure 2-13. Dual-regulation in the salicylic acid pathway.
(**A**) Schematic of the regulatory strategy. The genes encoding the salicylic acid pathway enzymes, *entC* and *pchB*, are expressed with increasing cell-density to balance growth and generation of salicylic acid, a toxic product. *pheA* and *tyrA* are silenced with increasing cell density to elevate chorismate levels without introducing an auxotrophy. (**B**) Diagram of the up-regulation module. *entC* and *pchB* are under control of the $P_{esaR\text{-}H}$ promoter such that increasing cell-density results in increased expression. (**C**) Diagram of the down-regulation module. *dCas9* and *sgRNAs* targeted towards silencing *pheA* and *tyrA* are expressed from the P_{lux} promoter.

Dynamically controlling *entC* and *pchB* expression only and testing salicylic acid production over a range of *esaI* expression levels resulted in a maximum observed salicylic acid titer of 291 ± 3 mg/L, a 10% improvement over that static strain with *entC* and *pchB* induced at inoculation. Addition of the down-regulation module and exploration of EsaI and LuxR levels resulted in a strain that produced 520 ± 7 mg/L salicylic acid, a 1.8-fold improvement over the static strain (Figure 2-14). This application demonstrates the generalizability of our control tool, confirming that independent control of two different targets—or sets of targets—can significantly improve production in some pathways.

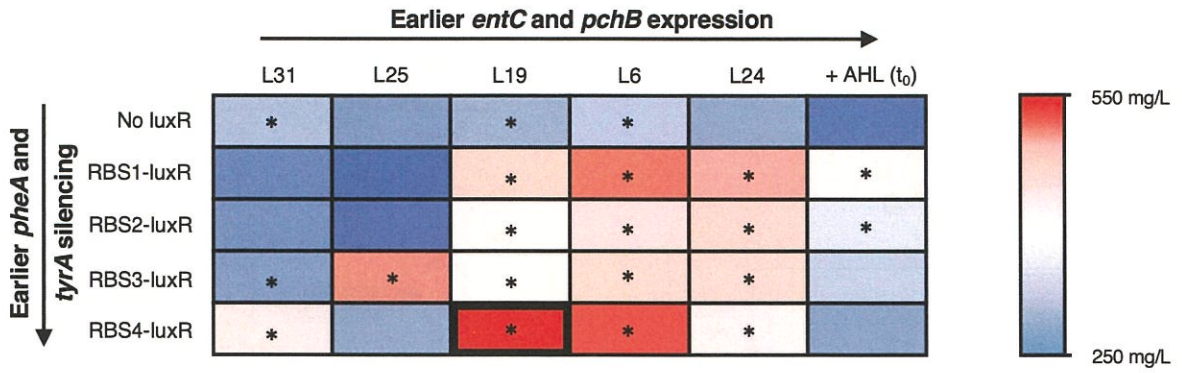

Figure 2-14. Heat map of salicylic acid titers at varying EsaI and LuxR expression levels.
Values represent the mean of triplicate trials. The rectangle corresponding to the top producer is bolded. *P < 0.01 compared to constitutive *entC* and *pchB* control with no AAA pathway downregulation.

2.4. Conclusion

Dynamic regulation is an important strategy in metabolic engineering for improving production in challenging pathways. We have developed an autonomous, pathway-independent, tunable, and bifunctional gene expression regulation system that can be applied to metabolic flux control. The system was applied to controlling key heterologous and endogenous enzymes in the naringenin and salicylic acid pathways, resulting in production benefits in both case studies. Our work demonstrates the importance of having two independently tunable modes of control for dynamic regulation to effectively manage trade-offs and builds on the collection of tools available for developing industrially feasible microbial production strains.

3. Development of a quorum-sensing based circuit for control of co-culture population composition

Abstract

As synthetic biology and metabolic engineering tools improve, it is feasible to construct more complex microbial synthesis systems that may be limited by the machinery and resources available in an individual cell. Co-culture fermentation is a promising strategy for overcoming these constraints by distributing objectives between sub-populations, but the primary method for controlling the composition of the co-culture of production systems has been limited to control of the inoculum composition. We have developed a quorum sensing (QS)-based growth-regulation circuit that provides an additional parameter for regulating the composition of a co-culture over the course of the fermentation. Implementation of this tool in a naringenin-producing co-culture resulted in a 60% titer increase over a system that was optimized by varying inoculation ratios only. We additionally demonstrated that the growth control circuit can be implemented in combination with a communication module that couples transcription in one sub-population to the cell-density of the other population for coordination of behavior, resulting in an additional 60% improvement in naringenin titer.

This chapter contains material adapted from:

Dinh, C. V., Chen, X. & Prather, K. L. J. Development of a quorum-sensing based circuit for control of co-culture population composition in a naringenin production system. Submitted.

3.1. Introduction

With more advanced understanding of cellular processes and improved synthetic biology tools, it is possible to design and construct systems that actuate increasingly complex cellular functions. In the context of metabolic engineering, these functions have resulted in an expansion in the set of molecules that can be produced through microbial synthesis and the types of production challenges that can be addressed. However, increasing complexity gives rise to potential problems such as growth burden or conflicting metabolic goals. To address situations in which achieving all design objectives in a single cell is not feasible, researchers have distributed functions between two or more strains in co-culture fermentations. For example, there have been a number of studies that partition metabolic pathways between sub-populations of a co-culture to alleviate metabolic burden in individual cells (21, 22, 84–89). Co-culture fermentations additionally offer strain construction advantages, allowing for more independent optimization of modules in separate strains and mitigating concerns for unpredictable interactions between the modules.

In some pathways, co-culturing could be a strategy for overcoming enzyme inhibition by an intracellular intermediate or product. One such example is the naringenin pathway that is commonly assembled in *E. coli* (12, 75, 81, 90). This pathway converts L-tyrosine and malonyl-CoA to naringenin using four heterologous enzymes. Tyrosine ammonia lyase (TAL) converts tyrosine to *p*-coumaric acid, which is converted to coumaryl-CoA by 4-coumaryl-CoA ligase (4CL). Chalcone synthase (CHS), and chalcone isomerase (CHI) then convert coumaryl-CoA to naringenin (Figure 2-3). Results from previous studies suggest that efficient naringenin production in this pathway is limited by inhibition of TAL by coumaryl-CoA. While most efforts to overcome this limitation have been focused on preventing accumulation of coumaryl-CoA by delaying its production or by flux balancing, this problem could also be addressed by separating TAL and coumaryl-CoA in different sub-populations. Such a system would contain one strain that expresses *TAL* to convert tyrosine to *p*-coumaric acid, which exits the cell, and a second strain which expresses *4CL*, *CHS*, and *CHI* to convert *p*-coumaric acid to naringenin. Since coumaryl-CoA is retained in the second strain, accumulation does not hinder the activity of TAL contained in the first strain. This approach was employed previously by Jones et al. to produce naringenin as part of an anthocyanin-producing polyculture (22) and Ganesan et al. improved naringenin production

by implementing a similar strategy in which one strain produces both tyrosine and *p*-coumaric acid for uptake in a second strain that expresses the entire naringenin pathway (89).

Co-culture fermentation studies have shown that the relative sub-population size is an important parameter (22, 23, 85, 87–89), but control of this key parameter in co-culture systems has so far been limited to varying the inoculation ratio, forcing the user to define the composition profile for the entire fermentation with one parameter. In nature, microbial cells alter their metabolism in response to the cell density of both their own and other communicating species through quorum-sensing (QS) circuits. Members of a population excrete signaling molecules such that the concentration of these molecules is coupled to the cell-density of that sub-population. Neighboring cells containing the appropriate circuitry can then sense the presence of the signaling molecule. In the canonical *lux* QS circuit, the signaling molecule (N-acyl homoserine lactone, AHL), binds to the regulator protein LuxR and this AHL-bound LuxR complex activates transcription from the P_{lux} promoter. QS promoters such as the P_{lux} promoter control expression of the genes associated with cell-density-dependent behavior.

We and others have implemented QS circuits to coordinate cellular behavior in mono- and co-cultures. For example, metabolic fluxes can be coupled to cell-density by placing genes which encode for key enzymes under control of QS promoters (15–17, 20). In the context of microbial synthesis, QS circuits offer a pathway-independent and autonomous method for dynamic control, which may be more industrially feasible than exogenous chemical addition. You et al. showed that cellular growth rates can be dynamically down-regulated by placing a gene encoding a toxic protein under control of a QS promoter (91) and Stephens et al. showed dynamic up-regulation of cellular growth rate by QS-mediated regulation of *ptsH* in a knockout strain background (30). These ideas have been applied to co-culture systems to facilitate communication between sub-populations, resulting in coordinated expression or growth behavior, although these tools have not yet been applied to microbial synthesis systems (24–30).

We aimed to develop a QS-based growth-regulation circuit that would provide an additional parameter to control co-culture composition profiles. This circuit down-regulates growth rate by decreasing glycolytic flux with increasing cell density. The relationship between cell-density and

growth down-regulation can be tuned by varying the expression level of the AHL synthase to give varied co-culture dynamics with the same inoculation ratio. We applied the circuit towards regulating population compositions in a naringenin-producing co-culture to achieve a significant improvement over the optimal co-culture that lacks the control circuit. The growth down-regulation circuit was then implemented in combination with a communication module in which the cell-density of one sub-population regulates transcription of a regulatory module in the other to show how these strategies can be used in combination to improve co-culture synthesis systems.

3.2. Materials and Methods

All strains and plasmids used in this study are summarized in Table 3-1 and Table 3-2, respectively. Sequences for promoters and RBS sequences are provided in Appendix Table 3 and primer sequences are provided to Appendix Table 4. For plasmid construction and gene/genome editing, cells were cultured in Luria-Bertani (LB) broth at either 30 or 37 °C. Temperature-sensitive plasmids were cured at 42 °C.

Table 3-1. All strains and corresponding genotypes relevant in Chapter 3.
The generalized denotation and genotype of strains containing esaI expression cassettes with different promoter and/or RBS sequences is given as "LXX" for esaI.

Strain	Genotype	Description
IB1643	MG1655 Δ*endA* Δzwf Δ*pfkB* *ΔsspB pfkA::114-pfkA(DAS+4)*	Brockman and Prather (2015)(13)
IB1643(DE3)	MG1655 Δ*endA* Δzwf Δ*pfkB* *ΔsspB pfkA::114-pfkA(DAS+4)* *P21::DE3*	Strain IB1643 with λDE3 cassette under the lacUV5 promoter in the P21 locus
IB1643(DE3)-lux	MG1655 Δ*endA* Δzwf Δ*pfkB* *ΔsspB pfkA::114-pfkA(DAS+4)* *P21::DE3 HK022::P_{con}-luxR-P_{lux}-sspB*	Strain IB1643(DE3) with P_{con}-*luxR* and P_{lux}-*sspB* in the HK022 locus
IB1643(DE3)-LXX	MG1655 Δ*endA* Δzwf Δ*pfkB* *ΔsspB pfkA::114-pfkA(DAS+4)* *P21::DE3 HK022::P_{con}-luxR-P_{lux}-sspB 186(O)::apFABXX-apFABXX-esaI*	Strain IB1643(DE3)-lux + *esaI* driven by a specific promoter and RBS, generalized as LXX here (Supplemental Table 3)

Table 3-2. Summary of plasmids used in Chapter 3.

Plasmid	Functional Genotype	Source
pCOLA-P_{esaR-H}-*TAL-4CL*	*TAL* (*Rhodotorula glutinis*) and *4CL* (*Petroselinum crispum*) under P_{esaR-H} promoters	Table 2-2
pCOLA-*4CL*	*4CL* under T7 promoter	This study
pETM6-*TAL*	*TAL* (*Rhodotorula glutinis*) under T7 promoter	Jones et al. (2017)(22)
pETM6-*TAL-GFP*	*TAL* (*Rhodotorula glutinis*) and GFP each under T7 promoters	This study
pET-P_{T7}-*CHS-CHI*	*CHS* (*Petunia hybrida*) and *CHI* (*Medicago sativa*) under T7 promoters	Table 2-2
pACYC-P_{lux}- *dCas9*-P_{con10} -RBSX-*luxR*	*dCas9* under the P_{lux} promoter and *luxR* under control of a constitutive Anderson library promoter	Table 2-2
pCDF-P_{lux}-*sg(fabF-sucC)*	*sgRNA(s)* targeted towards *fabF* and *sucC* under the P_{lux} promoter	Table 2-2
pACYC-P_{con}-*luxR*-P_{lux}-*sspB*	*luxR* under a constitutive promoter and *sspB* under the P_{lux} promoter	This study
pOSIP-KH	Vector for integration into the HK022 locus	St. Pierre (2013)(68)
pOSIP-KT	Vector for integration into the P21 locus	St. Pierre (2013)(68)
pTet-FLP	*FLP* recombinase expressed from the Tet promoter	Modified from St. Pierre (2013)(68)
pTrc-GFP	GFP expressed from the P_{trc} promoter	Shiue (2014)(73)
pTrc-RFP	RFP expressed from the P_{trc} promoter	Shiue (2014)(73)

3.2.1. Strain construction

Genomic integrations

The λDE3 expression cassette with T7 RNA polymerase under the lacUV5 promoter was integrated into strain IB1643(13) using "clonetegration" (68). The DE3 expression cassette was amplified from the genome of BL21(DE3) using primers DE3_fwd and DE3_rev and inserted into the pOSIP-KT backbone using restriction digestion and ligation. The ligation product was used to transform *E. coli* strain IB1643 for integration into the P21 locus. The phage integration genes and antibiotic resistance cassette were cured by transforming with a plasmid containing FLP under control of the P_{tet} promoter (pTet-FLP) yielding strain IB1643(DE3). An *sspB* expression library containing constitutive *luxR* and *sspB* under the P_{lux} promoter was then integrated into the HK022 locus of IB1643(DE3) using "clonetegration" yielding strain IB1643(DE3)-RBSX-lux. The expression cassettes were digested from the pACYC-P_{con}-*luxR*-P_{lux}-RBSX-*sspB* series and ligated into pOSIP-KH for transformation into IB1643(DE3). The *esaI* expression cassette was integrated into the genome of IB1643(DE3)-RBS2-lux under a several different constitutive synthetic promoters (15) via "clonetegration" to yield the IB1643(DE3)-LXX strain series.

sspB expression plasmids

The pACYC-P_{con}-*luxR*-P_{lux}-RBSX-*sspB* strain series was constructed using a Golden Gate Assembly reaction containing a pACYC-P_{con}-*luxR*-P_{lux}-2xBbsI-*sspB* plasmid and annealed oligos containing the RBS sequence library and the appropriate sticky ends. pAYC-P_{con}-*luxR*-P_{lux}-2xBbsI-*sspB* was constructed using Golden Gate Assembly with the backbone fragment amplified from pACYC-duet using primers Lux_sspB1 a Lux_sspB2, the *luxR,* P_{lux}, and *sspB* terminator fragments amplified from pSB1A2-P_{con}-*luxR*-P_{lux}-*GFP*(73) using primers Lux_sspB3-6, 9 and 10, and the *sspB* gene amplified from the genome of MG1655 using primers Lux_sspB7 and Lux_sspB8.

Naringenin pathway

Plasmid pETM6-*TAL-GFP* was constructed using Golden Gate Assembly. Primers TAL_GFP1 – TAL_GFP4 were used to amplify PCR fragments from pETM6-*TAL* (Addgene plasmid # 100947) (22) – a gift from Mattheos Koffas (Rensselear Polytechnic Institute, Department of Chemical and Biological Engineering) – and primers TAL_GFP5 and TAL_GFP6 were used to amplify fragments from pET-*GFP* (73). The pCOLA-*4CL* plasmid was constructed using restriction digest and ligation cloning using primers 4CL_CC1 and 4CL_CC2 to amplify the *4CL* gene from pCOLA-$P_{esaR\text{-}H}$-*TAL-4CL* (20).

3.2.2. Culturing and fermentations

Fluorescence characterization

Switching dynamics of the *lux* QS circuit over varying *esaI* expression levels were quantified using the BioLector microbioreactor system (m2p-labs, Baesweiler, Germany). Individual colonies were inoculated in LB medium and grown overnight at 30 °C. 1 mL cultures were inoculated from these seeds at OD_{600} 0.05 into BioLector 48-well flower plates and incubated at 30 °C, 1200 rpm (3 mm orbit), and 80% relative humidity. The plate was sealed with a gas-permeable sealing foil (m2p-labs). Cultures were monitored for OD (BioLector units) and RFP fluorescence over time.

Growth characterization

Individual colonies were inoculated in 3 mL LB broth and grown overnight at 30 C, then diluted 1:100 into 3 mL MOPS minimal medium containing 5 g/L glycerol, 500 mg/L tyrosine, 4 g/L NH_4Cl, 1 g/L K_2HPO_4, 2 mM $MgSO_4$, 0.1 mM $CaCl_2$, 40 mM MOPS, 4 mM Tricine, 50 mM NaCl, 100 mM Bis-Tris, 143 uM EDTA, 31 uM $FeCl_3$, 6.2 uM $ZnCl_3$, 0.76 uM $CuCl_2$. 0.42 uM $CoCl_2$, 1.62 uM H_3BO_3 and 0.081 uM $MnCl_2$ at 30 C for ~6 h. These were used to inoculate into 5 mL working cultures of MOPS minimal medium containing 5 g/L D-glucose at OD_{600} 0.1. Samples were taken periodically for quantification of cell density and relative population size until 24 h.

Fermentations

Naringenin production trials were performed in glass vials with 5 mL working volume at 30 C and 80% humidity with 250 rpm shaking in modified MOPS minimal medium containing 5 g/L D-glucose, 500 mg/L tyrosine, 4 g/L NH_4Cl, 1 g/L K_2HPO_4, 2 mM $MgSO_4$, 0.1 mM $CaCl_2$, 40 mM MOPS, 4 mM Tricine, 50 mM NaCl, 100 mM Bis-Tris, 143 uM EDTA, 31 uM $FeCl_3$, 6.2 uM $ZnCl_3$, 0.76 uM $CuCl_2$. 0.42 uM $CoCl_2$, 1.62 uM H_3BO_3 and 0.081 uM $MnCl_2$. For strains containing plasmids with pET, pCOLA, pACYC, and pCDF vector backbones, the medium was also supplemented with 100 μg/mL carbenicillin, 50 μg/mL kanamycin, 34 μg/mL chloramphenicol, and 100 μg/mL spectinomycin, respectively, for plasmid maintenance. Strains were initially grown in 3 mL of LB medium at 30 C overnight, then diluted 1:100 into 3-mL seed cultures of modified MOPS medium with 5 g/L glycerol for ~6 h at 30 C. These were used to inoculate working cultures at OD_{600} 0.1. Samples were taken periodically for quantification of cell density, relative population size, and extracellular metabolites. Fermentations were carried out for 48 hours.

3.2.3. Estimation of relative population sizes

Relative population sizes within co-cultures were estimated using fluorescence assisted cell sorting (FACS). 1-10 μL of cell culture was suspended in 1 mL of PBS and stored at 4 C until analysis. FACS screening was performed on a FACS LSRII (Becton Dickinson) at the Koch Institute Swanson Biotechnology Center Cytometry Core facility (Cambridge, MA).

3.2.4. Quantification of metabolites

p-Coumaric acid and naringenin titers were quantified as previously described in Chapter 2.

3.3. Results

3.3.1. Growth control circuit

To construct a QS-based circuit which dynamically down-regulates growth rate in response to increasing cell density, we modified a circuit previously developed in our group. Brockman and Prather developed a circuit that dynamically down-regulates glycolytic flux with the goal of accumulating glucose-6-phosphate by controlling phosphofructokinase (Pfk) levels (13). They placed *pfkA* under control of a constitutive synthetic promoter and appended the gene with an SspB-dependent degradation tag such that Pfk-1 is degraded upon *sspB* expression. The background strain (IB1643) additionally contained knockouts of *pfkB, zwf,* and *sspB* to achieve tight regulation, and a new copy of *sspB* was introduced under the control of a small molecule (anhydrotetracycline, aTc) inducible promoter. The circuit was intended to be a glycolytic flux control system, which resulted in a titratable growth down-regulation effect with increasing *sspB* expression when cells were grown in minimal medium with glucose as the sole carbon source (13).

To obtain a QS-based system for autonomous and dynamic growth control, we integrated a *lux* QS circuit, which contains *luxR* under the control of a constitutive promoter and *sspB* under the P_{lux} promoter and an RBS library into a variant of IB1643 that contains the DE3 lysogen (IB1643(DE3)) (Figure 3-1A). We screened the resulting RBS variants for the desired phenotype of growth rate down-regulation with AHL addition, with maintenance of a fast growth rate in the absence of AHL. The strain selected (IB1643(DE3)-lux) showed AHL-dependent growth behavior in which AHL addition at inoculation or during mid-exponential phase exhibits a decreased growth rate (Figure 3-1B). We then integrated a library of *esaI* expression levels into IB1643(DE3)-lux to make the IB1643(DE3)-LXX strain series. Based on previous characterization, we expect that increasing *esaI* expression leads to faster production of AHL, resulting in stronger growth down-regulation effects at lower cell-densities (20). An estimation of the specific growth rate of the IB1643-LXXesaI strain series at mid-exponential phase confirms this trend (Figure 3-1C).

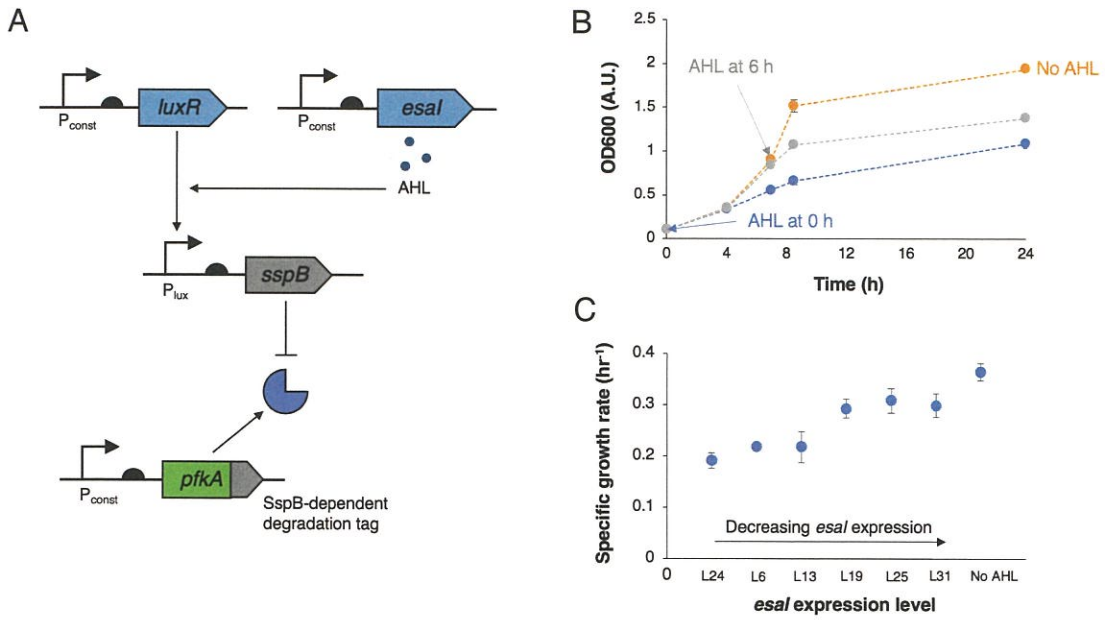

Figure 3-1. Growth regulation circuit and characterization.
(A) Diagram of the growth regulation circuit. The native copy of *pfkA* is under control of a synthetic constitutive promoter and appended with an SspB-dependent degradation tag. The only copy of *sspB* is under control of the P_{lux} promoter, which is activated by AHL-bound LuxR. AHL is produced in a cell-density dependent manner though constitutive expression of *esaI*. The background strain contains knockouts of *sspB, zwf,* and *pfkB.* (**B**) Growth curves of strains containing the growth regulation circuit with various AHL treatments. AHL addition at inoculation or during mid-exponential phase results in decreased growth rate. (**C**) Effect of *esaI* expression level on the specific growth rate of strains containing the growth regulation circuit during mid-exponential phase. Each data point represents the growth rate a strain expressing a different level of *esaI* (promoter-RBS indicated on x-axis). Increasing *esaI* expression generally results in decreased specific growth rate. Error bars represent the s.d. of triplicate trials.

3.3.2. Co-culture population characterization

Next, we evaluated whether the growth regulation circuit could offer a method for regulating co-culture population dynamics. All co-cultures tested contain an RFP-expressing strain (Strain R, BL21(DE3) + pTrc-RFP), and a GFP-expressing strain containing the growth regulation circuit (Strain G, IB1643(DE3)-lux or IB1643(DE3)-LXX + pTrc-GFP). With this regulation scheme, we expected that each strain would initially grow at its baseline rate, or the rate without AHL, until a sufficient concentration of AHL accumulates, resulting in down-regulation in the growth rate of Strain G (Figure 3-2A). A time course study of the population dynamics shows that at every inoculation ratio tested, the presence of EsaI results in a lower fraction of Strain G by 24 hours and final population compositions correlate well with the predicted *esaI* expression levels (Figure 3-2B).

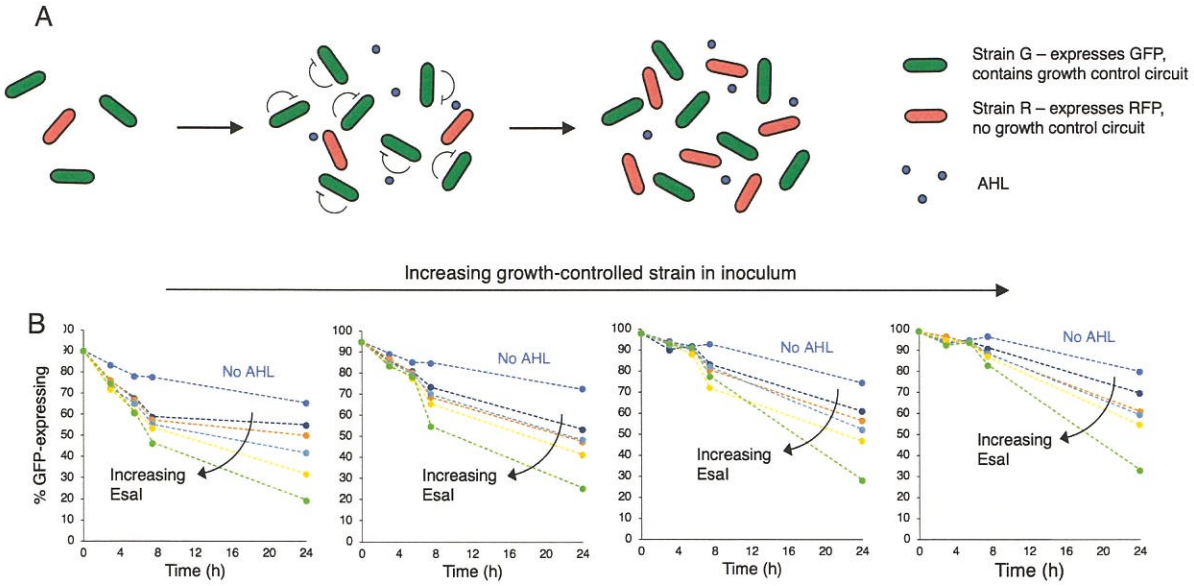

Figure 3-2. Effect of the growth regulation circuit in a co-culture.
(**A**) Illustration of the different stages of the co-culture fermentation in which the GFP-expressing strain (Strain G) contains the growth regulation circuit. At low cell density, both strains will grow at their baseline rates. Once the culture has accumulated a certain concentration of AHL, corresponding to a cell-density of Strain G, the growth rate of the green sub-population slows down. At the end of the fermentation, Strain R represents a greater fraction of the population than it would in the absence of growth regulation. (**B**) Representative population profiles for co-culture of varying inoculation compositions (L to R: 90%, 95%, 98%, and 99% Strain G) and esaI expression levels (different curves). For all inoculation ratios, increasing the esa expression level leads to a smaller fraction of Strain G by 24 h.

3.3.3. Growth rate control in the naringenin pathway

We then applied the growth control circuit to a naringenin-producing co-culture system to demonstrate how this additional control parameter can result in more favorable population dynamics to improve production. The co-culture naringenin production system includes one strain (Strain 1) that expresses *TAL* (pET-*TAL-GFP*) to convert L-tyrosine to *p*-coumaric acid and GFP for tracking population composition, and a second strain (Strain 2) that expresses *4CL, CHS*, and *CHI* (pCOLA-*4CL* and pET-*CHS-CHI*) to convert *p*-coumaric acid to naringenin. Since we hypothesized that successful co-cultures would contain relatively high levels of Strain 2 by the end of the fermentation, we implemented the growth control circuit with varying *esaI* expression levels in Strain 1 (Figure 3-4A).

To search for efficient naringenin producers, we co-cultured the Strain 1 *esaI* library with Strain 2 at varying inoculation ratios. Analysis of the final co-culture composition confirms that the trends

between *esaI* expression level and composition seen in Figure 3-2 still hold in this context (Figure 3-3). Characterization of the final co-culture composition and titers shows that *p*-coumaric acid titer increases with the fraction of Strain 1 as expected (Figure 3-4B). The relationship between naringenin titer and co-culture composition suggests that efficient production relies on achieving a balance between *p*-coumaric acid production and consumption capabilities. Cultures containing low levels of Strain 1 are limited by low *p*-coumaric acid production rates while cultures with low levels of Strain 2 are limited by their low rates of *p*-coumaric acid conversion to naringenin (Figure 3-4C).

To evaluate impact of the growth regulation circuit on production, we compared naringenin titers from co-cultures with and without the growth control circuit. The variant of Strain 1 used for the "without growth circuit" sample has the same genetic background as the "with growth circuit" strains, but lacks *esaI* such that the Pfk degradation rate is low and constant. When this variant of Strain 1 was co-cultured with Strain 2 at varying inoculation ratios, the best sample produced 0.1 mM naringenin (Figure 3-5), about 60% less than the top naringenin production system which employed the growth regulation circuit. This result suggests that the additional control parameter is beneficial in this context (Figure 3-11, bars 2 and 5). The composition of the optimal "no growth control" sample increases from 5% to 29% Strain 1 whereas the composition of the optimal strain with growth control decreases from 40% to 21% Strain 1 over the course of the fermentation.
We hypothesize that higher starting fraction of Strain 1 in the growth-controlled sample corresponds to earlier p-coumaric acid production, leading to more effective conversion by Strain 2.

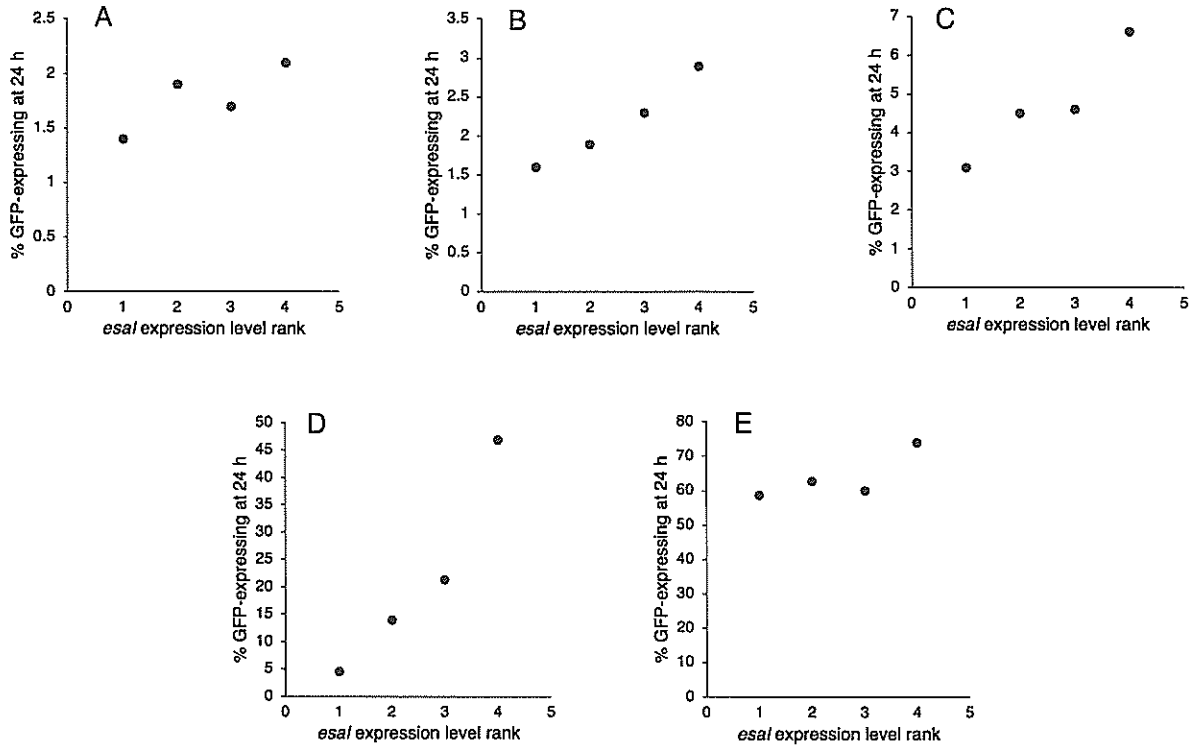

Figure 3-3. Stationary phase compositions of naringenin-producing co-cultures with growth control.
Panels show compositions that result from varying esaI expression levels at a single inoculation ratio. The esaI expression level rank is ordered as follows: 1 (highest) = L24-esaI, 2 = L6-esaI, 3 = L19-esaI, 4 (lowest) = L25-esaI. The inoculation compositions are: (**A**) 20% Strain (**B**) 25% Strain 1 (**C**) 33% Strain 1 (**D**) 40% Strain 1 (**E**) 50% Strain 1. At all inoculation ratios, there is a general trend of increasing fraction of Strain 1 with decreasing esaI expression levels.

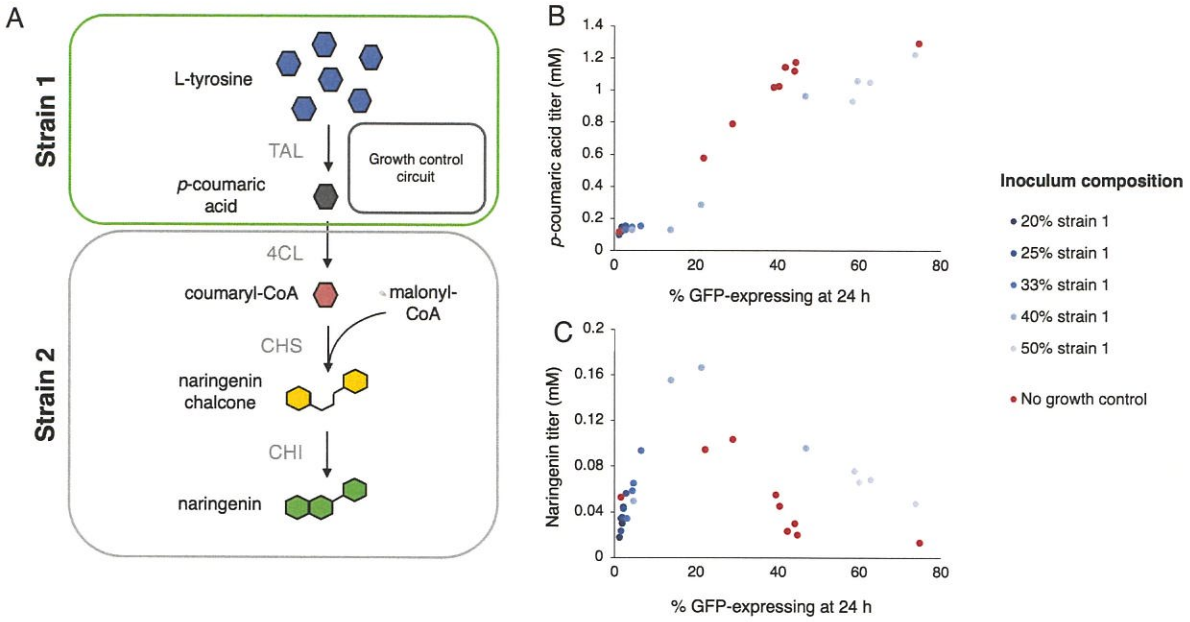

Figure 3-4. Naringenin co-culture system with growth regulation.

(**A**) Illustration of the sub-populations in the naringenin co-culture system. Strain 1 contains the growth control circuit (IB1643(DE3)-LXXesaI) and constitutively expresses TAL and GFP. Strain 2 is BL21(DE3) with constitutively expressed 4CL, CHS, and CHI. (**B**) *p*-Coumaric acid titers as function of the co-culture composition at 24 h. Data points with the same shade of blue represent samples in which Strain 1 contains different *esaI* expression levels, but the inocula contain the same fractions of Strains 1 and 2. Increasing the fraction of Strain 1 in the co-culture results in increased *p*-coumaric acid titers. (**C**) Naringenin titers as a function of the co-culture composition at 24 h. The intermediate fractions of Strain 1 in the co-culture results in the best naringenin production levels.

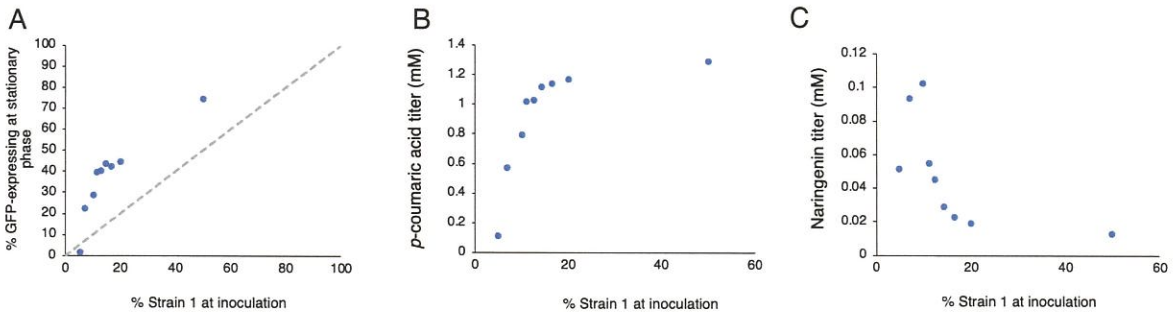

Figure 3-5. Characterization of naringenin-producing co-cultures without growth control.
Co-cultures were composed of *TAL*-expressing strain (IB1643-lux + pETM6-TAL-GFP, Strain 1) and a down-stream pathway strain (BL21(DE3) + pCOLA-4CLI + pET-CHS-CHI, Strain 2). (**A**) Comparison of co-culture composition in inoculation and stationary phases. For all inoculation ratios greater than 5 % Strain 1, the final composition of the co-culture has significantly more Strain 1 at stationary phase. (**B**) *p*-Coumaric acid titers with varying inoculation ratios of Strains 1 and 2. Increasing the fraction of Strain 1 results in an increased p-coumaric acid production. (**C**) Naringenin titers with varying inoculation ratios of Strains 1 and 2. The highest naringenin titer is observed with an inoculum that contains 10% Strain 1. Increasing the fraction of Strain 1 beyond from composition results in decreased naringenin production.

3.3.4. Growth rate control with sub-population communication in naringenin pathway

The maximum pathway flux in the co-culture system may be limited by the fact that each gene is only expressed in a fraction of the population. To evaluate the impact of this feature, we benchmarked the top co-culture naringenin titer against two relevant mono-culture controls. As previously mentioned, TAL inhibition is commonly addressed by delaying expression of *TAL* and *4CL*. This approach is subject to a different limitation in which there is low pathway flux early on in the fermentation before induction of *TAL* and *4CL* expression. In previous work, we controlled *TAL* and *4CL* expression under P_{esaR} promoters which are de-repressed in the presence of AHL. A screen of *esaI* expression levels corresponding to different *TAL* and *4CL* induction times identified a top strain that produces 0.17 mM naringenin (Figure 3-11, bar 4) (20). To study a naringenin production system that is free of both limitations, we cultured Strain 2 (BL21(DE3) + pCOLA-*4CL* + pET-*CHS-CHI*) with varying concentrations of *p*-coumaric acid supplied to the culture medium. This system, which is not limited by a fermentation phase with low pathway flux, *p*-coumaric acid levels, or the fraction of Strain 2, produced 0.18 mM naringenin at the optimal concentration of fed *p*-coumaric acid (Figure 3-11, bar 3 and Figure 3-6).

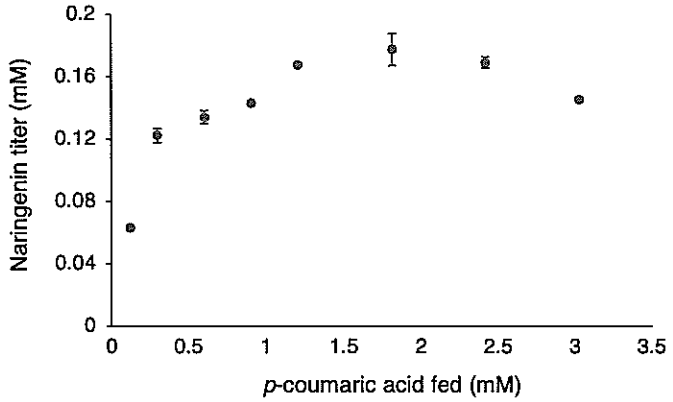

Figure 3-6. Naringenin titers with varying concentrations of p-coumaric acid fed.
BL21(DE3) expressing 4CL, CHS, and CHI was cultured with varying concentration of p-coumaric acid. Naringenin titers increase with p-coumaric acid concentration up to about 2 mM, after which high p-coumaric acid concentrations start to burden cell growth. Error bars represent s.d. of triplicate trials.

The different methods for overcoming TAL inhibition in the naringenin pathway (fed *p*-coumaric acid, delay of coumaryl-CoA production, and co-culture) result in naringenin titers that are not significantly different (Figure 3-11, bars 3-5). This observation led us to hypothesize that implementation of these strategies leads to a more significant limitation elsewhere in the pathway,

likely the malonyl-CoA-dependent step based on previous studies (12, 20, 75, 81). Our group and others have addressed the malonyl-CoA limitation by expressing silencing components to down-regulate TCA cycle and fatty acid synthesis pathways that consume the substrate (20, 77, 83, Chapter 2). However, altering these endogenous metabolic fluxes can result in undesired growth effects and thus, it is preferable to delay expression of the down-regulation system until the appropriate point in the fermentation, possibly once a sufficient concentration of *p*-coumaric acid is reached.

Since the *p*-coumaric acid concentration is expected to strongly correlate with the cell-density of Strain 1, we can implement a QS circuit in Strain 2 to regulate expression of silencing components for malonyl-CoA accumulation. To confirm that the AHL produced from Strain 1 is able to trigger expression from the P_{lux} promoter in a different sub-population, the Strain 1 *esaI* library was co-cultured with BL21(DE3) with *mCherry* controlled under the *lux* QS circuit. Analysis of the RFP fluorescence profiles confirmed that the AHL produced from the Strain 1 sub-population is able to trigger expression from the P_{lux} promoter in a second sub-population in an EsaI level-dependent manner (Figure 3-7).

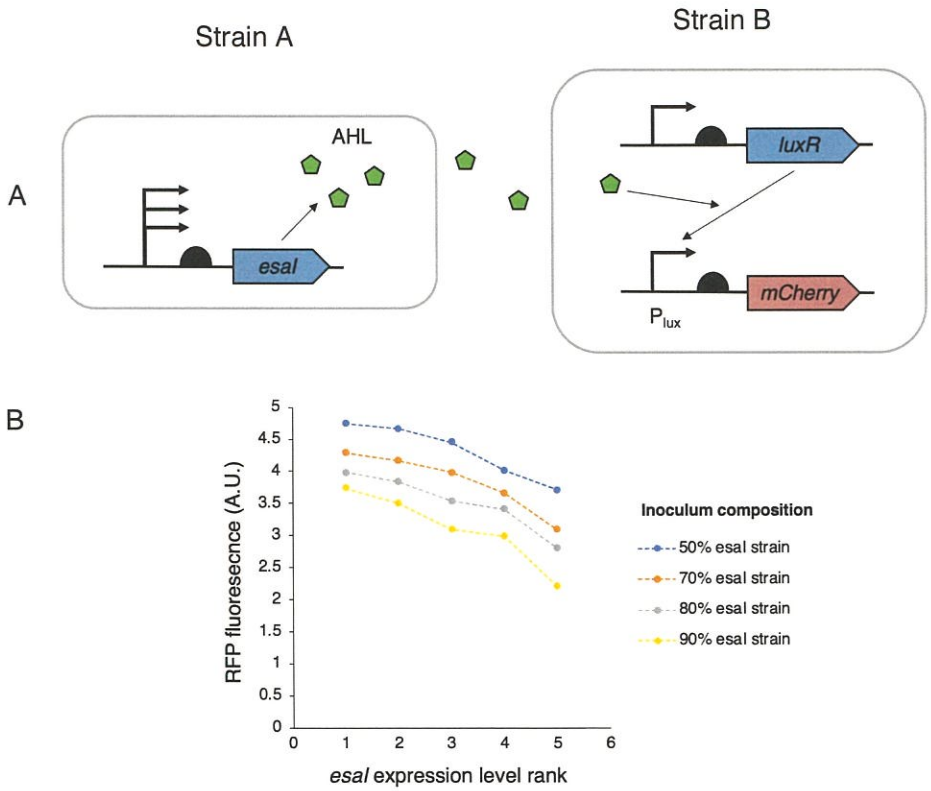

Figure 3-7. Separation of lux QS circuit components between two sub-populations in a co-culture.
(**A**) Diagram of how the components of the lux QS circuits are distributed between the two sub-populations of the co-culture. One strain (Strain A) expresses esaI to produce AHL at a rate that depends on both the esaI expression level and sub-population size. A second strain (Strain B) responds to the AHL levels produced by Strain A by activating the P_{lux} promoter to express mCherry. (**B**) Stationary phase RFP fluorescence with varying inoculation ratio and varying esaI expression levels. The promoter-RBS combinations that correspond to the esaI expression level ranks are: 1 = L24-esaI, 2 = L6-esaI, 3 = L13-esaI, 4 = L19-esaI, 5 = L25-esaI. Within each inoculation ratio, increasing esaI expression results in increased activation of the lux circuit.

In the previous chapter, we improved a mono-culture naringenin production system by controlling expression of CRISPRi components under a *lux* QS circuit for the purpose of increasing malonyl-CoA availability. A screen of gene target combinations and switching dynamics identified a best producer that targeted the endogenous genes, *fabF* and *sucC*, and employed the strongest *luxR* expression level(20). We implemented this top silencing system in Strain 2 by transforming plasmids containing *dCas9* and *sgRNA* under P_{lux} promoters (pACYC-P_{lux}-*dCas9*-P_{con}-RBS4-*luxR* and pCDF-P_{lux}-*sg(fabF-sucC)*). By incorporating this additional circuit, increasing cell-density of Strain 1 results in both growth-rate down-regulation of Strain 1 and expression of CRISPRi components in Strain 2 for malonyl-CoA accumulation (Figure 3-8).

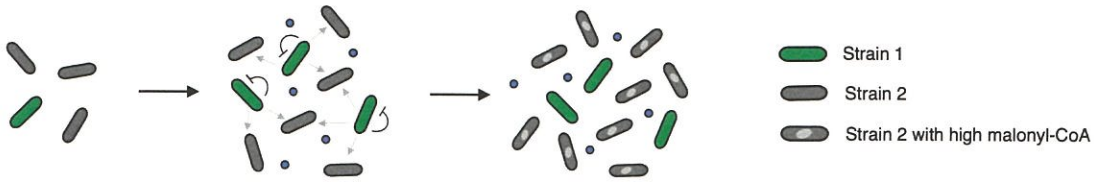

Figure 3-8. Illustration of the different stages of the co-culture system.
At low cell-densities, both strains grow at their baseline rates. As the cells grow, the AHL concentration in the media increases with the cell-density of Strain 1, resulting in decreased growth rate of Strain 1 and expression of CRISPRi components in Strain 2 for malonyl-CoA accumulation.

To again screen for top naringenin producers, the Strain 1 *esaI* library and Strain 2 with the CRISPRi modules were co-cultured with varying inoculation ratios. Analysis of final composition trends showed that within inoculation ratios, increasing *esaI* expression levels resulted in an increased fraction of Strain 1 (Figure 3-9), suggesting that *fabF* and *sucC* down-regulation has a stronger growth effect than Pfk degradation. Although both modules are controlled under *lux* QS circuits, the relative growth effects can be tuned independently by varying the expression level of *luxR* in each strain. This is a promising tuning parameter for further expanding the range of composition profiles, which could potentially lead to additional production benefits. In general, *p*-coumaric acid titers again increase with increasing fractions of Strain 1 at stationary phase (Figure 3-10A) and the naringenin titer dependence on the population composition again indicates a trade-off between *p*-coumaric acid production and consumption capabilities (Figure 3-10B), although the balance has shifted to favor higher fractions of Strain 1.

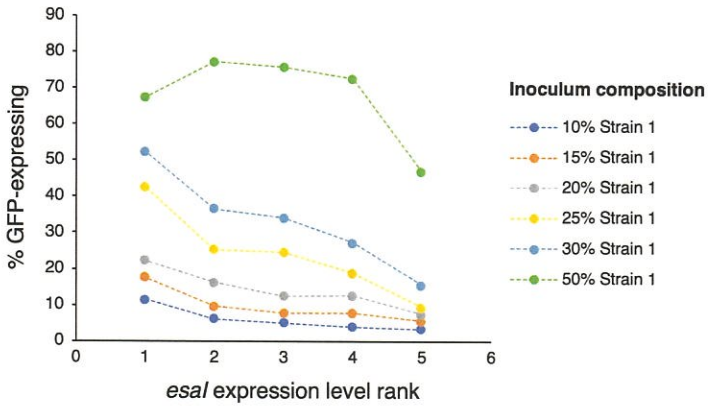

Figure 3-9. Stationary phase compositions of naringenin-producing co-cultures with growth control.
Curves show compositions that result from varying esaI expression levels at a single inoculation ratio. The esaI expression levels rank is ordered as follows: 1 = L24-esaI, 2 = L6-esaI, 3 = L13-esaI, 4 = L19-esaI, 5 = L25-esaI. For all inoculation compositions except the 50% Strain 1, increasing the esaI expression level results in an increased fraction of Strain 1 in the culture at stationary phase.

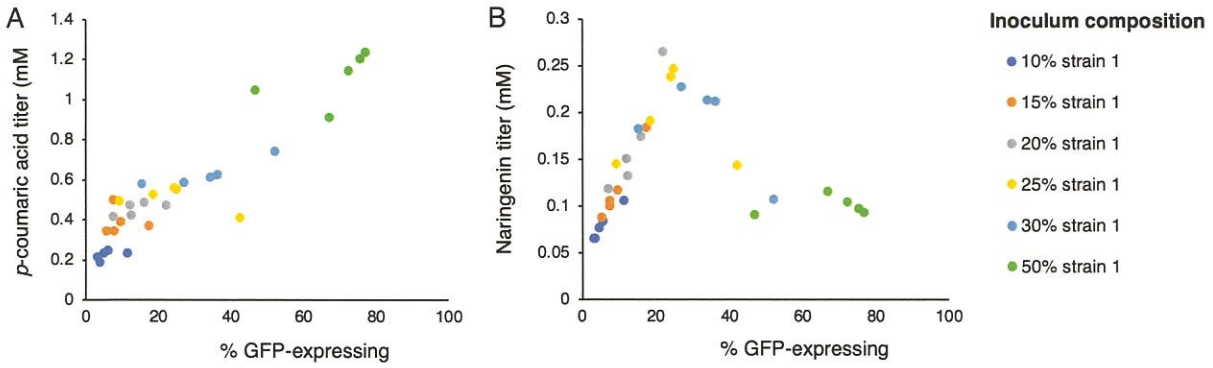

Figure 3-10. Naringenin co-culture system with growth regulation and malonyl-CoA accumulation.
(**A**) *p*-Coumaric acid titers as a function of the percentage of GFP-expressing cells (Strain 1) in the co-culture. Data points with the same color represent samples in which Strain 1 contains different esaI expression levels, but the inocula contain the same fractions of Strains 1 and 2. Generally, increasing the fraction of Strain 1 at stationary phase results in increased p-coumaric acid titers. (**B**) Naringenin titers as a function of the fraction of Strain 1 at stationary phase. High naringenin titers occur when neither strain dominates the co-culture.

3.3.5. Comparison of naringenin production systems

To summarize, constitutive expression of all naringenin pathway genes in a mono-culture suffers from poor production due to TAL inhibition by coumaryl-CoA, which can be relieved through a co-culture approach to separate TAL and coumaryl-CoA to give a 6-fold increase in naringenin titers (Figure 3-11, bars 1 and 2). Implementation of a growth control circuit into one of the co-culture strains (Strain 1) allows for an additional parameter for tuning population dynamics, resulting in a 60% increase in naringenin titers over the titers without this control capability (Figure 3-11, bars 2 and 5). These titers are comparable to the ones achieved by feeding *p*-coumaric acid to Strain 2 and by delaying production of coumaryl-CoA in a mono-culture, demonstrating the efficacy of the co-culture strategy with growth control (Figure 3-11, bars 3 and 4). To further increase naringenin titers, we implemented a CRISPRi-mediated down-regulation module which responds to the cell-density of the *p*-coumaric acid producing strain, resulting in an additional 60% increase in naringenin titer (Figure 3-11, bars 5 and 6).

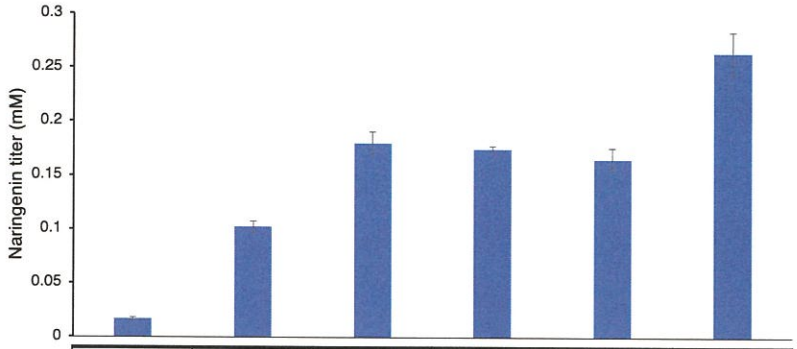

Culture strategy	mono	co	mono + pCA	mono	co	co
Control layer 1	-	-	-	*TAL/4CL*	growth	growth
Control layer 2	-	-	-	-	-	*fabF/sucC*

Figure 3-11. Comparison of various naringenin production systems.
The titer shown for the mono-culture strategy without dynamic control represents the titer that results from high constitutive expression of all naringenin pathway genes (bar 1). The titer shown for the co-culture strategy with no dynamic control is the higher titer achieved by varying inoculation ratios only using a Strain 1 variant that lacks EsaI (bar 2; Figure 3-5C). The titer shown for the mono-culture with added *p*-coumaric acid strategy is the highest titer achieved by varying fed p-coumaric acid concentrations a mono-culture of Strain 2 (bar 3; Figure 3-6). The titer shown for the mono-culture with TAL/4CL control is highest titer achieved by controlling TAL and 4CL expression from $P_{esaR\text{-}H}$ promoters and varying esaI expression levels (bar 4). The two right-most bars are the top titers shown in Figure 3-4C and Figure 3-10B (bars 5 and 6).

3.4. Conclusion

In conclusion, co-culturing presents a promising solution for overcoming the physiological limitations imposed by individual cells. In the context of metabolic engineering, previous studies have demonstrated the importance of co-culture composition for achieving efficient production, but co-culture composition during the entire fermentation is commonly controlled only by the inoculum composition. With the aim of obtaining greater control over the population dynamics of a co-culture, we developed a QS-based circuit that down-regulates the growth rate of a sub-population in response to an increase in its own cell-density in a tunable manner. Application of this system to a naringenin-producing co-culture resulted in an expansion of the range of possible population dynamics, which led to a significant increase in titer compared to an uncontrolled sample. We then implemented a second QS module to facilitate coordination between sub-population size and malonyl-CoA accumulation to achieve additional production improvements. To our knowledge, this is the first application of QS-based control tool for composition regulation in a co-culture production system.

4. Quorum-sensing-mediated control of enzyme clustering for metabolic flux control

Abstract

Metabolic engineering typically controls reaction rates by changing enzyme levels. However, the ability to increase protein levels may be limited by the host cell transcriptional or translational capacity or can result in growth burden. In the context of dynamic control, changes in metabolic flux are commonly achieved through control of transcription, or RNA or protein degradation, which also depend on dynamics of these host cell processes. Inspired by the mechanisms by which eukaryotic cells overcome these challenges, this study aimed to construct and characterize a quorum-sensing-based method for enzyme co-localization. Attempts at applying this co-localization system to regulating metabolic fluxes were limited by decreased enzymatic activity when enzymes were tagged and/or clustered. This suggests that future application will depend on protein engineering to decrease the size of the oligomerization domain to minimize its impact on the enzymatic domain.

4.1. Introduction

Traditionally, metabolic engineering has relied on changing enzyme levels or activity to achieve desired changes in metabolic fluxes, whether for relieving pathway bottlenecks or for implementing dynamic control. However, there are limitations to these approaches. Increasing enzyme levels can result in burdened growth or may not be attainable due to constraints imposed by host cell machinery. Additionally, the response dynamics of control circuits that rely on host transcription or protein degradation machinery can be limited by the dynamics of these cellular processes.

In natural production pathways, eukaryotic cells compartmentalize enzymes into membrane-bound organelles to efficiently utilize resources (92). Similarly, researchers have developed a number of methods to increase the rate of limiting reactions without increasing protein demand by co-localizing two or more enzymes. These co-localization strategies have involved the use of synthetic systems such as scaffolds (37, 38) and encapsulins (39), along with the use of natural systems such as membrane-bound organelles (40–42), and have resulted in significant production improvements in diverse pathway applications. Enzyme co-localization has also been used to increase specificity for a desired product in a branched pathway (34, 35). However, in some contexts, co-localization to favor a certain branch can result in depletion of an essential metabolite, burdening growth (36). This finding motivates the development of dynamic co-localization systems.

Recent studies have shown that in addition to compartmentalization of metabolic pathways in membrane-bound organelles, eukaryotic cells contain membrane-less organelles that dynamically co-localize certain biomolecules. These membrane-less organelles form in phase transition processes that are triggered when a threshold concentration of certain protein sequences, called intrinsically disordered regions (IDRs), is reached. Phase separation events are typically triggered when IDR-containing proteins undergo binding events which increase their local concentration, allowing for promiscuous interactions between IDRs. This mechanism is responsible for sequestering biomolecules, facilitating certain reactions, and channeling intracellular signaling in eukaryotic cells.

Previous studies have constructed synthetic systems that undergo clustering behavior by fusing an IDR domain to an oligomerizing protein. One such IDR domain that has been incorporated into synthetic clustering systems is the N-terminal of the FUS, an RNA-binding protein involved in DNA repair, transcription, and pre-mRNA splicing. Shin et al. developed a light-induced clustering system by constructing a fusion protein that consists of a FUS domain and a Cry2 domain, where Cry2 is a light-sensitive protein that self-associates with light exposure (46).

Researchers have since applied this clustering mechanism to the context of controlling metabolic fluxes. Zhao et al. applied phase separation to microbial synthesis as a method for clustering heterologous pathway enzymes to mitigate side-product formation in the deoxyviolacein pathway. The deoxyviolacein pathway contains a branchpoint at which the product of the VioE-catalyzed reaction can either be converted to deoxyviolacein by VioC or to prodeoxyviolacein non-enzymatically. With the goal of selectively producing deoxyviolacein, they constructed two fusion proteins consisting of a light-sensitive oligomerizing domain, an N-terminal FUS domain, and an enzymatic domain, where the enzymatic domains in the two proteins are VioE and VioC. Induction of clustering in this system resulted in an 18.4-fold increase in ratio of the desired to undesired product, demonstrating that phase separation is a viable method of metabolic flux control (31).

The goal of this study was to develop a QS-based system for protein co-localization that can be used to facilitate co-localization of enzymes for dynamic metabolic flux control. LasR is a transcriptional regulator in the *las* QS circuit that dimerizes in the presence of its cognate signaling molecule, *N*-(3-oxododecanoyl)-L-homoserine lactone (3OC12HSL). Construction of a fusion protein that contain a LasR domain, an IDR, and a fluorescent protein domain and image analysis to visualize the GFP distribution within cells showed 3OC12HSL-dependent clustering of the fusion protein. This behavior is consistent with what is expected based on the current understanding of dynamic phase separation systems. Interestingly, culturing cells expressing the fusion with 3OC12HSL added at inoculation results in a burdened growth phenotype, motivating the construction of a system which gradually accumulates 3OC12HSL. Incorporation of an AHL synthase expression library resulted in varying levels of clustering and growth burden. By inserting enzymatic domains in place of the GFP domain, this system can be used to autonomously control metabolic fluxes.

4.2. Materials and methods

All strains and plasmids used in this study are summarized in Table 4-1 and 4-2, respectively. Sequences for promoters and RBS sequences are provided in Appendix Table 5 and primer sequences are provided in Appendix Table 6. For plasmid construction and gene/genome editing, cells were cultured in Luria-Bertani (LB) broth at either 30 and 37 °C. Temperature-sensitive plasmids were cured at 42 °C.

Table 4-1. All strains and corresponding genotypes relevant in Chapter 4.

The generalized denotation and genotype of strains containing esaI expression cassettes with different promoter and/or RBS sequences is given as "LXX" for esaI.

Strain	Genotype	Description
LXX	MG1655 *186::LXX-esaI HK022::apFAB104-esaR*	Gupta et al. (2017)(15)
MG1655(DE3)-LXXlasI	MG1655(DE3) *186::LXX-lasI*	MG1655(DE3) with *lasI* driven by a specific promoter and RBS, generalized as LXX here (Appendix Table 5)
NST74	*aroH367, tyrR366, tna-2, lacY5, aroF394^{fbr}, -malT384, pheA101^{fbr}, pheO352, aroG397^{fbr}*	Tribe (1987)(67)

Table 4-2. Summary of plasmids used in Chapter 4.

Plasmid	Functional Genotype	Source
pCOLA-*4CL*	*4CL* (*Petroselinum crispum*) under T7 promoter	Chapter 3
pCOLA-*FUS4CL*	*lasR-FUS-4CL* fusion under T7 promoter	This study
pCOLA-*TAL-4CL*	*TAL* (*Rhodotorula glutinis*) and *4CL* (*Petroselinum crispum*) under P_{trc} promoters	Chapter 3
pCOLA-*TAL-FUS4CL*	*TAL* (*Rhodotorula glutinis*) and *lasR-FUS-4CL* fusion under P_{trc} promoters	This study
pET-*CHS-CHI*	*CHS* (*Petunia hybrida*) and *CHI* (*Medicago sativa*) under T7 promoters	Table 2-2
pET-*FUSCHS-CHI*	*lasR-FUS-CHS* fusion and *CHI* (*Medicago sativa*) under T7 promoters	Table 2-2
pCOLA-P_{trc}-*TAL*	*TAL* (*Rhodotorula glutinis*) under trc promoter	This study
pTrc-*tyrA*	*tyrA* (*E. coli*) under P_{trc} promoter	This study
pTrc-*FUStyrA*	*lasR-FUS-tyrA* fusion under P_{trc} promoter	This study
pro4IUP	*ck* (*Saccharomyces cerevisiae*), *ipk* (*Arabidopsis thaliana*), and *idi* (*E. coli*) operon expressed from the constitutive pro4 promoter	Chatzivasileiou et al. (2019) (93)
pro4-*ipk-ck*	*ck* (*Saccharomyces cerevisiae*) and *ipk* (*Arabidopsis thaliana*) operon expressed from the constitutive pro4 promoter	This study
pAC-LYCipi	*crtE, idi, crtB,* and *crtI* expressed from their native promoters from *Ewinia herbolica*	Cunningham et al. (2007) (94)

pACYC-*crtB-crtI*	*crtB* and *crtI* in an operon expressed under the T7 promoter	This study
pCDF-*idi-crtE*	*idi* and *crtE* expressed under T7 promoters	This study
pCDF-*FUSidi-crtE*	*lasR-FUS-idi* fusion and *crtE* under T7 promoters	This study
pCDF-*idi-FUScrtE*	*idi* and *lasR-FUS-crtE* fusion under T7 promoters	Table 2-2
pCDF-*FUSidi-FUScrtE*	*lasR-FUS-idi* and *lasR-FUS-crtE* fusions under T7 promoters	Table 2-2
pOSIP-KO	Vector for integration into the 186 locus	St. Pierre et al. (2013)(68)
pTet-FLP	*FLP* recombinase expressed from the Tet promoter	Modified from St. Pierre et al. (2013)(68)
pTrc-FUSGFP	*lasR-FUS-GFP* fusion expressed from the P_{trc} promoter	This study
pSB1A2-P_{con}-*lasR*-P_{las}-GFP	*lasR* under a constitutive promoter and GFP under the P_{las} promoter	Shiue (2014)(73)

4.2.1. Strain construction

Genomic integrations

A five-member *lasI* expression library was constructed using overlap extension PCR to join a promoter-RBS fragment, a *lasI* gene fragment, and a terminator fragment, and integrated into the 186 locus of BL21(DE3) using "clonetegration" (68). The primer pairs: CD_180 and CD_188, CD_180 and CD_181, CD_180 and CD_69, CD_74 and CD_188, CD_68 and CD_188, and CD_68 and CD_181 were used to amplify the promoter-RBS sequences from L1, L3, L5, L20, L26, and L28(15) to construct L1-*lasI*, L3-*lasI*, L5-*lasI*, L20-*lasI*, L26-*lasI*, and L28-*lasI*, respectively. The *lasI* gene fragment was amplified from the *Pseudomonas aeruginosa* genome using CD_189 and CD_36 for L1, L20, and L26, CD_182 and CD_36 for L3 and L28, and CD)70 and CD_36 for L5. The terminator fragment was amplified from pSB1S2-P_{con}-*lasR*-P_{las}-GFP using CD_37 and CD_71. The overlap extension PCR products were digested with KpnI and PstI and ligated into pOSIP-KO for transformation into MG1655(DE3). The phage integration genes and antibiotic resistance cassette were cured by transforming with the pE-FLP plasmid yielding the MG1655(DE3)-LXXlasI strain series.

GFP fusion plasmid

The expression cassette for the GFP fusion protein was constructed using overlap extension PCR to join a *lasR* domain, a N-terminal *FUS* domain, and a GFP domain. The *lasR* and GFP fragments were amplified from pSB1A2-P_{con}-*lasR*-P_{las}-GFP using primers PS_8 and PS_9, and PS_11 and PS_14, respectively. The FUS domain was amplified from a synthesized DNA fragment codon-optimized for *E. coli* (Appendix Table 10). The overlap extension PCR product was cloned into the multiple cloning site of the pTrc99A backbone using restriction digestion and ligation, yielding pTrc-FUSGFP.

Naringenin pathway plasmids

The pCOLA-*FUS4CL* plasmid was constructed using Golden Gate Assembly. Primers PS_nar1, PS_nar2, PS_nar5, and PS_nar6 were used to amplify fragments from pCOLA-*4CL*. Primers

PS_nar3 and PS_nar4 were used to amplify the *las-FUS* fragment from pTrc-*FUSGFP*. pET-*FUSCHS-CHI* was constructed by digesting pET-duet using NcoI and AvrII and using the digested product along with custom synthesized fragments *FUSCHSCHI1*, *FUSCHSCHI2*, and *FUSCHSCHI3* in a Gibson Assembly reaction (Appendix Table 10).

p-Coumaric acid/cinnamic acid plasmids

The pCOLA-P_{trc}-*TAL* plasmid was constructed using Golden Gate Assembly. Primers Trc_TAL1/2, Trc_TAL3/4, and Trc_TAL5/6 were used to amplify DNA fragments from pCOLA-duet, pTrc99A, and pETM6-*TAL*(22), respectively. The pTrc-*tyrA* plasmid was constructed by amplifying *tyrA* from the pY3 plasmid (95) using primers TyrA_fwd and PS_19 and inserting into the pTrc99A backbone using restriction digestion and ligation. The pTrc-*FUStyrA* plasmid was constructed using restriction digestion and ligation of the pTrc99A backbone with an insert prepared via overlap extension PCR. The overlap extension PCR product was constructed from DNA fragments using primers PS_8/22 to amplify the *lasR-FUS* sequence from pTrc-FUSGFP and primers PS18/19 to amplify *tyrA* from pY3 (95).

Lycopene pathway plasmids

The pACYC-*crtB-crtI* plasmid was constructed by amplifying the *crtB-crtI* operon from the pAC-LYCipi plasmid using LYC_25 and LYC_26 and inserting into the pACYC-duet backbone by restriction digestion and ligation. The pro4-*ipk-ck* plasmid was constructed using Gibson Assembly of DNA fragments amplified from pro4IUP using primers IUP_GA1 and IUP_GA2, IUP_GA3 and IUP_GA4, and IUP_GA5 and IUP_GA6. The plasmid pCDF-*idi* was constructed by amplifying *idi* from pro4IUP using primers LYC_1 and LYC_2 and inserting into MCS2 of pCDF-duet using Gibson Assembly with a linearized pCDF-duet backbone. The plasmid pCDF-*crtE* was constructed by amplifying *crtE* from pAC-LYCipi using primers LYC_3 and LYC_4 and inserting into MCS1 using Gibson Assembly with a linearized pCDF-duet backbone. The plasmid pCDF-*FUSidi* was constructed by amplifying *lasR* and *FUS* from custom synthesized gBlocks using primers LYC_12/13 and LYC_14/15, respectively and amplifying *idi* from pro4IUP using LYC_16 and LYC_2 and assembling into MCS2 of pCDF-duet using Gibson Assembly. The

plasmid pCDF-*FUScrtE* was constructed by amplifying *lasR* and *FUS* from custom synthesized gBlocks using primers LYC_12b/13 and LYC_14/17, respectively and amplifying *crtE* from pAC-LYCipi using LYC_18 and LYC_14 and assembling into MCS1 of pCDF-duet using Gibson Assembly. The plasmids pCDF-*idi-crtE*, pCDF-*FUSidi-crtE*, pCDF-*idi-FUScrtE*, and pCDF-*FUSidi-FUScrtE* were constructed using Golden Gate Assembly. The pCDF backbone was amplified using primers LYC_19 and LYC_20, the *crtE* or *FUScrtE* expression cassette was amplified using primers LYC_21 and LYC_22, and the *idi* or *FUSidi* expression cassette was amplified using primers LYC_23 and LYC_24.

4.2.2. Culturing and fermentation

Imaging experiments

Individual colonies were inoculated in LB medium and grown overnight at 30 °C. 3 mL cultures were inoculated from these seeds at OD_{600} 0.05 and incubated at 30 °C and 80% humidity with 250 rpm shaking in LB medium. The medium was supplemented with 100 µg/mL carbenicillin for plasmid maintenance and 100 µM IPTG for induction gene expression from the pTrc99A plasmid.

Growth characterization

Growth characterization was conducted using the BioLector microbioreactor system (m2p-labs, Baesweiler, Germany). Individual colonies were inoculated in LB medium and grown overnight at 30 °C. 1 mL cultures were inoculated from these seeds at OD_{600} 0.05 into BioLector 48-well flower plates and incubated at 30 °C, 120 rpm (3 mm orbit), and 80% relative humidity. The plate was sealed with a gas-permeable sealing foil (m2p-labs). Cultures were monitored for OD (BioLector units) over time.

Fermentations

Naringenin and *p*-coumaric acid/cinnamic acid production trials were performed in a glass vial with 5 mL working volume at 30 °C and 80% humidity with 250 rpm shaking in modified MOPS minimal medium containing 5 g/L D-glucose, 500 mg/L tyrosine, 4 g/L NH_4Cl, 1 g/L K_2HPO_4, 2 mM $MgSO_4$, 0.1 mM $CaCl_2$, 40 mM MOPS, 4 mM Tricine, 50 mM NaCl, 100 mM Bis-Tris, 143 uM EDTA, 31 uM $FeCl_3$, 6.2 uM $ZnCl_3$, 0.76 uM $CuCl_2$. 0.42 uM $CoCl_2$, 1.62 uM H_3BO_3 and 0.081 uM $MnCl_2$. For strains containing plasmids with pET, pCOLA, and pACYC vector backbones, the medium was also supplemented with 100 μg/mL carbenicillin, 50 μg/mL kanamycin, and 34 μg/mL chloramphenicol, respectively, for plasmid maintenance. Individual colonies were initially inoculated in 3 mL of LB medium at 30 °C for ~6 h. These were used to inoculate working cultures at OD_{600} 0.1 in modified MOPS medium. Samples were taken periodically for quantification of cell density and extracellular metabolites. Fermentations were carried out for 48 h.

Lycopene production trials were performed in a glass vial with 5 mL working volume at 37 °C and 80% humidity with 250 rpm shaking in LB medium. For strains containing plasmids pro4IUP, pCDF, and pACYC vector backbones, the medium was also supplemented with 50 μg/mL kanamycin, 50 μg/mL streptomycin, and 34 μg/mL chloramphenicol, respectively, for plasmid maintenance. Individual colonies were initially inoculated in 3 mL of LB medium with the appropriate antibiotics and 100 μM IPTG to express genes from the pACYC and pCDF backbones at 37 °C for ~6 h. These were used to inoculate working cultures at OD_{600} 0.1 in LB medium. When samples reached OD_{600} 0.5, 25 mM isoprenol was added to the medium. Samples were taken periodically for quantification of cell density and extracellular metabolites. Fermentations were carried out for 48 h.

4.2.3. Microscopy

Approximately 3 μL of cell culture was placed on microscope glass coated with a thin agarose pad (1 % w/v agarose). A coverslip was added and the cells were left for ~5 min so they were immobilized. All imaging was carried out using a 100x oil immersion objective on a Zeiss

AxioVert 200M inverted microscope with a Yokogawa CSU-22 spinning disk confocal scan head, a Hamamatsu Orca-ER cooled CCD camera and appropriate laser lines, dichronics and filters.

4.2.4. Quantification of metabolites

p-Coumaric acid, cinnamic acid and naringenin titers were quantified as previously described in Section 2.2.3.

Relative lycopene levels were estimated by measuring the absorbance of cell lysates at a wavelength of 475 nm. Lysates were prepared by pelleting 1 mL of the culture at maximum speed for 5 min, removing the supernatant, adding 1 mL of methanol and incubating in a 100 °C water bath until the pellet appears to be white. These samples were then spun down at maximum speed for 10 min and the supernatant was transferred to a cuvette for the absorbance measurement.

4.3. Results

4.3.1. Construction of a QS-mediated clustering system

In natural phase separation systems, phase separation is triggered by biomolecular binding events that increase the local concentration of proteins that contain an IDR. One such method is oligomerization of these proteins. Since some QS transcription factors regulate gene expression by assembling or disassembling in the presence of its cognate signaling molecule, we can construct synthetic clustering systems by fusing these transcription factors to IDRs. The *las* QS circuit contains a LasR transcription factor that dimerizes in the presence of *N*-(3-Oxododecanoyl)-L-homoserine lactone (C12-AHL). The resulting fusion protein contained a LasR dimerizing domain, an IDR domain taken from the N-terminal region of FUS, and a GFP domain for visualization of clustering events. Since the ligand-binding domain on the N-terminus of LasR must be retained, the FUS and GFP domains were appended to the C-terminal DNA binding domain of LasR (Figure 4-1A). The resulting plasmid (pTrc-FUSGFP) was transformed into MG1655 and cultures were grown with and without C12-AHL and imaged using confocal microscopy at mid-exponential

phase. These images revealed that cells grown without C12-AHL contained no detectable clusters characterized by regions within the cell with significantly higher GFP fluorescence levels, whereas cells grown with C12-AHL contained multiple clusters (Figure 4-1B-C). Growth rate characterization of these cultures showed that induction of clustering at inoculation results in significant growth burden (Figure 4-1D). Based on this finding along with the observation that clustering results in filamentous cell structures, we suspect that clustering could be interfering with cell division processes.

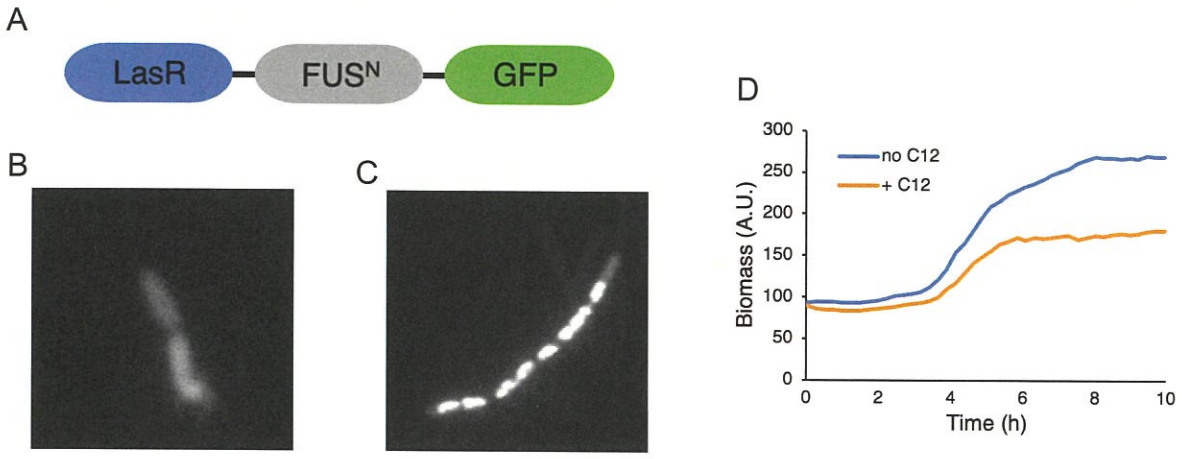

Figure 4-1. Characterization of LasR-mediated clustering.
(**A**) Structure of the fusion protein. LasR is present at the N-terminal of the fusion protein to preserve the ligand-binding domain and is tagged with an IDR sequence and GFP. Each domain is separated by a GSGS linker. (**B**) Representative image of a cell expressing the fusion protein grown without C12-AHL. There are no apparent clusters. (**C**) Representative image of a cell expressing the fusion protein grown with C12-AHL. Multiple clusters, characterized by regions of high GFP fluorescence levels, are present. (**D**) Representative growth curves of cultures growth with and without C12-AHL. Samples with induced clustering exhibit a burdened growth phenotype.

This growth effect can be addressed by delaying cluster formation. We can achieve dynamic and autonomous control by expressing the synthase for C12-AHL, *lasI*. A library of *lasI* expression levels was integrated into MG1655 and the resulting strains were transformed with pTrc-FUSGFP. Confocal imaging showed that every *lasI* expression level tested led to cluster formation and the degree of clustering generally correlates with the *lasI* expression level (Figure 4-2A). Although clusters are present, the shape of the cells induced with endogenous C12-AHL are more similar to

that of wild-type *E. coli.* Additionally, periodic biomass measurements showed that dynamic induction of cluster formation can partially restore growth rates (Figure 4-2B).

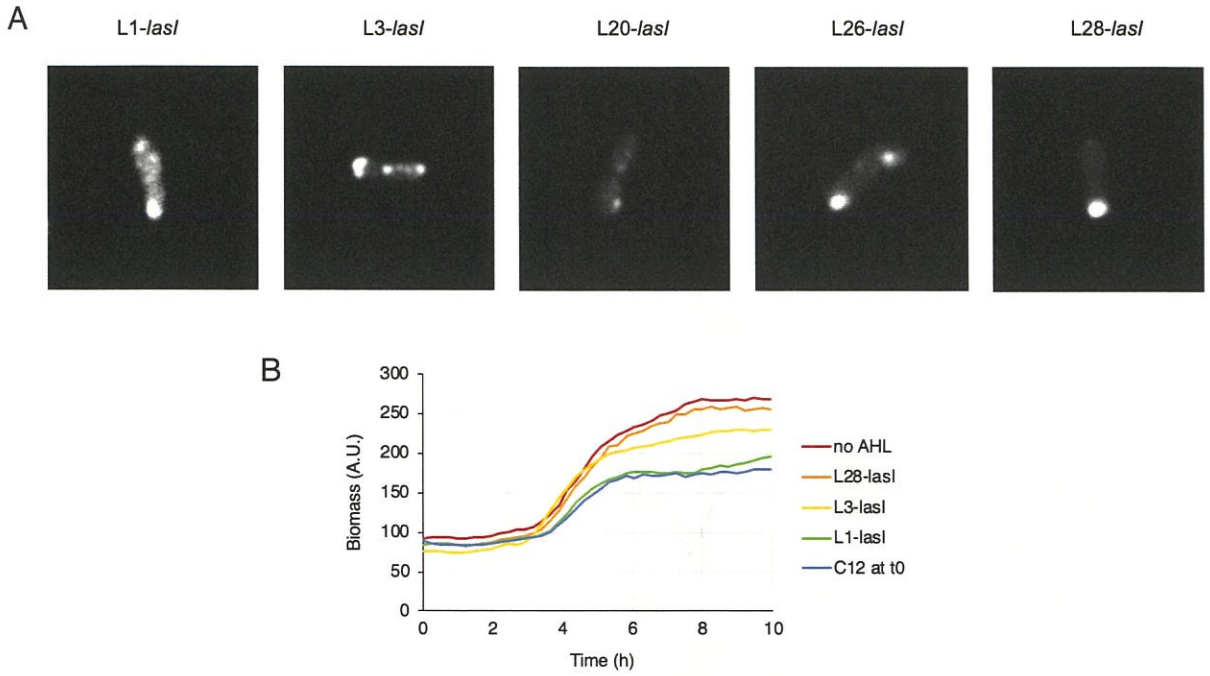

Figure 4-2. Characterization of strains containing autonomously induced clusters.
(**A**) Representative images of cells containing autonomously induced clusters. The predicted *lasI* expression levels decrease from left to right. Clustering is observed with all *lasI* expression levels tested. The degree of clustering observed at mid-exponential phase roughly correlates with the predicted *lasI* expression level. Increasing *lasI* expression corresponds to more clustering. (**B**) Growth curves of strains containing autonomously induced clusters. AHL accumulation occurs earlier from top to bottom. The time at which clustering is induced influences the growth profile.

4.3.2. Characterization of enzyme activity in tagged and clustered forms

The clustering system was then applied to regulating metabolic fluxes in three different pathway contexts in attempts to improve production. For the first implementation, we envisioned increasing selectivity for *p*-coumaric acid over cinnamic acid by shifting from both tyrosine and phenylalanine production to only tyrosine production in a strain expressing tyrosine ammonia lyase (*TAL*), which takes either tyrosine or phenylalanine as substrates to produce *p*-coumaric acid and cinnamic acid, respectively. To accomplish this regulation scheme, the goal was to co-localize chorismate synthase (AroC) and prephenate dehydrogenase (TyrA) by expressing the fusions *lasR*-

FUS-aroC and *lasR-FUS-tyrA* in a phenylalanine producer strain and stimulating enzyme clustering with C12-AHL. The first step was to construct the fusion enzyme constructs to test for enzyme activity with and without C12-AHL induction. A phenylalanine producer strain (NST74) (67) was transformed with pCOLA-P_{trc}-*TAL* in addition to pTrc-*tyrA* or pTrc-*FUStyrA*. Expression of all genes was induced at inoculation with 100 μM IPTG and the strain containing pTrc-*FUStyrA* was inoculated both with and without C12-AHL. Characterization of these samples shows that expression of *tyrA* or *FUStyrA* both result in an increase in ratio of *p*-coumaric acid to cinnamic acid, but induction of clustering with C12-AHL addition results in a complete loss of TyrA activity (Figure 4-3).

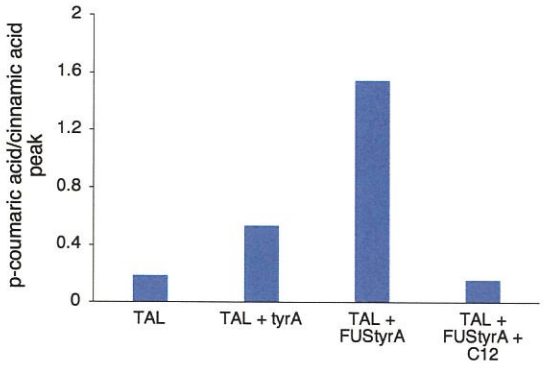

Figure 4-3. *p*-Coumaric acid and cinnamic acid production with different forms of prephenate dehydrogenase. All test strains express *TAL* in a phenylalanine producer background. *tyrA* expression results in an increase in the relative level of *p*-coumaric acid production and expression of the *lasR-FUS-tyrA* fusion (FUStyrA) results in an even greater increase, confirming that tagged TyrA retains activity. Addition of C12-AHL to the sample expressing tagged *tyrA* results in a complete loss of TyrA activity.

The second application sought to improve naringenin production by accelerating coumaryl-CoA consumption through co-localization of the enzymes responsible for coumaryl-CoA production and consumption, 4-coumaryl-CoA ligase (4CL) and chalcone synthase (CHS), respectively. Previous characterization of the naringenin pathway suggests that inhibition of the first pathway enzyme, tyrosine ammonia lyase (TAL), by coumaryl-CoA is a major limitation to efficient naringenin production that can be addressed by delaying production of coumaryl-CoA(12, 96). While effective, this approach is limited by the period of low pathway flux at the beginning of the fermentation, motivating this alternative strategy. Again, the activity of tagged and clustered 4CL and CHS were each evaluated by quantification of naringenin titers. To evaluate 4CL activity, BL21(DE3) was transformed with pCOLA-*4CL* or pCOLA-*FUS4CL* and pET-*CHS-CHI* and

strains were cultured with 0.6 mM *p*-coumaric acid, 100 μM IPTG, and with and without C12-AHL. Expression of *FUS4CL* leads to *p*-coumaric acid consumption and naringenin production levels that are comparable to the corresponding strain expressing untagged *4CL*. Induction of clustering with addition of C12-AHL results in about a 50% decrease in naringenin titer (Figure 4-4A). To evaluate the activity of tagged and clustered CHS, BL21(DE3) was transformed with pCOLA-*4CL* and pET-*CHS-CHI* or pET-*FUSCHS-CHI* and strains were incubated with 0.6 mM of *p*-coumaric acid, 100 μM IPTG to induce gene expression, and with and without C12-AHL. Tagged CHS resulted in a significant decrease in naringenin titer compared to corresponding strain expressing untagged CHS and induction of clustering results in a further reduction in naringenin titer (Figure 4-4B).

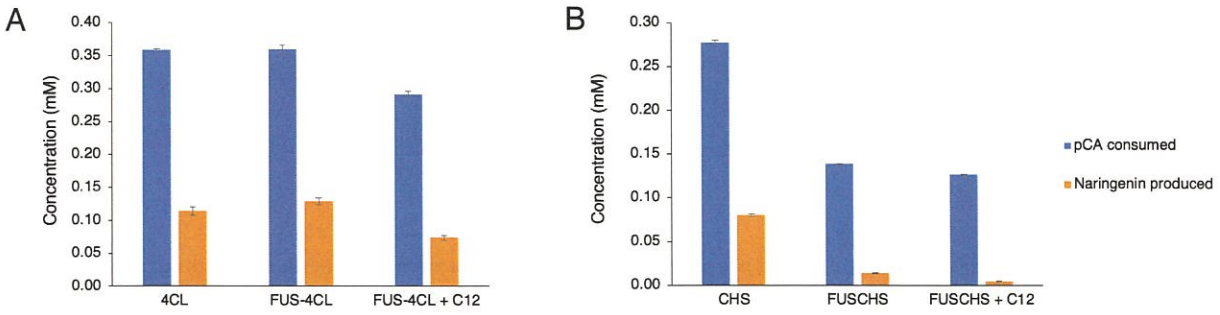

Figure 4-4. *p*-Coumaric acid consumed and naringenin titers with 4CL and CHS variants.
All samples express tagged or untagged *4CL*, tagged or untagged *CHS*, and untagged CHI. 0.6 mM of *p*-coumaric acid was added at inoculation. (**A**) Characterization of 4CL variants. Appending a *lasR-FUS* tag on the N-terminus of 4CL does not significantly impact the amount of *p*-coumaric acid consumed or naringenin produced, but induction of clustering results in about a 50% decrease in naringenin titer. (**B**) Characterization of CHS variants. Appending a *lasR-FUS* tag on the N-terminus of CHS results in a significant decrease in both *p*-coumaric acid consumption and naringenin production and induction of clustering leads to an even greater reduction in both. Error bars represent s.d. of triplicate trials.

The third application aimed to improve isoprenoid production by addressing a pathway bottleneck. Isoprenoids are produced through condensation of isopentyl diphosphate (IPP) and its isomer dimethylallyl diphosphate (DMAPP). The isopentenol utilization pathway (IUP) is a promising new method for isoprenoid production that converts isoprenol to IPP using two enzymatic steps(93). However, characterization of metabolite pools shows significant IPP and DMAPP accumulation even in the presence of the lycopene pathway. Kang et al. (2019) developed an

enzyme assembly system, to co-localize the enzymes responsible for producing and consuming IPP and DMAPP, isopentenyl diphosphate isomerase (Idi) and geranylgeranyl diphosphate synthase (CrtE), respectively(97). Their assembly system involved construction of fusion proteins containing one of two enzymatic domains and one of two assembly domains. The assembly domains bind to one another in a defined ratio and orientation, resulting in multi-enzyme complexes which facilitate fast consumption of IPP and DMAPP. Co-localization of these enzymes led to a two-fold increase in the intermediate geranylgeranyl pyrophosphate (GGPP), the product of the CrtE-catalyzed reaction. This led to significant improvements in carotenoid production over controls expressing only free enzymes.

This study sought to apply the QS-mediated clustering system to accelerate IPP and DMAPP consumption to improve lycopene production via the IUP. The lycopene production system consists of three plasmids: pro4-*ipk-ck* expresses *ipk* encoding isopentenyl phosphate kinase and *ck* encoding choline kinase in an operon from a constitutive promoter; pCDF-*(FUS)crtE-(FUS)idi* expresses *idi* and *crtE* in all combinations of each gene in both tagged and untagged forms from their own T7 promoters; and pACYC-*crtB-crtI* expresses *crtB* encoding phytoene synthase and *crtI* encoding phytoene desaturase in an operon from a T7 promoter. Expression of *lasR-FUS-idi* did not significantly impact lycopene production both with and without induction of clustering. However, expression of *lasR-FUS-crtE* resulted in undetectable lycopene production levels. Induction of cluster formation led to a decrease in the final cell density of both samples expressing *lasR-FUS-idi* and *lasR-FUS-crtE* even though C12 was added at mid-exponential phase (Figure 4-5).

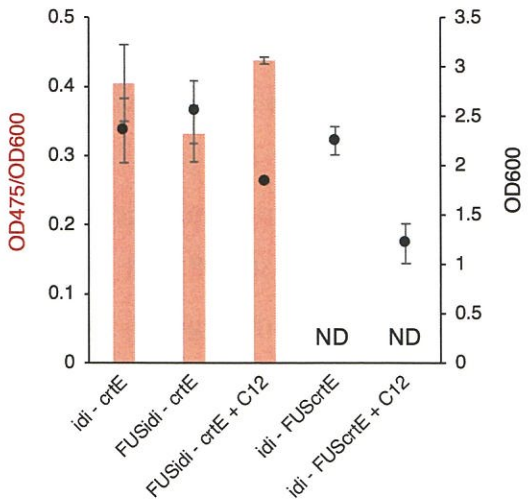

Figure 4-5. Relative lycopene production and cell density of samples expressing different *idi* and *crtE* variants. Expression of *lasR-FUS-idi* both with and without induction of clustering does not hinder lycopene production compared to the corresponding strain expressing untagged *idi*. Expression of *lasR-FUS-crtE* leads to a significant decrease in lycopene production. Induction of clustering results in a decrease in the final cell density. Error bars represent s.d. of triplicate trials.

4.3.3. Characterization of lycopene production with enzyme co-localization

Although incorporation of the LasR-FUS tag significantly hinders CrtE activity, we evaluated the effect of co-localization on lycopene production by testing strains expressing both tagged *idi* and *crtE*. Induction of clustering by addition of exogenous C12-AHL at mid-exponential phase resulted in a greater-than 20-fold increase in lycopene production, confirming that enzyme co-localization can partially restore lycopene production. Evaluation of this production system in the MG1655(DE3)-LXX*lasI* strain series showed that induction of cluster formation with endogenous C12-AHL can provide a similar improvement in lycopene production compared to the exogenous C12-AHL control. The best lycopene production resulted from an intermediate *lasI* expression level and in general, earlier induction of clustering with higher *lasI* expression levels leads to lower final cell densities (Figure 4-6).

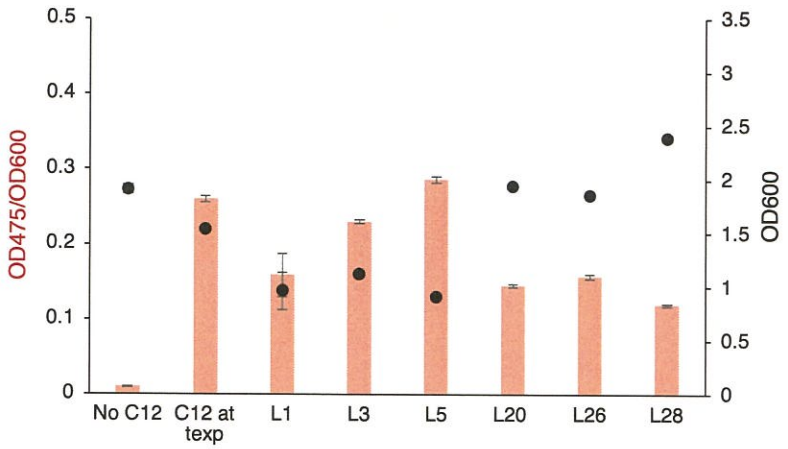

Figure 4-6. Relative lycopene production and cell density of samples expressing *FUSidi* and *FUScrtE* with exogenous and endogenous C12-AHL.
Induction of clustering with exogenous C12-AHL at mid-exponential phase results in a greater-than 20-fold increase in lycopene production. Endogenous induction of clustering with varying *lasI* expression levels (labeled LXX, decreasing predicted expression from left to right) results in improved lycopene production compared to the no-C12-AHL control. In general, increasing *lasI* expression, which corresponds to earlier induction of clustering, leads to a decrease in the final cell density. Error bars represent s.d. of triplicate trials.

4.4. Conclusions

In summary, a QS-mediated system for protein co-localization was constructed and characterized. Induction of cluster formation at inoculation was found to cause a growth burden, which can be relieved by delaying induction of cluster formation through expression of AHL synthase. Studies of enzymatic activity when pathway enzymes are tagged and clustered revealed that application to metabolic flux control is limited by the impact of the large tag on the enzyme activity of CHS and CrtE. TyrA showed a loss of enzyme activity with the induction of clustering, although the tagged variant retained activity. Application of the strategy to lycopene production shows how dynamic enzyme co-localization can be used to improve production by addressing a low-activity enzyme, but broad implementation of this system will rely on protein engineering efforts to decrease the size of the protein tag.

5. Characterization of other quorum-sensing circuits

Abstract

Prior to characterizing the *lux* QS system, circuits based on QS systems that do no share a signaling molecule with the *esa* QS system were constructed and characterized. This chapter summarizes the results from characterization of the *lsr* and *las* QS circuits.

5.1. Introduction

In addition to the *lux* and *esa*-based QS circuits described in Chapter 2, ones based on the *lsr* and *las* QS systems were also characterized. These QS circuits were selected as ones expected to show improved orthogonality to the *esa* QS system.

The *lsr* system is an autoinducer-2 (AI-2)-based QS system that is native to *E. coli*. Since the chemical structure of AI-2 is completely different from that of AHL (or AI-1), the *lsr* QS circuit should be completely orthogonal to any AHL-based QS system. The *lsr* QS system contains a regulator protein, LsrR, which represses expression from the P_{lsr} promoter and is released from the promoter upon binding to phosphorylated AI-2. In addition to these circuit components, AI-2 is exported through transporter protein, TqsA, transported into the cell through a complex composed of LsrACDB, phosphorylated by LsrK, and degraded by LsrF and LsrG (98). In the native *E. coli* system, all these components except the exporter are controlled under the P_{lsr} promoter. Additionally, *E. coli* produces AI-2 through two enzymatic conversions by Pfs and LuxS from *S*-adenosyl homocysteine to make dihydroxypentanedione (DPD), which spontaneously cyclizes to form AI-2 (99). In *E. coli*, the *lsr* system is subject to carbon catabolite repression at two different levels: expression from the P_{lsr} promoter relies on cAMP-CRP activation (100) and LsrR loses its DNA-binding ability through interaction with the phosphotransferase system protein HPr (101).

The *las* QS system is a *lux*-type QS circuit that responds to the signaling molecule, *N*-(3-oxododecanoyl)-L-homoserine lactone (3OC12HSL). The regulator protein, LasR, dimerizes in the presence of 3OC12HSL to activate transcription from the P_{las} promoter. Whereas the *lux* and *esa* QS system share a signaling molecule, the *las* QS system responds to a different, but similar AHL, possibly allowing for improved independent tunability between the individual circuits. The *las* QS system was characterized in combination with the *esa* QS system containing the P_{esaS} promoter and the *lux* QS system. In contrast to the QS promoters discussed thus far, the P_{esaS} promoter turns transcription from ON to OFF with increasing cell density as unbound EsaR activates expression from P_{esaS}.

5.2. Materials and Methods

All strains and plasmids used in this study are summarized in Table 5-1 and Table 5-2, respectively. Sequences for promoters and RBS sequences are provided in Appendix Table 7 and primers are provided in Appendix Table 8. For plasmid construction and gene/genome editing, cells were cultured in Luria-Bertani (LB) broth at either 30 and 37 °C. Temperature-sensitive plasmids were cured at 42 °C.

Table 5-1. All strains and corresponding genotypes relevant in Chapter 5.

The generalized denotation and genotype of strains containing *esaI* expression cassettes with different promoter and/or RBS sequences is given as "LXX" for *esaI* and *lasI*.

Strain	Genotype	Description
LXXesaI	MG1655 *186::LXX-esaI*	MG1655 with *esaI* driven by a specific promoter and RBS, generalized as LXX here (Appendix Table 7)
LXXlasI	MG1655 *HK022::LXX-lasI*	MG1655 with *lasI* driven by a specific promoter and RBS, generalized as LXX here (Appendix Table 7)
LXXesaI-LXXlasI	MG1655 *186::LXX-esaI HK022::LXXlasI*	MG1655 with *esaI* and *lasI* driven by their own specific promoter and RBS, generalized as LXX here (Appendix Table 7)
LXXesaI/luxR-LXXlasI/R	MG1655 *186::LXX-esaI Phi80::P_{con}-luxR HK022::LXXlasI P21::P_{con}-lasR*	MG1655 with *esaI* and *lasI* driven by their own specific promoter and RBS, generalized as LXX here and *luxR* and *lasR* under constitutive promoters (Appendix Table 7)

Table 5-2. Summary of plasmids used in Chapter 5.

Plasmid	Functional Genotype	Source
pSB3K3-P_{esaR}-GFP-P_{con}-esaR	*esaRI70V* under a constitutive promoter and GFPmut3b under the P_{esaR} promoter	Gupta et al. (2017)(15)
pSB3K3-P_{esaS}-GFP(LVA)-P_{con}-esaR	*esaRI70V* under a constitutive promoter and GFPmut3b under the P_{esaS} promoter	Gupta et al. (2017)(15)
pSB3K3-P_{lsr}-GFP-P_{con}-lsrR	*lsrR* under a constitutive promoter and GFPmut3b under the P_{lsr} promoter	This study
pSB1A2-P_{las}-GFP-P_{con}-lasR	*lasR* under a constitutive promoter and GFPmut3b under the P_{las} promoter	Shiue (2014) (73)
pSB3K3-P_{las}-GFP-P_{con}-lasR	*lasR* under a constitutive promoter and GFPmut3b under the P_{las} promoter in the pSB3K3 backbone	This study
pSB3K3-P_{las}-mCherry-P_{esaS}-GFP(LVA)	*lasR* under a constitutive promoter, esaRI70V under a constitutive promoter, mCherry under the P_{las} promoter, and GFP(LVA) under the P_{esaS} promoter	This study
pCOLA-P_{lux}-mCherry	mCherry under the P_{lux} promoter	Table 2-2
pOSIP-KO	Vector for integration into the 186 locus	St. Pierre (2013)(68)
pOSIP-KH	Vector for integration into the HK022 locus	St. Pierre (2013)(68)
pOSIP-CT	Vector for integration into the P21 locus	St. Pierre (2013)(68)
pOSIP-KP	Vector for integration into the Phi80 locus	St. Pierre (2013)(68)
pE-FLP	FLP recombinase under a constitutive promoter	St. Pierre (2013)(68)

5.2.1. Strain construction

Synthase expression library integrations

The *lasR* expression cassette was integrated into the genome under one constitutive promoter (BBa_J23100) by inserting the desired *lasR* cassette into the pOSIP-CT backbone using restriction digestion and ligation. The ligation product was used to transform *E. coli* strain MG1655 for integration into the P21 locus, yielding MG1655-lasR. The *luxR* expression cassette was integrated into the genome under one constitutive promoter (BBa_J23105) by inserting the desired *luxR* cassette into the pOSIP-KP backbone using restriction digestion and ligation. The ligation product was used to transform *E. coli* strain MG1655-*lasR* for integration into the Phi80 locus, yielding MG1655-lasR/luxR. The *esaI* expression cassette was integrated into the genome under two different constitutive synthetic promoters (denoted L19esaI and L24esaI) (15). Integration was performed via "clonetegration" (68). The desired *esaI* expression cassette was inserted into the pOSIP-KO backbone using restriction digestion and ligation. The ligation product was used to transform *E. coli* strain MG1655 or MG1655-*lasR/luxR* for integration into the 186 locus, yielding MG1655-lasR/luxR/LXXesaI. The *lasI* expression cassette was integrated into the genome under a library of several different constitutive synthetic promoters (denoted LXXlasI) (15) using "clonetegration". The desired *lasI* expression cassette was inserted into the pOSIP-KH backbone using restriction digestion and ligation. The ligation production was used to transform *E. coli* strains MG1655, MG1655-LXXesaI, and MG1655-lasR/luxR/LXXesaI for integration into the HK022 locus, yielding LXXlasI, LXXesaI-LXXlasI, and LXXesaI/luxR-LXXlasI/R, respectively. The phage integration genes and antibiotic resistance cassette were cured by transforming with the pE-FLP plasmid between each subsequent integration.

Fluorescence characterization of QS circuits

The plasmid pSB3K3-P_{lsr}-GFP-P_{con}-*lsrR* was constructed by restriction digestion and ligation of an overlap extension PCR product and the pSB3K3 backbone. The overlap extension PCR product was assembled from three DNA fragments – GFPmu3b was amplified from pSB3K3-P_{esaR}-GFP-P_{con}-*esaR* using primers CD_001 and CD_007 and the P_{lsr} promoter and *lsrR* gene were amplified from the *E. coli* genome using CD_002 and CD_003, and CD_004 and CD_005, respectively.

The plasmid pSB3K3-P_{las}-GFP-P_{con}-*lasR* was constructed by amplifying the P_{las}-GFP-P_{con}-*lasR* cassette from pSB1A2-P_{las}-GFP-P_{con}-*lasR* using CD_038 and CD_039. This DNA fragment was inserted into the pSB3K3 backbone by restriction digestion and ligation. The plasmid pSB3K3-P_{las}-mCherry-P_{esaS}-GFP(LVA) was constructed by Golden Gate Assembly using primers Esa_lux1/2 and a pSB3K3-P_{las}-GFP-P_{con}-*lasR* template, primers Esa_lux3/4 and a pFM301 template, and primers Esa_lux5/6 and a pSB3K3-P_{esaS}-GFP(LVA)-P_{con}-*esaR* template.

5.2.2. Culturing and fermentation

Fluorescence characterization

Switching dynamics over varying expression levels of QS circuit components (*esaI* and *luxR*) were quantified using the BioLector microbioreactor system (m2p-labs, Baesweiler, Germany). Individual colonies were inoculated in LB medium and grown overnight at 30 °C. 1 mL cultures were inoculated from these seeds at OD_{600} 0.05 into BioLector 48-well flower plates and incubated at 30 °C, 1200 rpm (3 mm orbit), and 80% relative humidity. The plate was sealed with a gas-permeable sealing foil (m2p-labs). Cultures were monitored for OD (BioLector units), GFP, and RFP fluorescence over time.

5.3. Results

5.3.1. Characterization of an *lsr* QS circuit

To construct a QS circuit based on these components, a plasmid containing a P_{con}-*lsrR* cassette and a P_{lsr}-GFP cassette was assembled (pSB3K3-P_{104}-*lsrR*-P_{lsr}-GFP) and used to transform MG1655. DPD was synthesized *in vitro* from *S*-adenosylhomocysteine (Sigma Aldrich) and purified Pfk and LuxS. The concentration of the resulting DPD stock was quantified as previously described using Ellman's assay. This strain harboring pSB3K3-P_{104}-*lsrR*-P_{lsr}-GFP was cultured in varying concentrations of DPD and GFP measurements were taken periodically. In the absence of the endogenous components, it is expected that the GFP fluorescence should increase with the

concentration of AI-2. However, Figure 5-1 shows that the circuit exhibited the opposite trend. It is hypothesized that this trend results from activation of the endogenous *lsr* QS circuit genes. For example, increased *lsrR* expression could result in decreased levels of LsrK or LsrACDB to lower the intracellular concentration of phosphorylated AI-2 or increased *lsrF* and *lsrG* expression could result in increased degradation of phosphorylated AI-2. While experiments to identify the cause of the unexpected response could have been conducted, it was instead decided that this QS system was not worth exploring further due to its relative complexity.

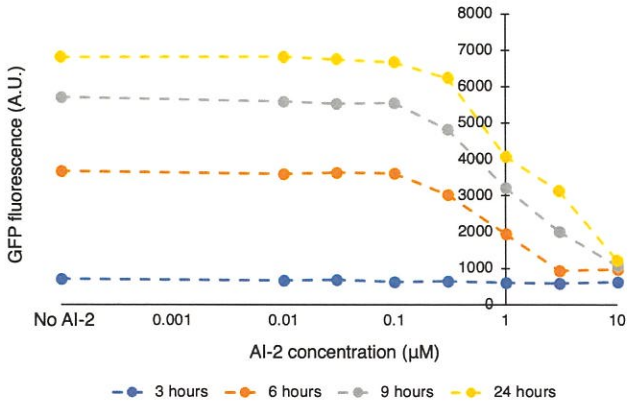

Figure 5-1. Activation of the P_{lsr} promoter with varying AI-2 treatments.
MG1655 harboring pSB3K3-P_{104}-*lsrR*-P_{lsr}-GFP was cultured in LB medium in varying concentrations of AI-2. It was expected that LsrR represses expression from P_{lsr} in the absence of AI-2 and this repression is relieved in its presence. The observed behavior shows the opposite trend, likely due to interaction with the endogenous *lsr* QS system components.

In addition to crosstalk with endogenous circuits, several studies suggest that the *lsr* QS circuit is subject to carbon catabolite repression. Activation of the P_{lsr} promoter does not occur in the presence of glucose or glycerol and the promoter contains binding sites for cAMP-CRP (100). While it would be possible to construct a hybrid promoter containing the *lsr* binding sequence to relieve the requirement for cAMP-CRP activation, a recent study suggests there is an additional layer of catabolite repression that may be more difficult to overcome. LsrK, the kinase responsible for phosphorylating AI-2 is inhibited by the phosphotransferase system protein HPr when they form a tight complex. However, knockout of *ptsH*, which encodes HPr results in significant growth burden (101). Alternatively, this layer of carbon catabolite repression could be addressed by evolving a variant of LsrR that loses HPr binding ability, but retains DNA-binding.

5.3.2. Characterization of a *las* QS circuit

First, a *las* QS circuit was constructed by transferring the *lasR* and P_{las}-GFP cassettes from pSB1A2-P_{con}-*lasR*-P_{las}-GFP to a pSB3K3 backbone (pSB3K3-P_{con}-*lasR*-P_{las}-GFP) and testing for GFP expression under varying concentrations of 3OC6HSL and 3OC12HSL. Results showed that GFP expression was induced with addition of 3OC12HSL only, suggesting that the similarity in the signaling molecule alone is not problematic (Figure 5-2).

Next, characterization of the *las* QS circuit was conducted in strains which also contain the entire *esa* QS circuit. This context allows for additional modes of crosstalk interactions that were not evaluated previously (i.e. activation or repression from non-cognate regulator protein). To conduct this characterization, a reporter plasmid containing *lasR* and *esaR* under constitutive promoters, P_{las}-RFP, and P_{esaS}-GFP(LVA) on the pSB3K3 backbone was constructed. The resulting plasmid was tested in two strain series – one which contains a *lasI* expression library and one that contains the same *lasI* library, along with *esaI* expressed from an intermediate strength promoter-RBS combination (L19-*esaI*). Periodic GFP and RFP measurements shows that the P_{las} promoter is activated in the *lasI*-expressing strains and the maximum RFP fluorescence follows the trend expected based on the predicted *lasI* expression level (i.e. increasing RFP with *lasI* expression level) (Figure 5-2A). While the maximum fluorescence from each *lasI* expression level is slightly higher in the presence of *esaI*, the general trend of increasing fluorescence with *lasI* expression holds (Figure 5-2C). Figures 5-2B and D shows that the activation of the P_{esaS} promoter is not impacted by the levels of 3OC12HSL represented in this *lasI* library, both with and without *esaI*.

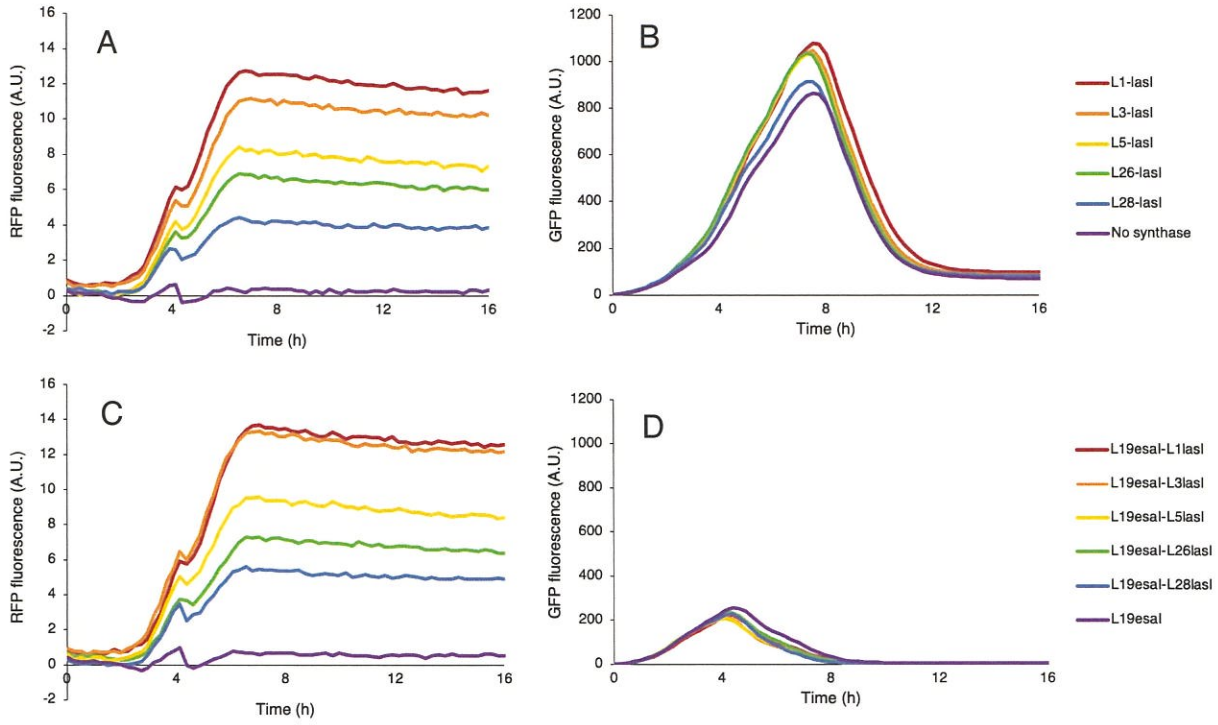

Figure 5-2. Fluorescence characterization of strains containing *las* and *esa* QS circuits.
All strains carry a reporter plasmid that contains P_{con}-lasR, P_{con}-esaR, P_{las}-RFP, and P_{esaS}-GFP(LVA). Panels A and B show data from the same set of strains, which contain *lasI* only. Panels C and D show data from the same set of strains that contain both *lasI* and *esaI*. (**A**) Activation of the P_{las} promoter under varying *lasI* expression levels. Increasing the *lasI* expression level results in earlier switching from the promoter as expected. (**B**) P_{esaS} promoter dynamics under a range of *lasI* expression levels without *esaI*. Increasing the *lasI* expression level results in a slight increase in the maximum GFP fluorescence. (**C**) Activation of the P_{las} promoter under varying *lasI* expression levels in strains containing L19-*esaI*. The maximum fluorescence of each curve is slightly higher than its counterpart in panel A, but switch time still follows the *lasI* expression level. (**D**) P_{esaS} promoter dynamics under a range of *lasI* expression levels in strains containing L19-*esaI*. Incorporation of the *lasI* cassette results in a slight decrease in fluorescence. Overall, the change in P_{esaS} behavior with the addition of *esaI* is much more significant than the changes that result from having any expression level of *lasI*.

While characterization of the *las* and *esa* QS systems showed they are a promising pair for orthogonal bifunctional control, characterization of a *lux* QS circuit was also showing promising results. Namely, characterization of the *lux* QS circuit showed that transcription from the P_{lux} promoter could be tuned by varying either the *esaI* or *luxR* expression level. Additionally, the circuit had been successfully applied to controlling expression of *TAL* and *4CL* in the naringenin pathway. Therefore, the *las* circuit was evaluated for use in combination to with the *lux* system. However, characterization of the *lux* circuit in a strain that constitutively expresses genomic *lasR* and *lasI* showed that these components significantly impact *lux* circuit dynamics (Figure 5-3).

Without *lasI*, increasing the *esaI* expression level leads to earlier switching from the P_{lux} promoter. However, with the addition of *lasI*, the *esaI* expression level no longer controls the switching dynamics from the P_{lux} promoter.

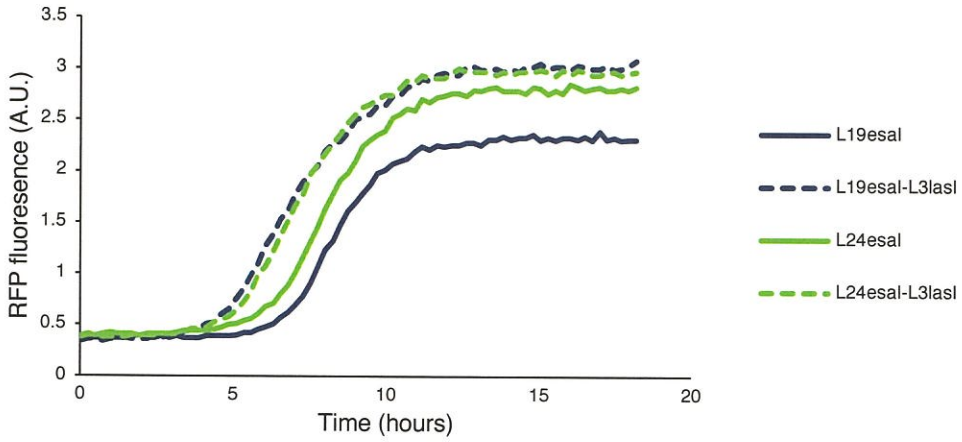

Figure 5-3. Fluorescence characterization of the *lux* QS system in the presence of *las* system components. All strains contain a reporter plasmid that expresses mCherry from the P_{lux} promoter. *esaI*, *lasI*, *luxR*, and *lasR* are all expressed from the genome under constitutive promoters. The *luxR* and *lasR* expression levels are constant across all strains and the *esaI* and *lasI* expression levels are specified in the legend. Without *lasI* increasing the *esaI* expression level from L19 to L24 shifts the switching time from the P_{lux} promoter earlier as expected. In the presence of *lasI*, the P_{lux} promoter is activated at the same time under both *esaI* expression levels.

5.4. Conclusions

In summary, these studies show that the combinations of QS systems significantly impact the independent tuning capabilities of a bifunctional circuit. Even though the *lux* and *esa* QS systems respond to the same signaling molecule, the *las* QS circuit showed little evidence of crosstalk with the *esa* circuit and significant levels of crosstalk with the *lux* circuit. This is not surprising as the *las* QS system shows *lux*-type interactions and there is homology between the regulator proteins. Recent studies have shown that other *lux*-type QS with dissimilar signaling molecules show high degrees of orthogonality (102, 103). Additionally, while non-AHL QS circuits are promising candidates for orthogonal behavior, the complexity and additional challenges of these circuits should be considered.

6. Conclusions and future directions

Abstract

The aims of this thesis were focused on the development of quorum-sensing based dynamic control circuits and the application of these strategies towards improving microbial synthesis processes. This chapter summarizes the major findings in this thesis and suggests directions for future exploration.

6.1. Thesis summary

In this thesis, quorum-sensing (QS) based dynamic control strategies were constructed and applied to microbial synthesis systems to improve production. The first control tool is a bifunctional QS circuit that controls two sets of target genes under two different modules. The two modules are semi-independent QS circuits that respond to the same signaling molecule, but contain different regulator proteins. This circuit was used to address two different production limitations in both the naringenin and salicylic acid pathways to achieve significant improvements in both contexts. The second control tool is a QS circuit that controls the activity of a target enzyme at the post-translational level. The circuit was used to control the growth rate of a sub-population in a co-culture to expand upon the achievable composition profiles. This added control parameter benefited production in a naringenin-producing co-culture system. The third control tool uses QS components to regulate protein co-localization dynamics. This system is a post-translational method for metabolic flux control that further decouples the switching dynamics from the dynamics of host cell processes.

6.1.1. QS-based transcriptional control

The first study in this thesis sought to develop a QS circuit for layered dynamic control of target gene transcription. Such a tool could be used to dynamically regulate multiple metabolic fluxes to address production limitations in some challenging pathways that require control at more than one metabolic node. To this end, a bifunctional QS circuit composed of modules derived from two different QS systems was constructed. Each module is an AHL-based circuit that controls transcription from its own QS promoter and responds to changes in the same signaling molecule (AHL). By using components from two different QS circuits, the switching dynamics of each module can be tuned independently by varying the expression level of the regulator proteins, which only impact the switching dynamics of their cognate promoter. Additionally, the OFF-to-ON response to increasing cell-density from one of the control modules was inverted by QS-based regulation of CRISPRi components to further expand upon the control capabilities of the circuit.

The bifunctional control circuit was then applied to regulating metabolic fluxes in the context of microbial synthesis systems to benefit production. This control circuit was implemented in two different production pathways to overcome enzyme inhibition by a pathway intermediate, product toxicity, and low precursor availability. Application of the bifunctional circuit to regulating metabolic fluxes in the naringenin and salicylic acid pathways resulted in a 16-fold and 2-fold higher titer compared to the respective static controls. Further, the wide range in product titers that result from varying switching dynamics in both pathways demonstrates the importance of tuning capabilities in a generalizable regulation tool.

6.1.2. QS-based control of co-culture composition

The second study in this thesis sought to develop a method to control the composition of a co-culture production system. This study addresses a limitation in the available strategies for composition control beyond defining the inoculation ratio. To this end, a growth-regulation circuit that dynamically down-regulates the growth rate of a target strain in response to its own cell density was constructed. The circuit uses the *lux* QS system components to control phosphofructokinase (Pfk) levels at the post-translational level by controlling expression of a protease linker required for degrading a tagged variant of Pfk. Pfk down-regulation results in a titratable decrease in cellular growth rate and the relationship between growth rate and cell-density can be tuned by varying the expression level of the AHL synthase. Implementation of this circuit allows for an expanded range of co-culture composition profiles.

To demonstrate the utility of such a control strategy, a co-culture naringenin production system was constructed and the control circuit was implemented in the sub-population containing the first enzyme of the pathway. A screen of naringenin producing co-culture systems with varying inoculum compositions and AHL synthase expression levels resulted in a top system that provides a 60% increase in naringenin titer compared to the top inoculation ratio without the circuit. Further, incorporation of a communication module that conveys cell-density of one strain to another allowed for coordination of precursor accumulation dynamics in the second strain, resulting in an additional 60% increase in naringenin titer. This study demonstrated that the application of a

simple QS circuit to dynamically regulate cell growth rates can lead to a significant improvement in microbial production processes.

6.1.3. QS-mediated control of enzyme clustering

The third study in this thesis aimed to develop a QS-mediated method for enzyme clustering for the purpose of sequestering inhibiting or toxic intermediates in production pathways or dynamically diverting metabolic fluxes from one pathway branch to another. The design for such a system was inspired by previous work on synthetic clustering systems composed of fusion proteins containing an oligomerizing domain, an intrinsically disordered domain (IDR), and a visualization (i.e. GFP) or enzymatic domain. In this system, the LasR regulator protein in the *las* QS system, was incorporated as the oligomerization domain since it has been previously shown to dimerize in the presence of its cognate AHL, 3OC12HSL. Image analysis of cells containing the fusion showed AHL-dependent clustering behavior of the fusion protein as expected. However, induction of clustering also resulted in burdened growth, which could be partially restored by expressing the AHL synthase to delay cluster formation. Attempts at applying this clustering system to co-localize enzymes to control metabolic fluxes were unsuccessful due to the significant loss of enzyme activity when the LasR-FUS tag is appended to the enzyme's N-terminal or when clustering is induced. These early studies suggest that broad applicability of a QS-mediated clustering system will depend on construction of tag variants with reduced impact on enzyme activity.

6.2. Future directions

6.2.1. Multiplexed dynamic control methods

While the bifunctional QS circuit described in Chapter 2 of this thesis did allow for independent tuning of the switching dynamics of each module, the range was limited since the two modules responded to the same signaling molecule. To achieve additional tunability, which could benefit

production in some contexts, each module could be comprised of QS systems that do not share any components. While this was the original intent for this thesis, the *las* QS circuit that was characterized alongside the *esa* and *lux* QS circuits showed significant levels of crosstalk with the *lux* QS circuit to the point that the added complexity afforded no additional tuning advantage (Figure 5-3). Since the start of this study, groups have conducted systematic analyses of crosstalk between various AHL-based QS circuits (102, 103). These studies can be used to guide the choice of promising QS combinations to study in the future. In addition to the increasing body of literature on combinations of QS circuit components, protein crystallography studies of QS regulator proteins complexed with different AHLs have informed specific amino acid changes that increase the specificity for a particular AHL (104). A directed-evolution-based approach could also be used to achieve the same goal of more specific regulator-AHL interactions. This strategy would involve a two-stage screen following the generation of a mutant regulator library – the first occurs in the presence of the cognate AHL and selects for activation behavior and the second occurs in the presence of one or more non-cognate AHLs and selects for a lack of activation behavior. Similar approaches have been applied for screening for ON/OFF sensor behavior (66).

While autonomous dynamic control strategies have shown promise in academic settings, it is uncertain whether these circuits will provide similar gains on an industrial scale. It is additionally unclear whether production trends obtained from small-scale fermentations will translate to larger-scale or high cell-density fermentations. For example, the switching cell-density that best manages the trade-off between growth and production phase may be higher when in contexts in which the maximum cell-density is higher. To address this potential limitation in transferability across fermentation conditions, researchers have constructed "multi-input" circuits which respond only when two or more conditions are met(64, 65). Although they hypothesize that the added specificity in the definition of switching time will facilitate a more successful translation between fermentation scales, a comprehensive study of the effect of changing fermentation scales on the optimal switching dynamics has not yet been conducted. Such a study will be key to defining the steps that should be taken may allow for the use of autonomous dynamic control circuits in industry.

With more advanced experimental methods available, there are now detailed dynamic models of cellular processes. This improvement in understanding may soon result in the ability to predict the optimal dynamic control profile, which may not follow the dynamics of any individual circuit. In this scenario, a set of characterized dynamic control systems could be assembled in a multi-input circuit to achieve the desired response. With this idea, Moser et al. achieved a response circuit that responded at all stages of the fermentation by incorporating three independent dynamic control circuits that exhibited dynamic behavior during the beginning, middle, and end of the fermentation (66).

6.2.2. Improving genetic stability regulation tools

In many contexts, dynamic regulation triggers a switch from growth to production phase, where the production phase may be characterized by low growth rates. This situation can lead to population drift towards a mutant phenotype that never switches to the production phase (i.e. no-production phenotype). Evidence of this behavior was observed in the circuit that regulates Pfk at the post-translational level. Sequencing analysis of colonies after observation of the mutant phenotype showed a mutation in the *sspB* gene in some of the colonies. In the context of *sspB* expression regulation under the *lux* QS circuit, mutations in the AHL synthase gene, *luxR,* or *sspB* can result in the no-production phenotype, although the AHL synthase mutation would not confer any immediate fitness advantage and thus can be ignored.

Especially for large scale fermentations in which cultures must undergo additional doublings before inoculation, it could be beneficial to implement a kill switch to mitigate genetic drift. In the context of the *lux*-controlled *sspB* circuit, one strategy could be to engineer a system that requires *sspB* expression for survival at high cell densities. For example, a copy of the *ccdB* gene (encodes toxin CcdB) controlled under a stationary phase promoter and appended with an SspB-dependent degradation tag could be incorporated into the existing strain. In the absence of a mutation, transcription of *ccdB* would occur at high cell densities, but the protein would be immediately degraded since SspB would already be present in the cell. However, acquisition of a mutation that prevents SspB-mediated degradation of Pfk will result in the failure to degrade CcdB as well, resulting in cell death. Table 6-1 compares the failure modes of the existing post-translational

regulation system, with and without the kill switch, to a transcription-based Pfk regulation system(15) that has not exhibited escape behavior. Notably, the sequences that result in escape behavior with the kill switch are promoter and degradation tag sequences which are less likely due to the short length of these sequences in combination with mutation in the CcdB cassette. While the suggested circuit is specific to the SspB-mediated post-translational control circuit, these ideas can be generalized to improve the robustness of other silencing systems as well.

Table 6-1. Summary of mutation loci that confer an escape phenotype.

Transcriptional	Post-translational	Post-translational (with kill switch)
P_{esaS} promoter	SspB	Pfk promoter AND CcdB cassette
EsaR ligand-binding domain	P_{lux} promoter	Pfk degradation tag AND CcdB cassette
Pfk degradation tag	LuxR DNA- or ligand-binding domains	
	Pfk promoter	
	Pfk degradation tag	

6.2.3. Methods for overriding QS-based control

While autonomous switching mechanisms provide important benefits, they can also cause problems in non-production contexts. For example, consider an autonomous control circuit that actuates a switch between a growth phase and production phase, during which there is no growth. During strain construction, failure could be due to procedural mistake or due to the low fitness of the resulting strain. Additionally, when growing seed cultures for inoculation of the working culture, slight variation in the cell density at the end of the seed culture could result in significantly different initial states of the inoculum leading to differences in production. When screening a

library of different switching dynamics, seed cultures used for inoculating working cultures may be at different metabolic states along the transition between growth and production phase. This variation could propagate to different lag times or nonsensical production trends. To address these scenarios, it would be beneficial to have a mechanism for overriding the autonomous control for non-production contexts.

To address these scenarios, a control circuit can be implemented to control expression of the AHL synthase. While researchers have placed expression of the AHL synthase under IPTG-inducible promoters, it would beneficial to instead suppress AHL synthase expression in the presence of a chemical inducer to minimize cost. Such a control scheme could be constructed through a few different strategies. First, an IPTG-inducible circuit could be used to control silencing components targeted to the AHL synthase. Second, the *aiiA* gene, which encodes an AHL-degrading enzyme, can be placed under control of an IPTG-inducible circuit. And third, if the main control circuit is orthogonal to the *esa* QS system, the P_{esaS} promoter could be used to control the AHL synthase of the orthogonal QS circuit. When *esaR* is also present, expression level of the orthogonal AHL synthase without 3OC6HSL can be tuned by changing the strength of the RBS for synthase translation and/or the *esaR* expression level. With this system, expression of the orthogonal AHL synthase is repressed with 3OC6HSL addition.

References

1. R. L. Perlman, B. De Crombrugghe, I. Pastan, Cyclic AMP regulates Catabolite and Transient Repression in E. coli. *Nature* **223**, 810–812 (1969).
2. A. Zaslaver, *et al.*, Just-in-time transcription program in metabolic pathways. *Nat. Genet.* **36**, 486–491 (2004).
3. F. Wessely, *et al.*, Optimal regulatory strategies for metabolic pathways in Escherichia coli depending on protein costs. *Mol. Syst. Biol.* **7**, 515 (2011).
4. K. G. Gadkar, F. J. D. Iii, J. S. Edwards, R. Mahadevan, Estimating Optimal Profiles of Genetic Alterations Using Constraint-Based Models. *Biotechnol. Bioeng.* **89**, 243–251 (2004).
5. N. Anesiadis, W. R. Cluett, R. Mahadevan, Dynamic metabolic engineering for increasing bioprocess productivity. *Metab. Eng.* **10**, 255–266 (2008).
6. N. Anesiadis, H. Kobayashi, W. R. Cluett, R. Mahadevan, Analysis and Design of a Genetic Circuit for Dynamic Metabolic Engineering. *ACS Synth. Biol.*, 442–452 (2013).
7. E. Klipp, R. Heinrich, H.-G. Holzhütter, Prediction of temporal gene expression. *Eur. J. Biochem.* **269**, 5406–5413 (2002).
8. W. R. Farmer, J. C. Liao, Improving lycopene production in Escherichia coli by engineering metabolic control. *Nat. Biotechnol.* **18**, 533–537 (2000).
9. F. Zhang, J. M. Carothers, J. D. Keasling, Design of a dynamic sensor-regulator system for production of chemicals and fuels derived from fatty acids. *Nat. Biotechnol.* **30**, 354–359 (2012).
10. P. Xu, L. Li, F. Zhang, G. Stephanopoulos, M. Koffas, Improving fatty acids production by engineering dynamic pathway regulation and metabolic control. *Proc. Natl. Acad. Sci.* **111**, 11299–11304 (2014).
11. R. H. Dahl, *et al.*, Engineering dynamic pathway regulation using stress-response promoters. *Nat. Biotechnol.* **31**, 1039–1046 (2013).
12. C. N. S. Santos, M. Koffas, G. Stephanopoulos, Optimization of a heterologous pathway for the production of flavonoids from glucose. *Metab. Eng.* **13**, 392–400 (2011).
13. I. M. Brockman, K. L. J. Prather, Dynamic knockdown of E. coli central metabolism for redirecting fluxes of primary metabolites. *Metab. Eng.* **28**, 104–113 (2015).
14. E. M. Zhao, *et al.*, Optogenetic regulation of engineered cellular metabolism for microbial chemical production. *Nature* **555**, 683 (2018).
15. A. Gupta, I. M. B. Reizman, C. R. Reisch, K. L. J. Prather, Dynamic regulation of metabolic flux in engineered bacteria using a pathway-independent quorum-sensing circuit. *Nat. Biotechnol.* **3** (2017).
16. Y. Soma, T. Hanai, Self-induced metabolic state switching by a tunable cell density sensor for microbial isopropanol production. *Metab. Eng.* **30**, 7–15 (2015).
17. E.-M. Kim, *et al.*, Autonomous control of metabolic state by a quorum sensing (QS)-mediated regulator for bisabolene production in engineered E. coli. *Metab. Eng.* **44**, 325–336 (2017).
18. Y. Yang, *et al.*, Sensor-regulator and RNAi based bifunctional dynamic control network for engineered microbial synthesis. *Nat. Commun.* **9**, 1–10 (2018).

19. S. J. Doong, A. Gupta, K. L. J. Prather, Layered dynamic regulation for improving metabolic pathway productivity in *Escherichia coli*. *Proc. Natl. Acad. Sci.*, 201716920 (2018).
20. C. V. Dinh, K. L. J. Prather, Development of an autonomous and bifunctional quorum-sensing circuit for metabolic flux control in engineered Escherichia coli. *Proc. Natl. Acad. Sci.* (2019).
21. Z. Li, X. Wang, H. Zhang, Balancing the non-linear rosmarinic acid biosynthetic pathway by modular co-culture engineering. *Metab. Eng.* **54**, 1–11 (2019).
22. J. A. Jones, *et al.*, Complete Biosynthesis of Anthocyanins Using E. coli Polycultures. *MBio* **8**, 1–9 (2017).
23. J. A. Jones, *et al.*, Experimental and computational optimization of an Escherichia coli co-culture for the efficient production of flavonoids. *Metab. Eng.* **35**, 55–63 (2016).
24. F. K. Balagaddé, *et al.*, A synthetic Escherichia coli predator–prey ecosystem. *Mol. Syst. Biol.* **4**, 187 (2008).
25. S. Gamby, *et al.*, Altering the Communication Networks of Multispecies Microbial Systems Using a Diverse Toolbox of AI-2 Analogues. *ACS Chem. Biol.* **7**, 1023–1030 (2012).
26. J. L. Terrell, *et al.*, Nano-guided cell networks as conveyors of molecular communication. *Nat. Commun.* **6**, 8500 (2015).
27. Y. Chen, J. K. Kim, A. J. Hirning, K. Josić, M. R. Bennett, Emergent genetic oscillations in a synthetic microbial consortium. *Science (80-.).* **349**, 986 LP – 989 (2015).
28. N. Marchand, C. H. Collins, Synthetic Quorum Sensing and Cell–Cell Communication in Gram-Positive Bacillus megaterium. *ACS Synth. Biol.* **5**, 597–606 (2016).
29. W. Kong, D. R. Meldgin, J. J. Collins, T. Lu, Designing microbial consortia with defined social interactions. *Nat. Chem. Biol.* **14**, 821–829 (2018).
30. K. Stephens, M. Pozo, C.-Y. Tsao, P. Hauk, W. E. Bentley, Bacterial co-culture with cell signaling translator and growth controller modules for autonomously regulated culture composition. *Nat. Commun.* **10**, 4129 (2019).
31. E. M. Zhao, *et al.*, Light-based control of metabolic flux through assembly of synthetic organelles. *Nat. Chem. Biol.* **15**, 589–597 (2019).
32. M. R. Parsek, M. Kivisaar, A. M. Chakrabarty, Differential DNA bending introduced by the Pseudomonas putida LysR-type regulator, CatR, at the plasmid-borne pheBA and chromosomal catBC promoters. *Mol. Microbiol.* **15**, 819–829 (1995).
33. K. W. George, *et al.*, Integrated analysis of isopentenyl pyrophosphate (IPP) toxicity in isoprenoid-producing Escherichia coli. *Metab. Eng.* **47**, 60–72 (2018).
34. J.-L. Lin, J. Zhu, I. Wheeldon, Synthetic Protein Scaffolds for Biosynthetic Pathway Colocalization on Lipid Droplet Membranes. *ACS Synth. Biol.* **6**, 1534–1544 (2017).
35. T. Thomik, I. Wittig, J. Choe, E. Boles, M. Oreb, An artificial transport metabolon facilitates improved substrate utilization in yeast. *Nat. Chem. Biol.* **13**, 1158 (2017).
36. M. Castellana, *et al.*, Enzyme clustering accelerates processing of intermediates through metabolic channeling. *Nat. Biotechnol.* **32**, 1011 (2014).
37. J. E. Dueber, *et al.*, Synthetic protein scaffolds provide modular control over metabolic flux. *Nat. Biotechnol.* **27**, 753–759 (2009).
38. T. Li, X. Chen, Y. Cai, J. Dai, Artificial Protein Scaffold System (AProSS): An efficient method to optimize exogenous metabolic pathways in Saccharomyces cerevisiae. *Metab. Eng.* **49**, 13–20 (2018).

39. Y. H. Lau, T. W. Giessen, W. J. Altenburg, P. A. Silver, Prokaryotic nanocompartments form synthetic organelles in a eukaryote. *Nat. Commun.* **9**, 1311 (2018).
40. J. L. Avalos, G. R. Fink, G. Stephanopoulos, Compartmentalization of metabolic pathways in yeast mitochondria improves the production of branched-chain alcohols. *Nat. Biotechnol.* **31**, 335 (2013).
41. W. C. DeLoache, Z. N. Russ, J. E. Dueber, Towards repurposing the yeast peroxisome for compartmentalizing heterologous metabolic pathways. *Nat. Commun.* **7**, 11152 (2016).
42. S. K. Hammer, J. L. Avalos, Harnessing yeast organelles for metabolic engineering. *Nat. Chem. Biol.* **13**, 823 (2017).
43. S. Elbaum-Garfinkle, *et al.*, The disordered P granule protein LAF-1 drives phase separation into droplets with tunable viscosity and dynamics. *Proc. Natl. Acad. Sci.* **112**, 7189 LP – 7194 (2015).
44. T. J. Nott, *et al.*, Phase Transition of a Disordered Nuage Protein Generates Environmentally Responsive Membraneless Organelles. *Mol. Cell* **57**, 936–947 (2015).
45. Y. Lin, D. S. W. Protter, M. K. Rosen, R. Parker, Formation and Maturation of Phase-Separated Liquid Droplets by RNA-Binding Proteins. *Mol. Cell* **60**, 208–219 (2015).
46. Y. Shin, *et al.*, Spatiotemporal Control of Intracellular Phase Transitions Using Light-Activated optoDroplets. *Cell* **168**, 159-171.e14 (2017).
47. K. V. Solomon, T. M. Sanders, K. L. J. Prather, A dynamic metabolite valve for the control of central carbon metabolism. *Metab. Eng.* **14**, 661–671 (2012).
48. J. B. Andersen, *et al.*, New Unstable Variants of Green Fluorescent Protein for Studies of Transient Gene Expression in Bacteria New Unstable Variants of Green Fluorescent Protein for Studies of Transient Gene Expression in Bacteria. *Appl. Environ. Microbiol.* **64**, 2240–2246 (1998).
49. K. E. McGinness, T. A. Baker, R. T. Sauer, Engineering Controllable Protein Degradation. *Mol. Cell* **22**, 701–707 (2006).
50. J. H. Davis, T. A. Baker, R. T. Sauer, Small-molecule control of protein degradation using split adaptors. *ACS Chem. Biol.* **6**, 1205–1213 (2011).
51. B. R. Sabari, *et al.*, Coactivator condensation at super-enhancers links phase separation and gene control. *Science (80-.).* **361**, eaar3958 (2018).
52. A. S. Holehouse, R. V Pappu, Functional Implications of Intracellular Phase Transitions. *Biochemistry* **57**, 2415–2423 (2018).
53. W. Stroberg, S. Schnell, Do Cellular Condensates Accelerate Biochemical Reactions? Lessons from Microdroplet Chemistry. *Biophys. J.* **115**, 3–8 (2018).
54. K. K. Nakashima, M. A. Vibhute, E. Spruijt, Biomolecular Chemistry in Liquid Phase Separated Compartments. *Front. Mol. Biosci.* **6**, 21 (2019).
55. S. Banjade, *et al.*, Conserved interdomain linker promotes phase separation of the multivalent adaptor protein Nck. *Proc. Natl. Acad. Sci.* **112**, E6426 LP-E6435 (2015).
56. S. Boeynaems, *et al.*, Protein Phase Separation: A New Phase in Cell Biology. *Trends Cell Biol.* **28**, 420–435 (2018).
57. E. Nevoigt, *et al.*, Engineering Promoter Regulation. *Biotechnol. Bioeng.* **96**, 550–558 (2006).
58. Z. Kang, Q. Wang, H. Zhang, Q. Qi, Construction of a stress-induced system in Escherichia coli for efficient polyhydroxyalkanoates production. *Appl. Microbiol. Biotechnol.* **79**, 203–208 (2008).
59. Q. Liang, H. Zhang, S. Li, Q. Qi, Construction of stress-induced metabolic pathway from

glucose to 1,3-propanediol in Escherichia coli. *Appl. Microbiol. Biotechnol.* **89**, 57–62 (2011).
60. S. Siedler, S. G. Stahlhut, S. Malla, J. Maury, A. R. Neves, Novel biosensors based on fl avonoid-responsive transcriptional regulators introduced into Escherichia coli. *Metab. Eng.* **21**, 2–8 (2014).
61. H. Liu, T. Lu, Autonomous production of 1,4-butanediol via a de novo biosynthesis pathway in engineered Escherichia coli. *Metab. Eng.* **29**, 135–141 (2015).
62. W. Xie, L. Ye, X. Lv, H. Xu, H. Yu, Sequential control of biosynthetic pathways for balanced utilization of metabolic intermediates in Saccharomyces cerevisiae. *Metab. Eng.* **28**, 8–18 (2015).
63. W. Bothfeld, G. Kapov, K. E. J. Tyo, A Glucose-Sensing Toggle Switch for Autonomous, High Productivity Genetic Control. *ACS Synth. Biol.* **6**, 1296–1304 (2017).
64. T. M. Lo, S. H. Chng, W. S. Teo, H. S. Cho, M. W. Chang, A Two-Layer Gene Circuit for Decoupling Cell Growth from Metabolite Production. *Cell Syst.* **3**, 133–143 (2016).
65. X. He, Y. Chen, Q. Liang, Q. Qi, Autoinduced AND Gate Controls Metabolic Pathway Dynamically in Response to Microbial Communities and Cell Physiological State. *ACS Synth. Biol.* **6**, 463–470 (2017).
66. F. Moser, *et al.*, Dynamic control of endogenous metabolism with combinatorial logic circuits. *Mol Syst Biol* **14**, 8605 (2018).
67. D. E. Tribe, Novel microorganism and method (1987) https:/doi.org/10.1016/j.(73).
68. F. St-Pierre, *et al.*, One-Step Cloning and Chromosomal Integration of DNA. *ACS Synth. Biol.*, 537–541 (2013).
69. I. M. Brockman, "Dynamic control of Escherichia coli central metabolism for improvement of glucaric acid production," Massachusetts Institute of Technology. (2015).
70. E. C.-J. Shiue, Improvement of D-Glucaric Acid Production in Escherichia coli (2008).
71. A. Gupta, "Dynamic Regulation of Bacterial Metabolic Pathways using Autonomous, Pathway-Independent Control Strategies," MIT. (2017).
72. L. S. Qi, *et al.*, Repurposing CRISPR as an RNA-Guided Platform for Sequence-Specific Control of Gene Expression. *Cell* **152**, 1173–1183 (2013).
73. E. Shiue, "Improvement of D-glucaric acid production in Escherichia coli," Massachusetts Institute of Technology. (2014).
74. P. Xu, *et al.*, Design and kinetic analysis of a hybrid promoter- regulator system for malonyl-CoA sensing in E. coli Design and kinetic analysis of a hybrid promoter-regulator system for malonyl-CoA sensing in E . coli. *ACS Chem. Biol.* **9**, 451–458 (2014).
75. J. Wu, G. Du, J. Chen, J. Zhou, Enhancing flavonoid production by systematically tuning the central metabolic pathways based on a CRISPR interference system in Escherichia coli. *Nat. Publ. Gr.*, 1–14 (2015).
76. Z. L. Fowler, M. A. G. Koffas, Biosynthesis and biotechnological production of flavanones: Current state and perspectives. *Appl. Microbiol. Biotechnol.* **83**, 799–808 (2009).
77. Y. Wang, S. Chen, O. Yu, Metabolic engineering of flavonoids in plants and microorganisms. *Appl. Microbiol. Biotechnol.* **91**, 949–956 (2011).
78. J. Zhou, G. Du, J. Chen, Novel fermentation processes for manufacturing plant natural products. *Curr. Opin. Biotechnol.* **25**, 17–23 (2014).

79. D. Yang, *et al.*, Repurposing type III polyketide synthase as a malonyl-CoA biosensor for metabolic engineering in bacteria. *Proc. Natl. Acad. Sci.* **115**, 9835–9844 (2018).
80. J. Wu, T. Zhou, G. Du, J. Zhou, J. Chen, Modular optimization of heterologous pathways for de Novo synthesis of (2S)-Naringenin in escherichia coli. *PLoS One* **9**, 1–9 (2014).
81. J. Wu, O. Yu, G. Du, J. Zhou, Fine-Tuning of the Fatty Acid Pathway by Synthetic Antisense RNA for Enhanced (2 S)-Naringenin Production from L-Tyrosine in Escherichia coli. *Appl. Environ. Microbiol.* **80**, 7283–7292 (2014).
82. S. Omura, The antibiotic cerulenin, a novel tool for biochemistry as an inhibitor of fatty acid synthesis. *Bacteriol. Rev.* **40**, 681–697 (1976).
83. Y. Lin, X. Sun, Q. Yuan, Extending shikimate pathway for the production of muconic acid. *Metab. Eng.* **23**, 62–69 (2014).
84. H.-D. Shin, S. McClendon, T. Vo, R. R. Chen, Escherichia coli Binary Culture Engineered for Direct Fermentation of Hemicellulose to a Biofuel. *Appl. Environ. Microbiol.* **76**, 8150 LP – 8159 (2010).
85. S.-L. Tsai, G. Goyal, W. Chen, Surface Display of a Functional Minicellulosome by Intracellular Complementation Using a Synthetic Yeast Consortium and Its Application to Cellulose Hydrolysis and Ethanol Production. *Appl. Environ. Microbiol.* **76**, 7514 LP – 7520 (2010).
86. K. Zhou, K. Qiao, S. Edgar, G. Stephanopoulos, Distributing a metabolic pathway among a microbial consortium enhances production of natural products. *Nat. Biotechnol.* **33**, 377 (2015).
87. H. Zhang, G. Stephanopoulos, Co-culture engineering for microbial biosynthesis of 3-amino-benzoic acid in Escherichia coli. *Biotechnol. J.* **11**, 981–987 (2016).
88. M. K. Ahmadi, L. Fang, N. Moscatello, B. A. Pfeifer, E. coli metabolic engineering for gram scale production of a plant-based anti-inflammatory agent. *Metab. Eng.* **38**, 382–388 (2016).
89. V. Ganesan, Z. Li, X. Wang, H. Zhang, Heterologous biosynthesis of natural product naringenin by co-culture engineering. *Synth. Syst. Biotechnol.* **2**, 236–242 (2017).
90. E. Il Hwang, M. Kaneko, Y. Ohnishi, S. Horinouchi, Production of Plant-Specific Flavanones by Escherichia coli Containing an Artificial Gene Cluster. *Appl. Environ. Microbiol.* **69**, 2699 LP – 2706 (2003).
91. L. You, R. S. Cox, R. Weiss, F. H. Arnold, Programmed population control by cell–cell communication and regulated killing. *Nature* **428**, 868–871 (2004).
92. H. C. Kistler, K. Broz, Cellular compartmentalization of secondary metabolism. *Front. Microbiol.* **6**, 68 (2015).
93. A. O. Chatzivasileiou, V. Ward, S. M. Edgar, G. Stephanopoulos, Two-step pathway for isoprenoid synthesis. *Proc. Natl. Acad. Sci.* **116**, 506 LP – 511 (2019).
94. F. X. Cunningham, H. Lee, E. Gantt, Carotenoid Biosynthesis in the Primitive Red Alga Cyanidioschyzon merolae. *Eukaryot. Cell* **6**, 533 LP – 545 (2007).
95. D. Juminaga, *et al.*, Modular engineering of L-tyrosine production in Escherichia coli. *Appl. Environ. Microbiol.* **78**, 89–98 (2012).
96. C. V. Dinh, K. L. J. Prather, Development of an autonomous and bifunctional quorum-sensing circuit for metabolic flux control in engineered Escherichia coli. *Proc. Natl. Acad. Sci.* (2019) https:/doi.org/10.1073/PNAS.1911144116 (December 3, 2019).
97. W. Kang, *et al.*, Modular enzyme assembly for enhanced cascade biocatalysis and metabolic flux. *Nat. Commun.* **10**, 4248 (2019).

98. M. D. Servinsky, *et al.*, Directed assembly of a bacterial quorum. *ISME J.* **10**, 1–12 (2015).
99. C. Y. Tsao, S. Hooshangi, H. C. Wu, J. J. Valdes, W. E. Bentley, Autonomous induction of recombinant proteins by minimally rewiring native quorum sensing regulon of E. coli. *Metab. Eng.* **12**, 291–297 (2010).
100. L. Wang, Y. Hashimoto, C. Tsao, J. Valdes, Cyclic AMP(cAMP) and cAMP Receptor Protein Influence both Synthesis and Uptake of Extracellular Autoinducer 2 in Escherichia coli. *J. Bacteriol.* **187**, 2066–2076 (2005).
101. J.-H. Ha, *et al.*, Evidence of link between quorum sensing and sugar metabolism in Escherichia coli revealed via cocrystal structures of LsrK and HPr. *Sci. Adv.* **4**, eaar7063 (2018).
102. S. R. Scott, J. Hasty, Quorum Sensing Communication Modules for Microbial Consortia. *ACS Synth. Biol.* **5**, 969–977 (2016).
103. A. D. Halleran, R. M. Murray, Cell-Free and In Vivo Characterization of Lux, Las, and Rpa Quorum Activation Systems in E. coli. *ACS Synth. Biol.* **7**, 752–755 (2018).
104. A. R. McCready, J. E. Paczkowski, B. R. Henke, B. L. Bassler, Structural determinants driving homoserine lactone ligand selection in the Pseudomonas aeruginosa LasR quorum-sensing receptor. *Proc. Natl. Acad. Sci.* **116**, 245 LP – 254 (2019).
105. V. K. Mutalik, *et al.*, Precise and reliable gene expression via standard transcription and translation initiation elements. *Nat. Methods* **10**, 354–60 (2013).
106. H. M. Salis, The ribosome binding site calculator. *Methods Enzymol.* **498**, 19–42 (2011).

Appendix

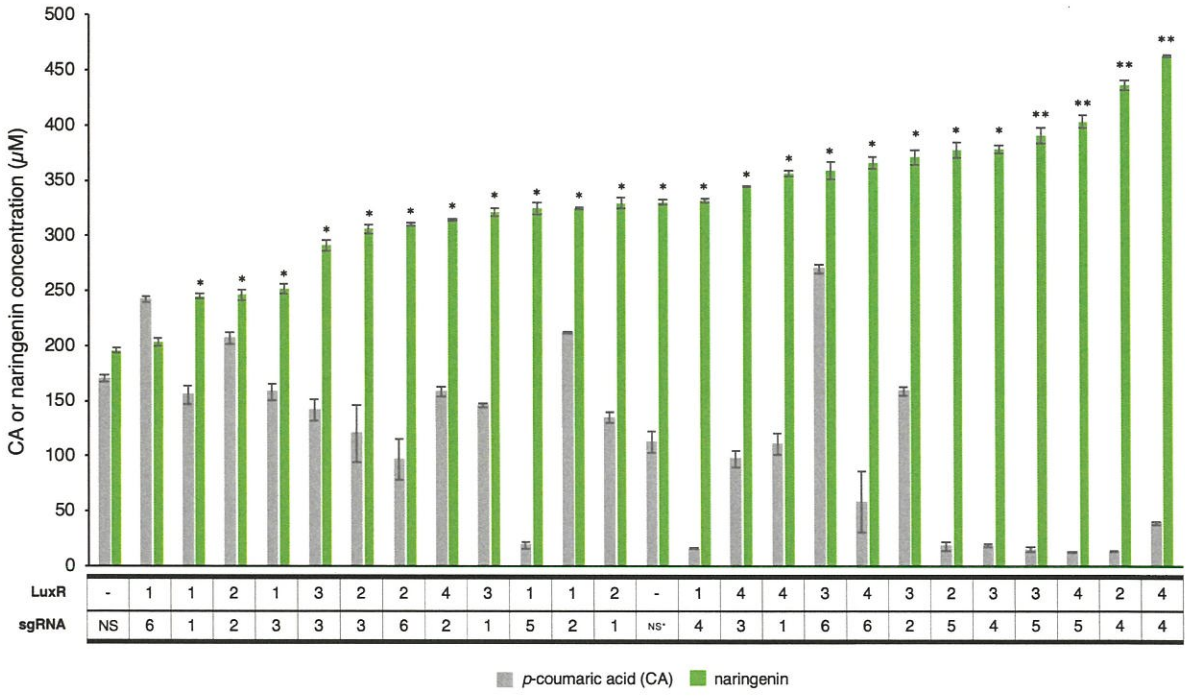

Appendix Figure 1. *p*-Coumaric acid and naringenin titers with QS-controlled *TAL* and *4CL* expression and endogenous gene downregulation.

Combinations of LuxR levels and sgRNA targets with upregulated genes under the $P_{esaR\text{-}H}$ promoter and downregulated genes under the P_{lux} promoter. All strains with the bifunctional regulation scheme improve naringenin titers compared to the non-specific sgRNA control and half of the strains exceeded the naringenin titers from the cerulenin-treated trial. *$P < 0.01$ compared to TAL and 4CL controlled strain in L19 background. **$P < 0.05$ compared to TAL and 4CL controlled strain in L19 background with cerulenin. Error bars indicate s. d. of triplicate trials.

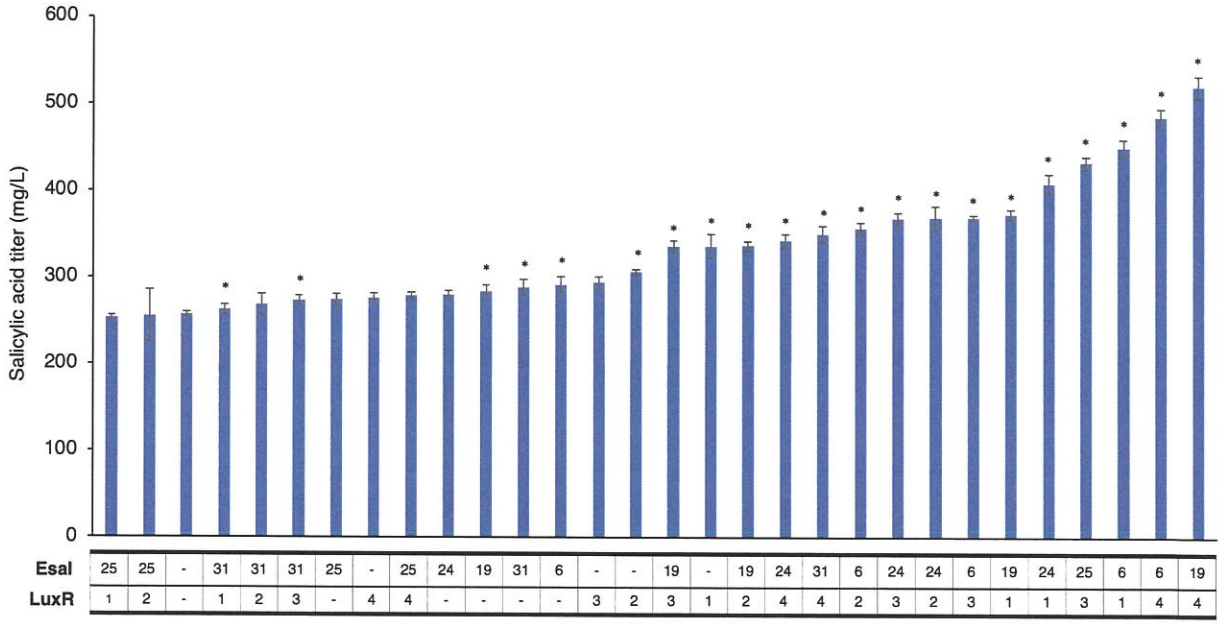

Appendix Figure 2. Salicylic acid at varying EsaI and LuxR levels.

The RBS number on the x-axis refers to the strength of the RBS driving *luxR* expression, increasing from 1 to 4 and the EsaI level is denoted with number corresponding to the NST74-LXX strain series. *P < 0.01 compared to constitutive entC and pchB control with no AAA pathway downregulation. Error bars represent s. d. from triplicate trials.

Appendix Table 1. Summary of promoter and RBS sequences used in Chapter 2.

Promoter RBS sequences denoted as LXX were taken from Mutalik et al. 2013 (105) and RBS sequences denoted RBSX were generated using the Salis RBS calculator (106).

Promoter sequence	**RBS sequence**	**Name and gene controlled**
AAAAAATTTATTTGCTTTCGCATCTTTTTGTACCTATAATGTGTGGA	GGGCCCAAGTTCACTTAAAAAGGAGATCAACAATGAAAGCAATTTTCGTACTGAAACATCTTAATCATGCCTAGGAAGTTTTCTAATG	L6-*esaI*
TTGACAATTAATCATCCGGCTCGTAATGTTTGTGGA	GGGCCCAAGTTCACTTAAAAAGGAGATCAACAATGAAAGCAATTTTCGTACTGAAACATCTTAATCATGCCTAGGAAGTTTTCTAATG	L13-*esaI*
TTCACTTTTAATCATCCGGCTCGTATAATGTGTGGA	GGGCCCAAGTTCACTTAAAAAGGAGATCAACAATGAAAGCAATTTTCGTACTGAAACATCTTAATCATGCCTAGGAAGTTTTCTAATG	L19-*esaI*
TTGCCTCTTAATCATCGGCTCGTATAATGTGTGGA	GGGCCCAAGTTCACTTAAAAAGGAGATCAACAATGAAAGCAATTTTCGTACTGAAACATCTTAATCATGCGAGGGATGGTTTCTAATG	L24-*esaI*
TTGCCTCTTAATCATCGGCTCGTATAATGTGTGGA	GGGCCCAAGTTCACTTAAAAAGGAGATCAACAATGAAAGCAATTTTCGTACTGAAACATCTTAATCATGCCTAGGAAGTTTTCTAATG	L25-*esaI*
TTGACATCAGGAAAATTTTTCTGTATAATGTGTGGA	GGGCCCAAGTTCACTTAAAAAGGAGATCAACAATGAAAGCAATTTTCGTACTGAAACATCTTAATCATGCCTAGGAAGTTTTCTAATG	L31-*esaI*
ACCTGTAGGATCGTACAGGTTTACGCAAGAAAATGGTTTGTTATAGTCGAATAAA	CTCGACTCTACTTAAGGAGGACCTTTT	P_{lux}-*TAL*

ACCTGTAGGATCGTACAGGTTT ACGCAAGAAAATGGTTTGTTAT AGTCGAATAAA	TTCACGAGGGATTGGTAAGGAAGGTA GGT	P_{lux}-*4CL*
ACCTGTAGGATCGTACAGGTTT ACGCAAGAAAATGGTTTGTTAT AGTCGAATAAA	TACTAGAGAAAGAGGAGAAATACTAG	P_{lux}-*dCas9*
TTGACAATTAATCATCCGGCTCG TATAATGTGTGGGCCTGTACTAT AGTGCAGGT	TACTAGAGAAAGAGGAGAAATACTAG	$P_{esaR\text{-}H}$-*TAL* $P_{esaR\text{-}H}$-*4CL* $P_{esaR\text{-}H}$-*mCherry*
TTGACAATTAATCATCCGGCTCG TATAATGTGTGGGCCTGTACTAT AGTGCAGGT	TAATATAATATTACAAAGAGGAGGTTT T	$P_{esaR\text{-}H}$-*entC*
TTGACAATTAATCATCCGGCTC GTATAATGTGTGGGCCTGTAC TATAGTGCAGGT	ACAATCATACTTGATAAGGAGGTTAT TGC	$P_{esaR\text{-}H}$-*pchB*
TCGACATAAAGTCTAACCTAT AGGATACTTACAGCCAT	TACTAGAGAAAGAGGAGAAATACTA G	P_{con}-*esaR*
TTTACGGCTAGCTCAGTCCTAG GTACTATGCTAGC	TACTAGAGAAAGGCTCGAAATACTA G	P_{con}-RBS1-*luxR*
TTTACGGCTAGCTCAGTCCTAG GTACTATGCTAGC	TACTAGAGAAAGAGGAGAAATACTA G	P_{con}-RBS2-*luxR*
TTTACGGCTAGCTCAGTCCTAG GTACTATGCTAGC	TACTAGAGAAGTACGGGAAATACTA G	P_{con}-RBS3-*luxR*
TTTACGGCTAGCTCAGTCCTAG GTACTATGCTAGC	TACTAGAGAACCTAAGGAAATACTA G	P_{con}-RBS4-*luxR*

Appendix Table 2. Summary of primers used in Chapter 2

Name	Sequence
CD_211	TCGACAAGCTTCACTGATAGTGCTAGTGTAGATCACTACTAGAGC
CD_212	CCCTTGCTCACCATCTAGTATTTCTCCTCTTTCTCTAGTATTTATTCGACTATAACAAAC
CD_213	GAGGAGAAATACTAGATGGTGAGCAAGGGCGAGGA
CD_214	GGTTTACCGGTCCGTTTTTTTGCCGGACTGCA
esa_RFP_1	ATGCCTCGGTCTCGTCCGCTCATGAATTAATTCTTAGAAAAACTC
esa_RFP_2	CCTCATCGGTCTCCCTCGACCGATGCCCTTGAGAGC
esa_RFP_3	CCTCATCGGTCTCGCGAGATGCTAGTTATTGCTCAGCGGTG
esa_RFP_4	CTTGGCAGAAGACGAACTCGACATAAAGTCTAACCTATAGGATACTTACAG
esa_RFP_5	CTTGGCAGAAGACGTGAGTTTGACAGCTTATCATCGACTGCA
esa_RFP_6	ATGCCTCGGTCTCGATCTAGTATTTCTCCTCTTTCTCTAGTAACCTG
esa_RFP_7	ATGCCTCGGTCTCCAGATGGTGAGCAAGGGCGAG
esa_RFP_8	ATGCCTCGGTCTCCCGGATTACCGCCTTTGAGTGAGCT
CD_215	CGTGCGGTACCTAGCTTTCGCTAAGGATGATTTCTGGAATTCG
CD_216	TCACTCTGCAGCTCTAGTATATAAACGCAGAAAGGCCCACC
lux_R1_a	CGGAACTGGTCTCCAGCCTTTCTCTAGTAGCTAGCATTGTACC
lux_R1_b	CGGAACTGGTCTCCGGCTCGAAATACTAGATGAAAAACATAAATGCC
lux_R3_a	CGGAACTGGTCTCCCGTACTTCTCTAGTAGCTAGCATTGTACC
lux_R3_b	CGGAACTGGTCTCGTACGGGAAATACTAGATGAAAAACATAAATGCC
lux_R4_a	CGGAACTGGTCTCCTTAGGTTCTCTAGTAGCTAGCATTGTACC
lux_R4_b	CGGAACTGGTCTCCCTAAGGAAATACTAGATGAAAAACATAAATGCC
C9_1	AGTGACCTAGGAGTCGAAGAGCATGCTCTTCATGGATAAGAAATACTCAATAGGCTTAGCTATCGG
C9_2	TCACTCTCGAGTTAGTCACCTCCTAGCTGACTCAAATCAATG
A15	AGTGAGCTCTTCGAGTTGGGACCTGTAGGATCGTACAGGTTTACG
A16	TCACTGCTCTTCTCCATCTAGTATTTCTCCTCTTTCTCTAGTATTTATTCGACTATAACAAACC
C9_lux_1	CGAAACCGGTCTCGAGGCGGTGGCAGCAGCCTAG
C9_lux_2	CGAAACCGGTCTCCAAAGGCATTTGAGAAGCACACGG
C9_lux_3	CGAAACCGGTCTCGCTTTATGGCTAGCTCAGTCCTAGG
C9_lux_4	CGAAACCGGTCTCGGCCTCTAGTATATAAACGCAGAAAGGCC
T4_R20_1	CAATCGCGAAGACAGTTCACGAGGGATTGGTAAGGAAGG
T4_R20_2	CAATCGCGAAGACAGTGTGAGAGCCTTCAACCCAGTCA
T4_R20_3	CAATCGCGAAGACAGCACAGGATCCTCTGCGTTTATATACTAGAGAC
T4_R20_4	CAATCGCGAAGACAGAGTTTATTCGACTATAACAAACCATTTTCTTGCG
T4_R20_5	CAATCGCGAAGACACAACTCGACTCTACTTAAGGAGGACCTTT
T4_R20_6	CAATCGCGAAGACACTGAATTTATTCGACTATAACAAACCATTTTCTTGCG
T4_esa_1	CCTCATCGGTCTCCTAGATGGCGCCGCGCCCGACT
T4_esa_2	CCTCATCGGTCTCCCTCGACCGATGCCCTTGAGAGC
T4_esa_3	CATCGGTCTCGCGAGATGCTAGTTATTGCTCAGCGGTG
T4_esa_4	CATCGGTCTCGCATCTAGTATTTCTCCTCTTTCTCTAGTAACCTGC
T4_esa_5	CCTCATCGGTCTCGGATGGGTGACTGCGTTGCC
T4_esa_6	CCTCATCGGTCTCGCAAACATATAAACGCAGAAAGGCCCACC
T4_esa_7	CATCGGTCTCGTTTGACAGCTTATCATCGACTGCAC
T4_esa_8	CATCGGTCTCGTCTAGTATTTCTCCTCTTTCTCTAGTAACCTGC
CHI_T7F2	TATACCATGGCGGCGAGCATTACCG
CHI_T7R2	ATTATGCGGCCGCTTAGTTACCAATCTTGAACGCACCCTC
CHS_T7F2	ATATACATATGGTGACCGTGGAAGAATACCG
CHS_T7R2	AGCAGCCTAGGTTAGGTCGCAACGCTATGCAGAA
EP_1	GAGAGACGGTCTCGTGACTGCTGCCACCGCTGAGC
EP_2	AGGGGAAGGTCTCGGGCATCTCGACCGATGCCCTTG
EP_3	AGGGGAAGGTCTCCTGCCACCTGACGTCTAAGAA
EP_4	AGGGGAAGGTCTCCAATCGACATAAAGTCTAACCTATAGGATACTTAC
EP_5	AGGGGAAGGTCTCCGATTTGACAGCTTATCATCGACTGC
EP_6	AGGGGAAGGTCTCCACCTGCACTATAGTACAGGCC
EP_7	AGGGGAAGGTCTCGAGGTTAATATAATATTACAAAGAGGAGGTTTTATGGATACG

EP_8	GAGAGACGGTCTCGAGTATTAATGCAATCCAAAAACGTTCAACA
EP_9	GAGAGACGGTCTCGTACTAGAGCCAGGCATCAAATAAAAC
EP_10	GAGAGACGGTCTCGACCTGCACTATAGTACAGGCC
EP_11	GAGAGACGGTCTCGAGGTACAATCATACTTGATAAGGAGGTTATTGCATGAAAACT
EP_12	GAGAGACGGTCTCGGTCATGCGGCACCCCGTGT
fapR_1	ACGTCTGGGTCTCGAAACCAGCAATAGACATAAGCGG
fapR_2	ACGTCTGGGTCTCGGAGCGCAACGCAATTAATGTAAGT
fapR_3	ACGTCTGGGTCTCGGCTCACTGCCCGCTTTCCAG
fapR_4	ACGTCTGGGTCTCGGTTTTTATTGACTACCGGAAGCAGTGT
A11	AGTGAGGTCTCGCTTCCGACCTGTAGGATCGTACAGGTTTACGC
A12	TCACTGGTCTCAAAAACAATTCTTGTTGAATTAGATGTTTATTCGACTATAACAAACCATTTTCTTGCGTAAACC
sg_1	CGTACCTGGTCTCGTAAGCGGCTATTTAACGACCCTGC
sg_2	CGTACCTGGTCTCGAGGGCATGACTAACATGAGAATTACAACTTATATCG
sg_3	CGTACCTGGTCTCGCCCTGCGTTTATATACTAGTAGCGGCCG
sg_4	CGTACCTGGTCTCGCGCAGAAAGGCCCACCCGAAGGT
sg_5	CGTACCTGGTCTCGTGCGTTTATATACTAGTAGCGGCCG
sg_6	CGTACCTGGTCTCGGAAAGGCCCACCCGAAGGT
sg_7	CGTACCTGGTCTCCTTTCTGCGTTTATATACTAGTAGCGGCCG
sg_8	CGTACCTGGTCTCCCAGAAAGGCCCACCCGAAGGT
sg_9	CGTACCTGGTCTCGTCTGCGTTTATATACTAGTAGCGGCC
sg_10	CGTACCTGGTCTCGCTTAAAAGGCCCACCCGAAGGT
adhE_lux_R	AGCGTGAATATGCCAGTTTCTTTATTCGACTATAACAAACCATTTTCTTGC
adhE_lux_F	GAAACTGGCATATTCACGCTGTTTTAGAGCTAGAAATAGCAAGTTAAAATAAG
fabB_lux_R	GGGCATTGTTTCCAGCATCGTTTATTCGACTATAACAAACCATTTTCTTGC
fabB_lux_F	CGATGCTGGAAACAATGCCCGTTTTAGAGCTAGAAATAGCAAGTTAAAATAAG
fabF_lux_R	GTACGCCGCTGGGCGTTGGTTTTATTCGACTATAACAAACCATTTTCTTGC
fabF_lux_F	ACCAACGCCCAGCGGCGTACGTTTTAGAGCTAGAAATAGCAAGTTAAAATAAGG
fumC_lux_R	GGCAGATAAGCTGTGGGGCGTTTATTCGACTATAACAAACCATTTTCTTGC
fumC_lux_F	CGCCCCACAGCTTATCTGCCGTTTTAGAGCTAGAAATAGCAAGTTAAAATAAG
sucC_lux_R	GCTATGGCTTACCAGCACCGTTTATTCGACTATAACAAACCATTTTCTTGC
sucC_lux_F	CGGTGCTGGTAAGCCATAGCGTTTTAGAGCTAGAAATAGCAAGTTAAAATAAG
sg_CPEC_1	CACATAAACAGACGCTTTTCCG
sg_CPEC_2	TCAGATTCATGGTTGAGCCTC

Appendix Table 3. Summary of promoter and RBS sequences used in Chapter 3.

Promoter and RBS sequences denoted as LXX were taken from Mutalik et al. (2013) (105) and RBS sequences denoted RBSX were generated using the Salis RBS calculator (106).

Promoter sequence	**RBS sequence**	**Name and gene controlled**
AAAAAATTTATTTGCTTTCGCA TCTTTTTGTACCTATAATGTGT GGA	GGGCCCAAGTTCACTTAAAAA GGAGATCAACAATGAAAGCAA TTTTCGTACTGAAACATCTTAA TCATGCCTAGGAAGTTTTCTAA TG	L6-*esaI*
TTGACAATTAATCATCCGGCTC GTAATGTTTGTGGA	GGGCCCAAGTTCACTTAAAAA GGAGATCAACAATGAAAGCAA TTTTCGTACTGAAACATCTTAA TCATGCCTAGGAAGTTTTCTAA TG	L13-*esaI*
TTCACTTTTAATCATCCGGCTC GTATAATGTGTGGA	GGGCCCAAGTTCACTTAAAAA GGAGATCAACAATGAAAGCAA TTTTCGTACTGAAACATCTTAA TCATGCCTAGGAAGTTTTCTAA TG	L19-*esaI*
TTGCCTCTTAATCATCGGCTCG TATAATGTGTGGA	GGGCCCAAGTTCACTTAAAAA GGAGATCAACAATGAAAGCAA TTTTCGTACTGAAACATCTTAA TCATGCGAGGGATGGTTTCTA ATG	L24-*esaI*
TTGCCTCTTAATCATCGGCTCG TATAATGTGTGGA	GGGCCCAAGTTCACTTAAAAA GGAGATCAACAATGAAAGCAA TTTTCGTACTGAAACATCTTAA TCATGCCTAGGAAGTTTTCTAA TG	L25-*esaI*
TTGACATCAGGAAAATTTTTCT GTATAATGTGTGGA	GGGCCCAAGTTCACTTAAAAA GGAGATCAACAATGAAAGCAA TTTTCGTACTGAAACATCTTAA TCATGCCTAGGAAGTTTTCTAA TG	L31-*esaI*

ACCTGTAGGATCGTACAGGTT TACGCAAGAAAATGGTTTGTT ATAGTCGAATAAA	TACTAGAGAATATCCAGAAAT ACTAG	P_{lux}-*sspB* (in IB1643(DE3)-lux)
ACCTGTAGGATCGTACAGGTT TACGCAAGAAAATGGTTTGTT ATAGTCGAATAAA	TACTAGAGAAGTGACAGAAAT ACTAG	P_{lux}-RBS1-*sspB*
ACCTGTAGGATCGTACAGGTT TACGCAAGAAAATGGTTTGTT ATAGTCGAATAAA	TACTAGAGAACCGTGAGAAAT ACTAG	P_{lux}-RBS3-*sspB*
ACCTGTAGGATCGTACAGGTT TACGCAAGAAAATGGTTTGTT ATAGTCGAATAAA	TACTAGAGAAGAAGGAGAAAT ACTAG	P_{lux}-RBS6-*sspB*
TTTATGGCTAGCTCAGTCCTAG GTACAATGCTAGC	TACTAGAGAAAGAGGAGAAAT ACTAG	P_{con}-*luxR* (in IB1643(DE3)-lux)
ATGGCTAGCTCAGTCCTAGGT ACAATGCTAGC	TACTAGAGAACCTAAGGAAAT ACTAG	P_{con}-RBS4-*luxR* (in pACYC-P_{lux}-*dCas9*-P_{con}-RBS4-*luxR)*

Appendix Table 4. List of primers used in Chapter 3

Name	Sequence
4CL_CC1	AGATATACCATGGGTGACTGCGTTGCC
4CL_CC2	ATTATGCGGCCGCAAGCTTTTACTTCGGCAGGTCGCC
TAL_GFP1	AGGTCTCCCACGATGGCATGAGATTATCAAAAAGGA
TAL_GFP2	AGGTCTCCAGGCGCCATCTCCTTGCATGCAC
TAL_GFP3	AGGTCTCCGCCTAGGATCGAGATCGATCTC
TAL_GFP4	AGGTCTCCCCATTCGCCAATCCGGATATAGTC
TAL_GFP5	AGGTCTCGATGGCGTCCGGCGTAGAGGAT
TAL_GFP6	AGGTCTCGCGTGGGCCGTGTACAATACGATTACTTT
Lux_sspB1	CCAGTAGGGTCTCCACTAAGCGGCTATTTAACGACCCT
Lux_sspB2	CCGTGATGGTCTCCCCATAAATTGCACTGAAATCTAGAAATATTTTATCTGAT
Lux_sspB3	CCGTGATGGTCTCGATGGATGATTTCTGGAATTCGCGG
Lux_sspB4	CCGTGATGGTCTCGGATATATAAACGCAGAAAGGCCCACC
Lux_sspB5	CCAGTAGGGTCTCGCCACCTTCGGGTGGGCCTTT
Lux_sspB6	CCAGTAGGGTCTCGATGAAGACCAGCTTTCGTGTACC
Lux_sspB7	CCAGTAGGGTCTCGTCATGAAGACAGATGGATTTGTCACAGC
Lux_sspB8	CCAGTAGGGTCTCGGTATTACTTCACAACGCGTAATGCC
Lux_sspB9	CCAGTAGGGTCTCGATACTAGAGCCAGGCATCAAATAAAAC
Lux_sspB10	CCAGTAGGGTCTCGTAGTGAGCGAGGAAGCCTGC
RBS_sspB1	AAGCTACTAGAGAAGACGAAGAAATACTAG
RBS_sspB2	CCATCTAGTATTTCTTCGTCTTCTCTAGTA
DE3_fwd	AGTGAGAATTCCTGCGCAACTCGTGAAAGGTAGG
DE3_rev	GCACTCTGCAGGGTCTTTCCTTCGAAGGGGATCCG

Appendix Table 5. Summary of promoter and RBS sequences used in Chapter 4

Promoter sequence	RBS sequence	Name and gene controlled
AAAAAATTTATTTGCTTTCGCA TCTTTTTGTACCTATAATGTGT GGA	GGGCCCAAGTTCACTTAAAAA GGAGATCAACAATGAAAGCAA TTTTCGTACTGAAACATCTTAA TCATGCTAAGGAGGTTTTCTA ATG	L1-*lasI*
AAAAAATTTATTTGCTTTCGCA TCTTTTTGTACCTATAATGTGT GGA	GGGCCCAAGTTCACTTAAAAA GGAGATCAACAATGAAAGCAA TTTTCGTACTGAAACATCTTAA TCATGCTGCGGAGGGTTTCTA ATG	L3-*lasI*
TTGCCTCTTAATCATCGGCTCG TATAATGTGTGGA	GGGCCCAAGTTCACTTAAAAA GGAGATCAACAATGAAAGCAA TTTTCGTACTGAAACATCTTAA TCATGCTAAGGAGGTTTTCTA ATG	L20-*lasI*
TTGACATCAGGAAAATTTTTCT GTATAATGTGTGGA	GGGCCCAAGTTCACTTAAAAA GGAGATCAACAATGAAAGCAA TTTTCGTACTGAAACATCTTAA TCATGCTAAGGAGGTTTTCTA ATG	L26-*lasI*
TTGACATCAGGAAAATTTTTCT GTATAATGTGTGGA	GGGCCCAAGTTCACTTAAAAA GGAGATCAACAATGAAAGCAA TTTTCGTACTGAAACATCTTAA TCATGCTGCGGAGGGTTTCTA ATG	L28-*lasI*

Appendix Table 6. List of primers used in Chapter 4

Name	Sequence
CD_36	CCTTTCGTTTTATTTGATGCCTGGCTCTAGTATTATTAGGAAACAGCCAGACGCTGTTCA
CD_37	CAGCGTCTGGCTGTTTCCTAATAATACTAGAGCCAGGCATCAAATAAAACGAAAGGCTCA
CD_68	GGTACCTTGACATCAGGAAAATTTTTCTGTATAATGTG
CD_71	GATCGCTGCAGGAGCCAGTGTGACTCTAGTAGAGAGC
CD_74	CGATCGGTACCTTGCCTCTTAATCATCGGCTC
CD_180	GATCGGTACCAAAAAATTTATTTGCTTTCGCATCTTTTTG
CD_181	ATCTGAACGATCATCATTAGAAACCCTCCGCAGCATGATTAAG
CD_182	CGGAGGGTTTCTAATGATGATCGTTCAGATCGGTCGTCGT
CD_188	CGATCTGAACGATCATCATTAGAAAACCTCCTTAGCATGATTAAGATGTTTCAG
CD_189	GGAGGTTTTCTAATGATGATCGTTCAGATCGGTCGTCGT
PS_3	GGTAGCGGCAGCGCCTCAAACGATTATACCCAACAA
PS_6	GCTGCCGCTACCCTGCTGCCCGTAAGACGAT
PS_8	AATTCGGTTCCATCATAAGGAGGTATTTATGGCCTTGGTTGACGGT
PS_9	GCGCTGCCGCTACCGAGAGTAATAAGACCCAAATTAACGGC
PS_11	GCAGGGTAGCGGCAGCCGTAAAGGAGAAGAACTTTTCACTGG
PS_14	CATGCCTGCAGTTATTATTTGTATAGTTCATCCATGCCATGTGT
PS_nar1	AGGTCTCGCGACTTTTCGGGGAAATGTGCG
PS_nar2	AGGTCTCGGTTTCCTGTGTGAAATTGTTATCCGC
PS_nar3	AGGTCTCCAAACAGACCATGGAATTCGGTTCC
PS_nar4	AGGTCTCCTTGCTGCCGCTACCCTGCTG
PS_nar5	AGGTCTCCGCAACAGACCTACTAGAGAAAGAGGAGA
PS_nar6	AGGTCTCCGTCGTATATAAACGCAGAAAGGCCC
PS_18	ATACGGCGGTGGTGGATCTGGAGGTGTTGCTGAATTGACCGCATTAC
PS_19	TCACTCTGCAGTTATTACTGGCGATTGTCATTCGC
PS_22	GATCCACCACCGCCGTATCCACCCTGCTGCCCGTAAGACGA
Trc_TAL1	AGGTCTCGGGCAAGTGGCACTTTTCGGGG
Trc_TAL2	AGGTCTCGAGTACAACTTATATCGTATGGGGCTGAC
Trc_TAL3	AGGTCTCGTACTATCGCTACGTGACTGGGT
Trc_TAL4	AGGTCTCGGAGGTCTGTTTCCTGTGTGAAATTGT
Trc_TAL5	AGGTCTCGCCTCTAGAAATAATTTTGTTTAACTTTAAGAAGGAGATATAC
Trc_TAL6	AGGTCTCGTGCCATTCGCCAATCCGGATATAG
TyrA_fwd	CTTATAATCGATACATTTAAGGAGATAAGAATGGTTGCTGAATTGACCGCATTAC
IUP_GA1	CCGCTTACATCTCGCGTTCTAAAGTTGGCTGTTTAATGCCAAAG
IUP_GA2	TGGAACACGCCTGGGT
IUP_GA3	TTGCAATGCACCAGGTCAT
IUP_GA4	GGCTGATCAGCCACTTGT
IUP_GA5	ATGGACATCGTCGATCGGT
IUP_GA6	CTTTGGCATTAAACAGCCAACTTTAGAACGCGAGATGTAAGCGG
LYC_1	CATCTTAGTATATTAGTTAAGTATAAGAAGGAGATATACATATGCAAACGGAACACGT
LYC_2	GTTATTGCTCAGCGGTGGCAGCAGCTTATTTAAGCTGGGTAAATGCA

LYC_3	ACTTTAATAAGGAGATATACCATGGTGAGTGGCAGTAAAG
LYC_4	TGTTCGACTTAAGCATTATGCTCAGGCGATTTTCATGACC
LYC_12	ATCTTAGTATATTAGTTAAGTATAAGAAGGAGATATACATATGGCCTTAGTTGATGGTT
LYC_13	GTATAATCATTCGATGCGGACCCACTACCAAGCGTGATCA
LYC_14	TGATCACGCTTGGTAGTGGGTCCGCATCGAATGATTATAC
LYC_15	ATGACGTGTTCCGTTTGCATACCACCGCTGCCACCACCCC
LYC_16	GGGGTGGTGGCAGCGGTGGTATGCAAACGGAACACGTCAT
LYC_12b	GTAGAAATAATTTTGTTTAACTTTAATAAGGAGATATACCATGGCCTTAGTTGATGGTT
LYC_17	CTTTACTGCCACTCACCATACCACCGCTGCCACCACCCC
LYC_18	GGGGTGGTGGCAGCGGTGGTATGGTGAGTGGCAGTAAAG
LYC_19	AGGTCTCGGGTCATCGTGGCCGGATC
LYC_20	AGGTCTCGCGGACACCATCGAATGGCG
LYC_21	AGGTCTCCTCCGGGATCTCGACGCTC
LYC_22	AGGTCTCCTACTTTCTGTTCGACTTAAGCATTATGC
LYC_23	AGGTCTCCAGTAATCGTATTGTACACGGCCG
LYC_24	GGTCTCCGACCCGGTCGTCGGTTCA
LYC_25	AGTGACATATGAAAAAAACCGTTGTGATTGGC
LYC_26	TCACTCCTAGGCTAAACGGGACGCTGCC

Appendix Table 7. Summary of promoter and RBS sequences used in Chapter 5

Promoter sequence	RBS sequence	Name and gene controlled
AAAAAATTTATTTGCTTTCGCA TCTTTTTGTACCTATAATGTGT GGA	GGGCCCAAGTTCACTTAAAAA GGAGATCAACAATGAAAGCAA TTTTCGTACTGAAACATCTTAA TCATGCTAAGGAGGTTTTCTA ATG	L1-*lasI*
AAAAAATTTATTTGCTTTCGCA TCTTTTTGTACCTATAATGTGT GGA	GGGCCCAAGTTCACTTAAAAA GGAGATCAACAATGAAAGCAA TTTTCGTACTGAAACATCTTAA TCATGCTGCGGAGGGTTTCTA ATG	L3-*lasI*
AAAAAATTTATTTGCTTTCGCA TCTTTTTGTACCTATAATGTGT GGA	GGGCCCAAGTTCACTTAAAAA GGAGATCAACAATGAAAGCAA TTTTCGTACTGAAACATCTTAA TCATGCGAGGGATGGTTTCTA ATG	L5-*lasI*
TTGACATCAGGAAAATTTTTCT GTATAATGTGTGGA	GGGCCCAAGTTCACTTAAAAA GGAGATCAACAATGAAAGCAA TTTTCGTACTGAAACATCTTAA TCATGCTAAGGAGGTTTTCTA ATG	L26-*lasI*
TTGACATCAGGAAAATTTTTCT GTATAATGTGTGGA	GGGCCCAAGTTCACTTAAAAA GGAGATCAACAATGAAAGCAA TTTTCGTACTGAAACATCTTAA TCATGCTGCGGAGGGTTTCTA ATG	L28-*lasI*
TTCACTTTTAATCATCCGGCTC GTATAATGTGTGGA	GGGCCCAAGTTCACTTAAAAA GGAGATCAACAATGAAAGCAA TTTTCGTACTGAAACATCTTAA TCATGCCTAGGAAGTTTTCTAA TG	L19-*esaI*
TTGCCTCTTAATCATCGGCTCG TATAATGTGTGGA	GGGCCCAAGTTCACTTAAAAA GGAGATCAACAATGAAAGCAA TTTTCGTACTGAAACATCTTAA TCATGCGAGGGATGGTTTCTA ATG	L24-*esaI*

AATTCATTCTTCACTTTGAACA TATTTAAATCTTTAATGCAATT GTTCAGTTCTTGCTCATTTATA TCTGTGATGGCAACCACAGTT TGACTCTACGAGCATGAACAA ACGCAACCGTGAAAATCAAAA TAGCATAAATTGTGATCTATTC GTCGGAAATATGTGCAATGTC CACCTAAGGTTATGAACAAAT TAAAAGCAGAAATACATTTGT TCAAAACTCACCTGCAAAACT GAACGGGGGAAAT	CAATTCATTAAAGAGGAGAAA GGATCC	P_{lsr}-GFPmut3b
GCTCACAACAGTGTAAGCGTA TCCGTTATTGTTTGATTTTCAA GGAAAAAAGAAAACATTCAG GCTCCATGCTGCTTCTTTTACT TAACGTGGACTTAACCTGCAC TATAGTACAGGCAAGATGATA CTTAAGAGTAACTTACAATGA ATCATTCAGAGGTTACAATGG	CAATTCATTAAAGAGGAGAAA GGATCC	P_{esaS}-GFP(LVA)
GCCCCTCGCTGAGCGCGTCCC GGAGCTGGGGGCAACCTAGCT GCCACCTGCTTTTCTGCTAGCT ATTCCAGCGAAAACATACAGA TTTCCGGCGAAATCAAGGCTA CCTGCCAGTTCTGGCAGGTTTG GCCGCGGGTTCTTTTTGGTACA CGAAAGC	TACTAGAGAAAGAGGAGAAAT ACTAG	P_{las}-RFP
TCGACATAAAGTCTAACCTAT AGGATACTTACAGCCAT	CAATTCATTAAAGAGGAGAAA GGATCC	P_{con}-*lsrR*
TTTATGGCTAGCTCAGTCCTAG GTACAATGCTAGC	CAATTCATTAAAGAGGAGAAA GGATCC	P_{con}-*lasR* (plasmid)
TTGACGGCTAGCTCAGTCCTA GGTACAGTGCTAGC	CAATTCATTAAAGAGGAGAAA GGATCC	P_{con}-*lasR* (genomic)
TCGACATAAAGTCTAACCTAT AGGATACTTACAGCCAT	CAATTCATTAAAGAGGAGAAA GGATCC	P_{con}-*esaR*
TTTATGGCTAGCTCAGTCCTAG GTACAATGCTAGC	TACTAGAGAAAGAGGAGAAAT ACTAG	P_{con}-*luxR*
ACCTGTAGGATCGTACAGGTTT ACGCAAGAAAATGGTTTGTTAT AGTCGAATAAA	TACTAGAGAAAGAGGAGAAATA CTAG	P_{lux}-mCherry

Appendix Table 8. List of primers used in Chapter 5

Name	Sequence
CD_001	CGACATAAAGTCTAACCTATAGGATACTTACAGCCATCAATTCATTAAAGAGGAGAAA GGATCCATGACAATCAACGATTCGGCAATTTCAGAA
CD_002	GGCTGTAAGTATCCTATAGGTTAGACTTTATGTCGAAATTCATTCTTCACTTTGAACAT ATTTAAATCTTTAATGCAATTGTTC
CD_003	CGCATGGATCCTTTCTCCTCTTTAATGAATTGATTTCCCCCGTTCAGTTTTGCAGG
CD_004	GGGGAAATCAATTCATTAAAGAGGAGAAAGGATCCATGCGTAAAGGAGAAGAACTTT TCACTGGA
CD_005	CCGTTTTTTTGCCGGACTGCAGTTATTATTTGTATAGTTCATCCATGCCATGTGTAATCC C
CD_007	TGATTTCTGGAATTCTTAACTACGTAAAATCGCCGCTGCTG
CD_038	ATGATTTCTGGAATTCGCGGCCG
CD_039	GAGGAAGCCTGCAGCGGC
Esa_las1	CGACGTTGCTCTTCCCTTAATACTAGAGCCAGGCATCAAATAAAACGAAAGGC
Esa_las2	CGACGTTGCTCTTCCTGTACGCTTTCGTGTACCAAAAAGAACCCGC
Esa_las3	CGACGTTGCTCTTCCACACGACCACACGAAGTCCTAAGAGAGGTAAAAATGGTG
Esa_las4	CGACGTTGCTCTTCCGGACTGCAGCGGCCGCTA
Esa_las5	CGACGTTGCTCTTCCTCCGGCTCACGAGGCAGAATTTCAGATAAAAAAAATCCTTAGC
Esa_las6	CGACGTTGCTCTTCCAAGCTACTAAAGCGTAGTTTTCGTCGTTTGC

Appendix Table 9. Guide RNA sequences

Target gene	20-bp complementary sequence
GFPmut3b	CATCTAATTCAACAAGAATT
tyrA	GAGAAGATGCTGACCCTCTC
pheA	ATCGCTTTTCTCGGCCCCAA
fabF (75)	ACCAACGCCCAGCGGCGTAC
fabB (75)	CGATGCTGGAAACAATGCCC
fumC (75)	CGCCCCACAGCTTATCTGCC
sucC (75)	CGGTGCTGGTAAGCCATAGC
adhE (75)	GAAACTGGCATATTCACGCT

Appendix Table 10. Custom synthesized DNA sequences

Gene	Sequence
RgTAL	ATGGCGCCGCGCCCGACTTCTCAAAGCCAGGCCCGCACTTGCCCGACCACCCAG GTTACCCAAGTTGATATCGTTGAGAAAATGCTGGCGGCTCCGACTGATAGCACC CTGGAGCTGGACGGTTATAGCCTGAACCTGGGTGATGTTGTGAGCGCTGCGCGT AAGGGTCGTCCGGTTCGTGTTAAAGATAGCGATGAAATCCGCAGCAAAATCGAC AAGAGCGTTGAATTTCTGCGCAGCCAACTGAGCATGTCTGTTTACGGTGTGACC ACCGGCTTTGGCGGCTCCGCGGACACCCGCACCGAGGACGCAATTAGCCTGCAA AAGGCGCTGCTGGAACACCAGCTGTGTGGTGTGCTGCCGAGCAGCTTCGACAGC TTTCGCCTGGGTCGTGGTCTGGAGAACAGCCTGCCGCTGGAAGTTGTTCGCGGT GCAATGACCATTCGTGTGAACTCTCTGACCCGTGGCCATAGCGCTGTTCGTCTGG TTGTTCTGGAAGCACTGACCAACTTTCTGAACCACGGTATTACCCCGATTGTTCC GCTGCGCGGTACCATCTCCGCGAGCGGCGATCTGTCTCCACTGTCTTACATTGCA GCGGCGATTAGCGGTCACCCGGATAGCAAAGTTCACGTGGTTCATGAAGGCAA AGAGAAGATCCTGTACGCGCGCGAAGCGATGGCGCTGTTTAACCTGGAGCCGGT GGTTCTGGGTCCGAAGGAGGGCCTGGGTCTGGTGAACGGTACCGCAGTTTCCGC GAGCATGGCAACCCTGGCACTGCACGACGCGCACATGCTGAGCCTGCTGAGCCA ATCTCTGACCGCGATGACCGTGGAGGCGATGGTTGGTCACGCGGGCAGCTTCCA TCCATTCCTGCACGATGTTACCCGTCCGCACCCGACCCAAATCGAGGTTGCGGG TAACATTCGCAAACTGCTGGAGGGCTCTCGCTTCGCGGTTCACCACGAGGAAGA GGTTAAGGTTAAGGATGATGAAGGCATTCTGCGTCAGGATCGTTATCCGCTGCG CACCAGCCCGCAATGGCTGGGTCCGCTGGTGTCCGACCTGATTCACGCTCATGC CGTTCTGACCATCGAAGCGGGTCAAAGCACCACCGATAACCCACTGATCGATGT TGAGAACAAGACCAGCCATCACGGTGGCAACTTTCAAGCGGCAGCGGTTGCCA ACACTATGGAAAAGACCCGTCTGGGCCTGGCCCAAATCGGTAAACTGAACTTCA CCCAGCTGACCGAGATGCTGAACGCGGGCATGAACCGTGGCCTGCCGAGCTGCC TGGCGGCTGAAGACCCATCCCTGAGCTATCATTGCAAAGGTCTGGACATTGCGG CGGCTGCATATACCAGCGAACTGGGCCACCTGGCTAACCCGGTTACCACCCACG TTCAACCGGCTGAAATGGCAAACCAGGCGGTGAACAGCCTGGCGCTGATTAGC GCACGTCGTACCACCGAATCTAACGACGTTCTGTCCCTGCTGCTGGCAACCCAC CTGTACTGCGTGCTGCAGGCGATCGACCTGCGTGCGATTGAGTTCGAGTTCAAG AAACAGTTTGGTCCGGCCATTGTTAGCCTGATCGACCAACACTTTGGTAGCGCG ATGACCGGTAGCAACCTGCGTGATGAGCTGGTTGAAAAGGTTAACAAGACTCTG GCCAAGCGTCTGGAGCAAACCAACAGCTACGATCTGGTTCCGCGCTGGCACGAC GCTTTTAGCTTCGCTGCAGGCACTGTTGTTGAGGTTCTGTCCAGCACCAGCCTGA GCCTGGCGGCCGTGAACGCATGGAAGGTTGCGGCAGCCGAGAGCGCGATCTCC CTGACCCGCCAGGTTCGTGAAACCTTTTGGTCCGCTGCAAGCACCTCCAGCCCG GCGCTGTCTTACCTGAGCCCGCGCACCCAGATCCTGTACGCATTTGTGCGTGAG GAACTGGGTGTTAAAGCCCGCCGTGGTGACGTTTTCCTGGGTAAACAAGAAGTT ACCATCGGCAGCAACGTTAGCAAGATTTACGAAGCCATCAAGAGCGGCCGTATC AACAACGTTCTGCTGAAGATGCTGGCATAA

Pc4CL	ATGGGTGACTGCGTTGCCCCGAAAGAGGATCTGATCTTCCGCAGCAAACTGCCG GACATTTACATTCCAAAGCATCTGCCGCTGCATACCTATTGTTTTGAGAACATCA GCAAGGTTGGCGACAAGAGCTGTCTGATCAACGGCGCAACCGGCGAAACCTTT ACCTACAGCCAGGTTGAGCTGCTGTCCCGTAAAGTTGCCAGCGGCCTGAACAAG CTGGGCATTCAACAAGGTGATACCATTATGCTGCTGCTGCCGAACTCCCCGGAG TACTTTTTCGCTTTCCTGGGTGCGAGCTATCGCGGTGCAATCAGCACTATGGCGA ACCCATTCTTTACCAGCGCAGAAGTGATCAAGCAACTGAAAGCGAGCCAAGCG AAGCTGATTATCACCCAGGCATGCTATGTTGACAAGGTTAAGGACTACGCAGCG GAGAAAAACATCCAGATCATTTGTATTGACGATGCACCGCAGGATTGCCTGCAC TTTAGCAAGCTGATGGAAGCGGATGAGAGCGAAATGCCGGAAGTGGTTATTAA CAGCGATGATGTGGTGGCACTGCCGTACAGCTCTGGCACCACCGGCCTGCCGAA AGGCGTTATGCTGACCCACAAGGGTCTGGTTACCAGCGTTGCACAACAGGTGGA TGGTGATAACCCGAACCTGTATATGCACTCCGAGGATGTTATGATCTGCATCCT GCCACTGTTCCATATCTATAGCCTGAACGCTGTTCTGTGTTGTGGTCTGCGTGCG GGCGTTACCATTCTGATCATGCAAAAGTTCGACATTGTGCCGTTTCTGGAGCTGA TTCAGAAGTATAAGGTTACCATTGGTCCGTTTGTTCCGCCGATCGTGCTGGCCAT CGCGAAAAGCCCGGTTGTTGACAAGTACGACCTGTCTAGCGTGCGCACCGTTAT GAGCGGTGCAGCGCCGCTGGGTAAAGAGCTGGAGGACGCTGTTCGTGCGAAAT TCCCGAACGCGAAGCTGGGTCAAGGCTATGGCATGACCGAAGCCGGTCCGGTTC TGGCGATGTGTCTGGCGTTCGCCAAAGAGCCGTATGAGATTAAGTCTGGCGCAT GCGGTACCGTTGTGCGTAACGCCGAGATGAAAATCGTTGACCCAGAAACCAAC GCGTCTCTGCCGCGTAACCAGCGTGGTGAGATTTGCATCCGTGGTGATCAGATT ATGAAAGGTTACCTGAACGACCCGGAAAGCACCCGCACCACCATCGACGAAGA GGGTTGGCTGCACACCGGTGACATTGGTTTCATCGACGATGACGATGAACTGTT CATTGTTGATCGTCTGAAAGAAATCATTAAGTACAAAGGTTTTCAAGTTGCTCC GGCGGAGCTGGAAGCACTGCTGCTGACCCACCCGACCATCAGCGATGCCGCGGT GGTTCCGATGATTGACGAGAAAGCGGGTGAAGTGCCAGTGGCGTTTGTTGTGCG TACCAACGGTTTTACCACCACCGAAGAAGAAATCAAACAATTTGTGAGCAAACA GGTTGTGTTCTACAAACGTATCTTCCGCGTTTTCTTCGTTGACGCTATTCCGAAA TCCCCGAGCGGCAAGATTCTGCGTAAGGATCTGCGCGCTCGTATTGCGAGCGGC GACCTGCCGAAGTAA
PhCHS	ATGGTGACCGTGGAAGAATACCGTAAGGCGCAACGTGCGGAAGGCCCGGCGAC CGTGATGGCGATTGGCACCGCGACCCCGAGCAACTGCGTTGACCAGAGCACCTA CCCGGATTTCTATTTTCGTATTACCAACAGCGAGCACAAAACCGACCTGAAGGA AAAATTCAAGCGTATGTGCGAGAAGAGCATGATTAAGAAACGTTACATGCACCT GACCGAGGAAATCCTGAAAGAGAACCCGAGCATGTGCGAATATATGGCGCCGA GCCTGGACGCGCGTCAGGATATCGTGGTTGTGGAAGTGCCGAAACTGGGCAAA GAGGCGGCGCAGAAAGCGATTAAGGAATGGGGTCAACCGAAAAGCAAGATCAC CCACCTGGTTTTCTGCACCACCAGCGGCGTGGACATGCCGGGTTGCGATTACCA ACTGACCAAACTGCTGGGCCTGCGTCCGAGCGTTAAGCGTCTGATGATGTATCA GCAAGGTTGCTTTGCGGGTGGCACCGTGCTGCGTCTGGCGAAAGATCTGGCGGA AAACAACAAGGGTGCGCGTGTTCTGGTTGTGTGCAGCGAGATTACCGCGGTGAC CTTCCGTGGCCCGAACGACACCCACCTGGATAGCCTGGTTGGTCAGGCGCTGTT TGGTGATGGTGCGGGTGCGATCATTATCGGCAGCGATCCGATTCCGGGTGTTGA GCGTCCGCTGTTCGAACTGGTGAGCGCGGCGCAAACCCTGCTGCCGGACAGCCA TGGTGCGATTGATGGTCACCTGCGTGAAGTTGGCCTGACCTTTCACCTGCTGAA

	AGACGTGCCGGGTCTGATTAGCAAAAACATCGAGAAGAGCCTGGAGGAAGCGT TCAAGCCGCTGGGCATTAGCGACTGGAACAGCCTGTTTTGGATTGCGCACCCGG GTGGCCCGGCGATTCTGGATCAAGTTGAAATCAAACTGGGCCTGAAGCCGGAG AAACTGAAGGCGACCCGTAACGTTCTGAGCAACTACGGTAACATGAGCAGCGC GTGCGTGCTGTTTATCCTGGATGAAATGCGTAAAGCGAGCGCGAAAGAGGGTCT GGGTACCACCGGCGAGGGTCTGGAATGGGGTGTGCTGTTCGGCTTTGGTCCGGG CCTGACCGTGGAAACCGTTGTTCTGCATAGCGTTGCGACCTAA
MsCHI	ATGGCGGCGAGCATTACCGCGATTACCGTGGAAAATCTGGAATATCCGGCGGTT GTGACCAGCCCGGTGACCGGCAAAAGCTACTTCCTGGGTGGCGCGGGCGAGCG TGGCCTGACCATCGAAGGCAACTTCATTAAATTTACCGCGATCGGTGTGTACCT GGAGGACATTGCGGTTGCGAGCCTGGCGGCGAAGTGGAAAGGCAAGAGCAGCG AGGAACTGCTGGAAACCCTGGACTTCTATCGTGATATCATTAGCGGTCCGTTTG AAAAACTGATTCGTGGCAGCAAGATCCGTGAGCTGAGCGGTCCGGAATACAGC CGTAAAGTGATGGAGAACTGCGTTGCGCACCTGAAGAGCGTGGGTACCTATGGC GATGCGGAGGCGGAAGCGATGCAGAAATTCGCGGAAGCGTTTAAACCGGTGAA CTTCCCGCCGGGTGCGAGCGTGTTCTACCGTCAAAGCCCGAACGGTATTCTGGG CCTGAGCTTCAGCCCGGACACCAGCATTCCGGAGAAAGAAGCGGCGCTGATCG AAAACAAGGCGGTGAGCAGCGCGGTTCTGGAAACCATGATCGGTGAACACGCG GTTAGCCCGGATCTGAAGCGTTGCCTGGCGGCGCGTCTGCCGGCGCTGCTGAAT GAGGGTGCGTTCAAGATTGGTAACTAA
FUS	GCCTCAAACGATTATACCCAACAAGCAACCCAAAGCTATGGGGCCTACCCCACC CAGCCCGGGCAGGGCTATTCCCAGCAGAGCAGTCAGCCCTACGGACAGCAGAG TTACAGTGGTTATAGCCAGTCCACGGACACTTCAGGCTATGGCCAGAGCAGCTA TTCTTCTTATGGCCAGAGCCAGAACACAGGCTATGGAACTCAGTCAACTCCCCA GGGATATGGCTCGACTGGCGGCTATGGCAGTAGCCAGAGCTCCCAATCGTCTTA CGGGCAGCAG
FUSCHSCHI1	CTAGAAATAATTTTGTTTAACTTTAAGAAGGAGATATACCATGGCGGCGAGCAT TACCGCGATTACCGTGGAAAATCTGGAATATCCGGCGGTTGTGACCAGCCCGGT GACCGGCAAAAGCTACTTCCTGGGTGGCGCGGGCGAGCGTGGCCTGACCATCG AAGGCAACTTCATTAAATTTACCGCGATCGGTGTGTACCTGGAGGACATTGCGG TTGCGAGCCTGGCGGCGAAGTGGAAAGGCAAGAGCAGCGAGGAACTGCTGGAA ACCCTGGACTTCTATCGTGATATCATTAGCGGTCCGTTTGAAAAACTGATTCGTG GCAGCAAGATCCGTGAGCTGAGCGGTCCGGAATACAGCCGTAAAGTGATGGAG AACTGCGTTGCGCACCTGAAGAGCGTGGGTACCTATGGCGATGCGGAGGCGGA AGCGATGCAGAAATTCGCGGAAGCGTTTAAACCGGTGAACTTCCCGCCGGGTGC GAGCGTGTTCTACCGTCAAAGCCCGAACGGTATTCTGGGCCTGAGCTTCAGCCC GGACACCAGCATTCCGGAGAAAGAAGCGGCGCTGATCGAAAACAAGGCGGTGA GCAGCGCGGTTCTGGAAACCATGATCGGTGAACACGCGGTTAGCCCGGATCTGA AGCGTTGCCTGGCGGCGCGTCTGCCGGCGCTGCTGAATGAGGGTGCGTTCAAGA TTGGTAACTAAGCGGCCGCATAATGCTTAAGTCGAACAGAAAGTAATCGTATTG TACACGGCCGCATAATCGAAATTAATACGACTCACTATAGGGGAATTGTGAGCG

	GATAACAATTCCCCATCTTAGTATATTAGTTAAGTATAAGAAGGAGATATACAT ATGGCCTTAGTTGATGGTTTCTTAGAATTGGAGCGTAGTTCAGGAAAGTTAGAG TGGAGTGCTATCTTACAAAAAATGGCAAGCGATTTGGGGTTTTCAAAAATTTTG TTTGGTTTGTTGCCAAAAGACAGCCAAGATTA
FUSCHSCHI2	AAATTTTGTTTGGTTTGTTGCCAAAAGACAGCCAAGATTATGAGAATGCCTTCAT TGTCGGGAACTATCCCGCAGCCTGGCGTGAGCATTACGACCGCGCCGGATATGC GCGCGTAGACCCTACAGTCTCCCATTGTACACAGTCTGTGCTTCCCATTTTTTGG GAACCCTCCATCTACCAAACACGTAAACAGCATGAATTCTTTGAAGAGGCCTCC GCAGCCGGGTTGGTGTATGGGTTGACTATGCCATTACACGGTGCTCGTGGAGAA CTGGGTGCTCTGTCACTGTCAGTAGAAGCAGAGAATCGCGCGGAGGCGAATCGC TTCATTGAGAGTGTGTTACCGACTCTGTGGATGCTTAAAGACTACGCGCTTCAAT CCGGTGCTGGACTGGCGTTTGAACACCCAGTATCAAAGCCAGTTGTATTAACCT CACGTGAAAAGGAGGTCCTGCAATGGTGCGCGATCGGGAAAACGAGTTGGGAG ATTTCCGTTATCTGCAATTGTTCAGAGGCAAATGTCAACTTTCACATGGGAAAC ATCCGCCGCAAATTCGGAGTAACAAGCCGTCGTGTCGCTGCCATCATGGCAGTT AATCTTGGTTTGATCACGCTTGGTAGTGGGTCCGCATCGAATGATTATACACAA CAGGCTACCCAATCCTATGGAGCGTACCCTACTCAACCGGGTCAAGGCTATTCT CAACAGAGTTCCCAGCCTTACGGGCAGCAGAGTTACTCGGGATATTCCCAATCT ACCGACACATCCGGGTACGGGCAGTCTTCCTACTCAAGCTACGGACAATCACAA AACACCGGATACGGGACACAGTCAACTCCACAGGGCTATGGCAGTACAGGCGG TTACGGGTCGTCCCAGTCCAGTCAGAGCAGTTATGGACAGCAAGGCGGATACGG GGGTGGTGGCAGCGGTGGTATGGTGACCGTGGAAGAATACCGTAAGGCGCAAC GTGCGGAAGGCCCGGCGACCGTGATGGC
FUSCHSCHI3	GTAAGGCGCAACGTGCGGAAGGCCCGGCGACCGTGATGGCGATTGGCACCGCG ACCCCGAGCAACTGCGTTGACCAGAGCACCTACCCGGATTTCTATTTTCGTATTA CCAACAGCGAGCACAAAACCGACCTGAAGGAAAAATTCAAGCGTATGTGCGAG AAGAGCATGATTAAGAAACGTTACATGCACCTGACCGAGGAAATCCTGAAAGA GAACCCGAGCATGTGCGAATATATGGCGCCGAGCCTGGACGCGCGTCAGGATA TCGTGGTTGTGGAAGTGCCGAAACTGGGCAAAGAGGCGGCGCAGAAAGCGATT AAGGAATGGGGTCAACCGAAAAGCAAGATCACCCACCTGGTTTTCTGCACCACC AGCGGCGTGGACATGCCGGGTTGCGATTACCAACTGACCAAACTGCTGGGCCTG CGTCCGAGCGTTAAGCGTCTGATGATGTATCAGCAAGGTTGCTTTGCGGGTGGC ACCGTGCTGCGTCTGGCGAAAGATCTGGCGGAAAACAACAAGGGTGCGCGTGT TCTGGTTGTGTGCAGCGAGATTACCGCGGTGACCTTCCGTGGCCCGAACGACAC CCACCTGGATAGCCTGGTTGGTCAGGCGCTGTTTGGTGATGGTGCGGGTGCGAT CATTATCGGCAGCGATCCGATTCCGGGTGTTGAGCGTCCGCTGTTCGAACTGGT GAGCGCGGCGCAAACCCTGCTGCCGGACAGCCATGGTGCGATTGATGGTCACCT GCGTGAAGTTGGCCTGACCTTTCACCTGCTGAAAGACGTGCCGGGTCTGATTAG CAAAAACATCGAGAAGAGCCTGGAGGAAGCGTTCAAGCCGCTGGGCATTAGCG ACTGGAACAGCCTGTTTTGGATTGCGCACCCGGGTGGCCCGGCGATTCTGGATC AAGTTGAAATCAAACTGGGCCTGAAGCCGGAGAAACTGAAGGCGACCCGTAAC GTTCTGAGCAACTACGGTAACATGAGCAGCGCGTGCGTGCTGTTTATCCTGGAT GAAATGCGTAAAGCGAGCGCGAAAGAGGGTCTGGGTACCACCGGCGAGGGTCT

	GGAATGGGGTGTGCTGTTCGGCTTTGGTCCGGGCCTGACCGTGGAAACCGTTGT TCTGCATAGCGTTGCGACCTAACCTAGGCTGCTGCCACCGCTGAGCAATAACTA GCATAAC